A parametric investigation into the membrane stresses of hydrostatically loaded circular and elliptic toroidal shells

Nishalin Govender

Thesis presented in partial fulfilment of the requirements of the degree of Master of Science in Civil Engineering

Structural Engineering and Mechanics Research Group

Department of Civil Engineering

University of Cape Town

2014 - 2016

Plagiarism Declaration

I know the meaning of plagiarism and declare that all the work in the document, save for that which is properly acknowledged, is my own. This dissertation has been submitted to the Turnitin module and I confirm that my supervisor has seen my report and any concerns revealed by such have been resolved with my supervisor.

Signature: signature removed Date: 17 November 2016

Abstract

This study explores the membrane stresses of hydrostatically loaded elliptical and circular toroidal tanks. Equations are derived, using the membrane theory of shells, to obtain equations which can accurately describe the meridional and hoop stress behaviour at locations sufficiently far away from any bending disturbance occurring within the shell. The derived expressions are validated using the finite element software ADINA, indicating excellent agreement between the analytical and numerical solutions.

A parametric study is undertaken, whereby the membrane profiles for prolate, oblate and circular toroidal shells is investigated. Parameters which are varied are the opening and aspect ratio of toroidal shells. Stress resultant profiles are shown for numerous cases in order to aid designers on suitable ratios to minimise membrane stresses for use when designing hydrostatically loaded toroidal shells.

Lastly, numerical examples are investigated, keeping the volume constant and comparing the surface area due to a variation of opening and aspect ratios. It was found that when investigating toroidal shells, considerations are required when choosing the aspect ratio and opening ratios. Based on the results obtained, compromises between prolate and circular cross-sections with relatively small opening ratios are recommended in order to minimise the cost and maximise the structural efficiency, based on the membrane stresses occurring within the shell.

Acknowledgements

First and foremost, I would like to thank my parents, Dr Dhana Sagree Govender and Manogran Govender for their support, love and encouragement. Words cannot express my gratitude for all they have done in my life.

Secondly, I would like to thank my supervisor, Professor Alphose Zingoni. The knowledge, understanding and patience exhibited by him is characteristic of a world class academic. I am indeed honoured to have been given the opportunity to work under him.

Thirdly, my gratitude goes out to Shathish Balendra, Christopher Long, Roya Amouhadi Nosakhare Enoma and Chad Ludwig. I have met these individuals during my studies and they have encouraged, provided insight and supported me at every step of the way. I am truly glad to have made such friendships along this journey.

Table of Contents

List of Tables

List of Figures

Chapter 1

Introduction

1.1 Background to investigation

A plated structure is defined as a structural member in which the length and breadth of the element are comparable to each other but are far greater in size than its thickness. Shell structures follow the same definition, with the difference being that shell structures have curvature, whilst plates do not. Shell elements have been historically documented for more than 2000 years, with a well-known example being the dome-shaped roof of the Pantheon, built at the height of the Roman empire. The curvature present in the element, is what gives shell structures their unique characteristic, which Zingoni (1997) describes as "their ability to resist transverse surface loading through the action of internal forces in the tangential plane of the shell's middle surface at any given point." Unlike beams or plates which resists such loading using flexural action, curvature allows shells to resist transverse loading using extensional action.

According to Ventsel et al (2001), there are five other advantages which enable shell structures to be a versatile structural element. They are:

- strength to weight ratio
- degree of strength and structural integrity
- high stiffness
- containment of space
- the aesthetic appeal

For modern man, shells are used in a variety of fields, ranging from civil and structural engineering, where roofs, fluid containment vessels, dams and even large structures, to mechanical engineering, whereby pipes, pressure vessels and numerous other applications are found. Apart from man-made applications, shells also do exist in nature, where besides the obvious connection to sea shells and egg shells, shells are present in the form of leaves, the human skull and even in the composition of DNA. From these natural examples and with the goal of modern society to create a sustainable environment, it can be argued that shell structures are by itself, a form of biomimicry, which is the creation of a man made object which mimics natural systems. Biomimicry often has the potential to create something far more intelligent than in comparison which man has created himself (Maglic, 2012).

Looking at our planet and by extension, the laws of physics itself, it is interesting to note that there is surface which is encountered in countless applications, present in the shape examined in magnetic fields and it is even postulated as the shape of our entire universe. This surface is commonly known as the torus. A torus is geometrically classified as being a surface of revolution which is revolved around an axis which is coplanar to the circle and does not intersect the circle. Given the natural applications of the torus and with the popularity of biomimicry gaining traction in modern times, an investigation merging both the torus and liquid containment capabilities of shell structures are undertaken in this dissertation.

1.2 Definition of a shell

Shell structures are defined by Novozhilov (1970) as being a "three-dimensional structure bounded primarily by two arbitrary curved surfaces a relatively small distance apart". This structure consists of a material or composite which is formed into the desired shape. Paramount to the definition of this shape is a property of the shell known as the middle surface, the surface which bisects the shell thickness at each point investigated. The classification of whether a shell is thick or not will vary, depending on the source consulted. According to Zingoni (1997), Novozilov suggests that the criteria for the definition of a thick and thin shell is defined as $\frac{h}{R} = \frac{1}{20}$, where h is the thickness and R is classified as the minimum radius of curvature of the middle surface of the shell. From the definition of the middle surface of the shell, it can be seen that there exists and inner and outer surface, named the intrados and the extrados respectively. Figure 1-1 below shows a typical shell element illustrating the thickness, radius of curvature and middle surface.

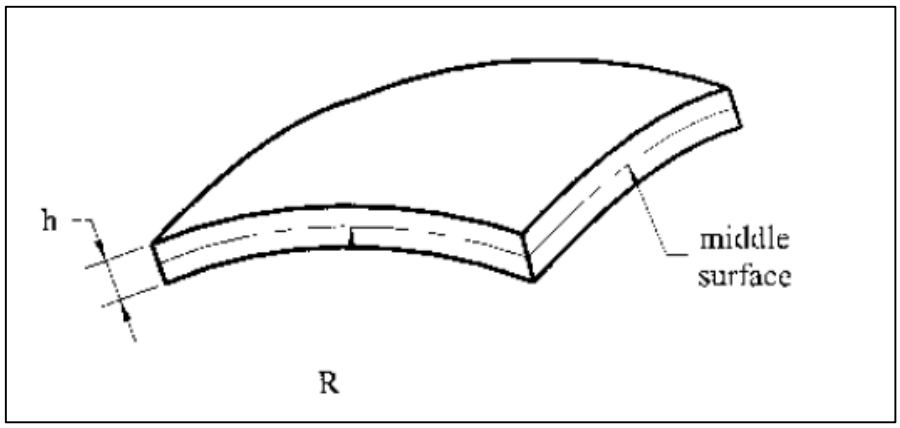

Figure 1-1: Typical shell element (Ventsel et al, 2013)

Shell structures exist in numerous shapes and classifications. According to Farshad (2013), there are three main categories of shells: translational surfaces, ruled surfaces and surfaces of revolution. Surfaces of translations are created by taking a plane curve, known as the meridian, and sliding it along a different plane curve and keeping the orientation of the curve which is sliding constant. Ruled surfaces are generated by

taking two curves and connecting line segments between these two curves. Surfaces of revolution are generated by the meridian, and rotating it about an axis called the axis of revolution, which will be shown later, does not necessarily intersect the meridian.

In addition to the above classification of shells, there exist further ways to differentiate different classes of shells. One such method is employing a property from multivariate calculus known as Gaussian curvature. Shells have two principal radii of curvature known as r_1 and r_2 respectively. The product of the principal radii at any point investigated can give three possible outcomes: positive, negative or zero, which correspond to synclastic, anticlastic or a surface which has zero Gaussian curvature respectively. Related to the Gaussian curvature, is the developability of a shell. Shells can be either developable or non-developable, which as the name suggests, a developable surface is one which can be folded out into a plane, without any distortion of the middle surface, whilst non-developable surfaces are ones which cannot. Those surfaces which are either anticlastic or synclastic are developable, in contrast to shells which have zero Gaussian curvature are non-developable.

In the analysis of a shell, a three dimensional structure, the application of linear elastic theories is possible, although the resulting equations are often complex to compute, despite the thickness of thin shells often being far smaller in comparison to the other dimensions. Love developed approximations for shell theory with regards to linear elasticity. His assumptions were obtained by taking the Kirchhoff assumptions for plates and applying them to shells. This resulted in the set of assumptions which would later give way to the first-order approximation shell theory. The Love-Kirchhoff assumptions which are given as follows:

- The shell thickness is negligibly small in comparison with the least radius of the shells middle surface
- Strains and displacements that arise within the shell are small
- Straight lines that are normal to the middle surface prior to deformation remain straight and normal to the middle surface during deformation, and experience no change in length

- The direct stress acting in the direction normal to the shell middle surface is negligible.

Although not entirely correct, these assumptions formed the basis of shell theories where Reissner (1941), Sanders (1959) and Timoshenko (1959) would later develop their popular shell theories and even further down the line, be the fundamental assumptions for the second-order approximation theory of shells. All of these theories are based on the theory of elasticity, of which small deflections are an important assumption which cannot be violated, providing accurate stresses as long as displacements occur in the linear elastic range. For those shells which experience large displacements, nonlinear theory of shells is required to be applied. Shells may be non-linear not only in their geometry, but also physically non-linear with respect to the material used.

In addition to the statics involved in shells, the initial problem of vibration in thin elastic shells were originally derived by Love. Following from his work, higher order approximations to vibration were derived by Flugge (1973). Buckling, however, was derived for both linear elastic and non-linear cases. Due to the complexities involved in vibration and buckling, numerical methods, such as the finite element method are employed in order to obtain solutions.

1.3 Thesis Overview

Chapter 1 provides a general introduction to the definition of a shell and the shape of the torus. It also gives a brief overview of the structure of this dissertation.

Chapter 2 provides an introduction to the membrane theory of shells – key to this investigation and derives the necessary equations for later use.

Chapter 3 discusses the previous literature undertaken on the statics and dynamics of toroidal shells

Chapter 4 introduces the theory behind the finite element method, which is used to validate the later derived expressions.

Chapter 5 derives the membrane expressions for elliptical toroidal shells and verifies them using finite element software

Chapter 6 provides a parametric study into the membrane stress profiles of elliptical and circular toroidal tanks

Chapter 7 investigated the effects of parameters using numerical examples for a fixed volume

Chapter 8 presents conclusions of the study and recommendations for future research

.

Chapter 2

The membrane theory of shells

This chapter introduces the membrane theory of shells – a theory crucial to the examination of the membrane stress resultants later derived in this investigation. The derivation, limitations and general aspects of this shell theory are discussed. The majority of this chapter is adapted from Zingoni (1997).

When investigating the stress static response of shell structures, there are two approaches which are used in conjunction with each other in order to derive expressions which govern the behaviour of the shell. These approaches are respectively known as the membrane and bending theories of shells.

The membrane theory of shells is applied to shells which have completely flexible membranes, negligible bending stiffness or shells which have a finite bending stiffness, but the moments which are formed are insignificantly small due to the geometric and loading properties. However, the exact state of stress in a shell is giving by the bending theory of shells, in which flexural and extensional effects are dealt with. However, Farnsworth (1999) shows that with general shell theory, a system of 11 equations and unknowns, which comprise of stress resultants, stress couples and displacements is difficult to solve. In contrast to this, the membrane theory, avoids a lot of these

complexities with a reduction of the number of unknowns by neglecting normal shear forces, along with bending and twisting moments.

In the absence of discontinuities explained in Section 2.2, the membrane theory of shells serves as a suitable approximation to the actual state of stress within a shell. In addition, the membrane solution has the added function of serving as an approximate particular integral to the equations of the bending theory.

2.1 Derivation of the membrane theory

Given a shell of revolution, where a meridional curve is rotated around an axis of revolution. From this shell, consider an element, bounded by two meridian curves and two circles of latitude as shown by Figure 2-1. The coordinate system describing this element is not Cartesian and there are two angular coordinates which are utilised. These angular coordinates are ϕ and θ, which for a given point describe the angle measured from the axis of revolution of the shell, known as the meridional angle and the angle measured in the horizontal plane of a circle of latitude respectively. Subsequently, any point on the shell may be described by these two coordinates.

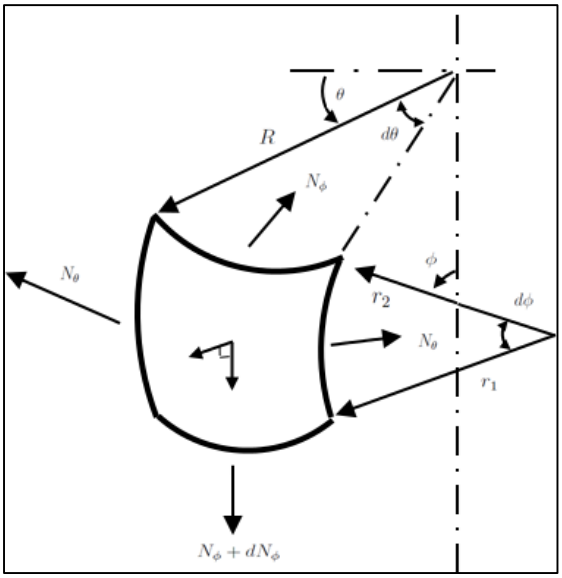

Figure 2-1: Axisymmetrically loaded shell element (As adapted from Zingoni, 1997)

Other parameters also introduced by Figure 2 are for a given point on the shell:

r_1 – the first principle radius of curvature.
r_2 – the second principle radius of curvature, which is denoted by the distance between the given point and the intercept of the normal and axis of revolution.
R – the radius of a horizontal circle of latitude
N_ϕ – the force per unit length in the meridional direction
N_θ – the force per unit length in the hoop direction
p_ϕ – load per unit area of the shell midsurface, in the meridional direction
p_r – load per unit area of the shell midsurface, normal to the given point

The radius R can also be described using the defined coordinate system, leading to the following relationships:

$$R = r_2 \sin\phi \tag{2-1}$$

It can also be seen that the length of vertical edges can be given by $r_1 d\phi$ of the upper and lower horizontal edges can be given by $Rd\theta$ and $(R + dR)d\theta$. The area of this element, may be approximated as $r_1 r_2 \sin\phi \, d\phi d\theta$.

When treated as a free body, force equilibrium of the shell element dictates that the sum of all forces in the directions of normal to the meridian and shell midsurface must be zero. Both the stress resultants and the loading components contributes a force in their corresponding direction.

Examining Figure 2-2a), which shows a section of the element, viewed from the horizontal plane of a circle of latitude, the force equilibrium can be given by:

$$\begin{aligned} F_1 &= N_\theta \, r_1 d\theta \left(\sin\frac{d\theta}{2}\right) + N_\theta \, r_1 d\theta \left(\sin\frac{d\theta}{2}\right) \\ &\approx N_\theta \, r_1 d\theta d\phi \end{aligned} \tag{2-2}$$

Since $\sin\phi \approx \phi$ for small angles of ϕ. Similarly, examining Figure 2-2b), which shows a section of the element along the vertical plane of the meridian, resolving F_1 along OT, which is the positive meridional direction gives:

$$-F_1 \cos\phi \tag{2-3}$$

Which, when substituted into Equation 2-2, results in:

$$-N_\theta r_1 \cos\phi d\phi d\theta \qquad 2\text{-}4$$

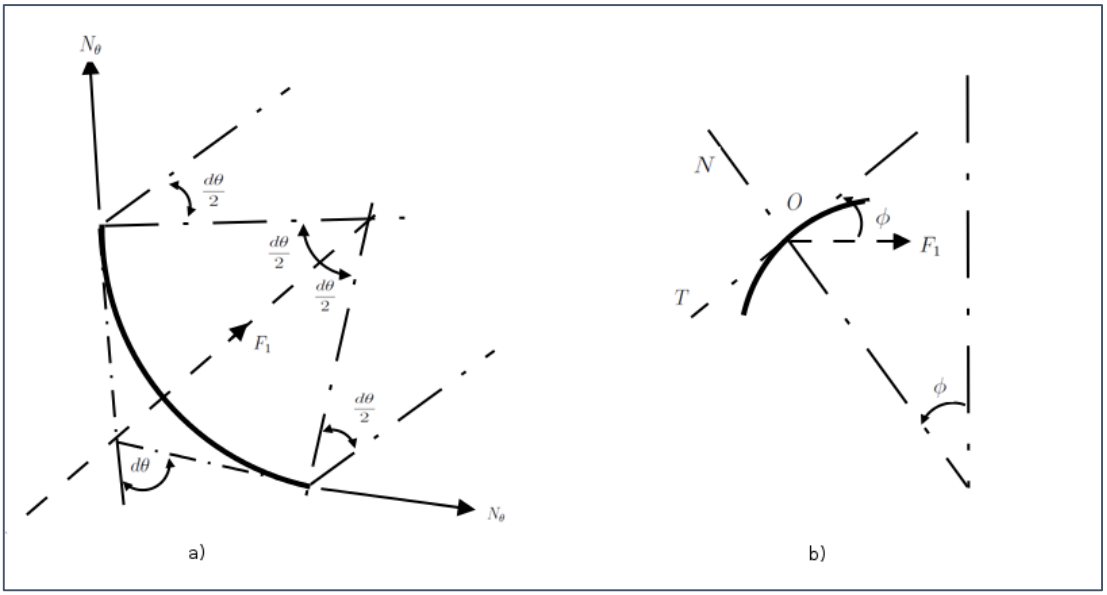

Figure 2-2: Various views of the axisymmetrically loaded shell element

With this expression obtained, the resultant F_2 from Figure 2-3 is obtained:

$$\begin{aligned} F_2 &= \left(N_\phi + dN_\phi\right)(R + dR)d\theta \cos\left(\frac{d\phi}{2}\right) - N_\phi R d\theta \cos\left(\frac{d\phi}{2}\right) \\ &\approx N_\phi dR d\theta + R dN_\phi d\theta \\ &= d\left(RN_\phi\right)d\theta \end{aligned} \qquad 2\text{-}5$$

Since for small angles of ϕ, $\cos\phi = 1$ and the term $dRdN_\phi d\theta$ is omitted due to it being negligibly small in comparison. Taking into account the contribution of external loading along OT is given by:

$$p_\phi r_1 R d_\phi d_\theta \qquad 2\text{-}6$$

Adding Equations 2-4 to 2-6 results in:

$$-N_\theta r_1 \cos\phi d\phi d\theta + d\left(RN_\phi\right)d\theta + p_\phi r_1 R d_\phi d_\theta = 0 \qquad 2\text{-}7$$

And dividing through by $d\theta$:

$$-N_\theta r_1 \cos\phi \, d\phi + d(RN_\phi) = -p_\phi r_1 R d_\phi \qquad 2\text{-}8$$

Similarly, forces must be resolved in the direction ON, which is the positive direction of the normal to the shell midsurface. Examining Figure 2-2b as was done in Equation 2-3 results in:

$$-N_\theta r_1 \sin\phi d\phi d\theta \qquad 2\text{-}9$$

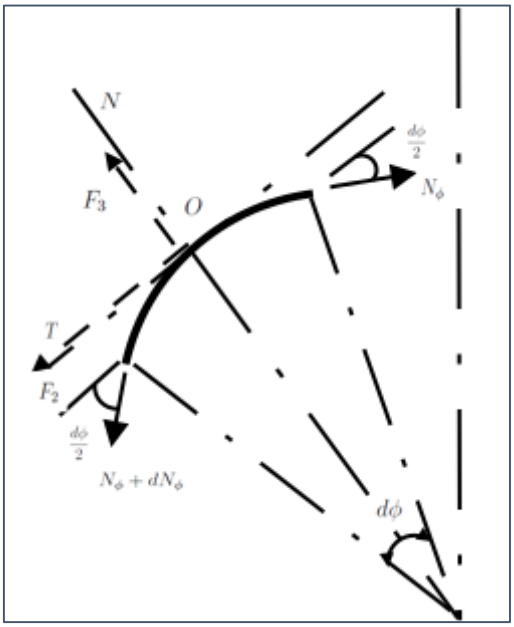

Figure 2-3: A section of the element in the vertical plane of the meridian

From Figure 2-3, resolving forces along the resultant of ON, F_3, yields:

$$\begin{aligned} F_3 &= -(N_\phi + dN_\phi)(R + dR)d\theta \sin\left(\frac{d\phi}{2}\right) - N_\phi R d\theta \sin\left(\frac{d\phi}{2}\right) \\ &\approx -RN_\phi d\theta d\phi \end{aligned} \qquad 2\text{-}10$$

Since for small values of ϕ, $\sin\phi = \phi$ and as done previously, smaller terms: $N_\phi dR d\theta \frac{d\phi}{2}$, $RdN_\phi d\theta \frac{d\phi}{2}$ and $dRdN_\phi d\theta \frac{d\phi}{2}$ are ignored.

The resultant force of the external loading normal to the shell midsurface is given by:

$$p_\phi r_1 R d_\phi d_\theta \qquad 2\text{-}11$$

And summation of terms from Equations 2-9 to 2-11 yields:

$$-N_\theta r_1 \sin\phi d\phi d\theta - RN_\phi d\theta d\phi + p_\phi r_1 R d_\phi d_\theta = 0 \qquad 2\text{-}12$$

Dividing through by $d\phi d\theta$, utilising the expression from Equation 2-1 and dividing through by $\sin\phi$ results in:

$$r_2 N_\phi + r_1 N_\theta = p_r \qquad 2\text{-}13$$

Dividing this expression throughout by $r_1 r_2$ gives the following expression, key to the membrane theory of shells:

$$\frac{N_\phi}{r_1} + \frac{N_\theta}{r_2} = r_1 r_2 p_r \qquad 2\text{-}14$$

Rearranging the above formula by making N_θ the subject of the formula and substitution of this into Equation 2-8 gives:

$$-\left(r_2 p_r - \frac{r_2}{r_1} N_\phi\right) r_1 \cos\phi \, d\phi + d\left(RN_\phi\right) = -p_\phi r_1 R d_\phi \qquad 2\text{-}15$$

Multiplying throughout by $\frac{\sin\phi}{d\phi}$ yields:

$$\left[\frac{d\left(RN_\phi\right)}{d\phi}\right] \sin\phi + r_2 \sin\phi \, N_\phi \cos\phi = r_1 r_2 p_r \cos\phi \sin\phi - p_\phi r_1 R \sin\phi \qquad 2\text{-}16$$

Back substitution of the relationship into Equation 2-1 into the above equation gives the left hand side as:

$$\left[\frac{d\left(RN_\phi\right)}{d\phi}\right] \sin\phi + RN_\phi \cos\phi \qquad 2\text{-}17$$

This term can be thought of as the result of the product rule from differential calculus. Applying this in reverse gives:

$$\left[\frac{d\left(RN_\phi\right)}{d\phi}\right] \sin\phi + RN_\phi \cos\phi = \frac{d}{d\phi}\left(RN_\phi \sin\phi\right) \qquad 2\text{-}18$$

Rewriting Equation 2-16 with the expression from Equation 2-18 yields:

$$\frac{d}{d\phi}\left(RN_\phi \sin\phi\right) = r_1 r_2 p_r \cos\phi \sin\phi - p_\phi r_1 R \sin\phi \quad 2\text{-}19$$

Integrating both sides of the above equations with respect to ϕ gives:

$$RN_\phi \sin\phi = \left[\int\left(r_1 r_2 p_r \cos\phi \sin\phi - r_1 R p_\phi \sin\phi\right)d\phi + k\right] \quad 2\text{-}20$$

Substitution of Equation 2-1 and rearranging the equation gives the general solution for N_ϕ as:

$$N_\phi = \frac{1}{r_2 \sin^2\phi}\left[\int r_1 r_2 (p_r \cos\phi - p_\phi \sin\phi) \sin\phi \, d\phi + k\right] \quad 2\text{-}21$$

k is a constant of integration which is obtained from an appropriate boundary condition. Once N_ϕ is calculated from the above expression, substitution of N_ϕ into Equation 2-14 gives the corresponding expression for N_θ.

2.2 Limitations

The validity of the membrane theory is dependent on the shell to which it is applied to. Consequently, there are various conditions which when employed will result in a breakdown of the membrane solution. These conditions are: external supports, discontinuities in the shell geometry and loading and concentrated line loadings. Locations where the above conditions may occur are known as edges and shear forces, bending and twisting moments occur at these locations. Gol'denveizer (1961) as cited by Zingoni (1997) named sources of edge effects as "lines of distortion". These lines of distortions are:

- The physical edges of the shell
- Discontinuities of surface loads or their derivatives
- Where the middle surface is discontinuous or the curvature changes suddenly
- Where their rigidity of the shell or its thickness abruptly changes

Illustrations of the above conditions are shown by Figure 2-4. In addition, the supports are required to be compatible with membrane theory.

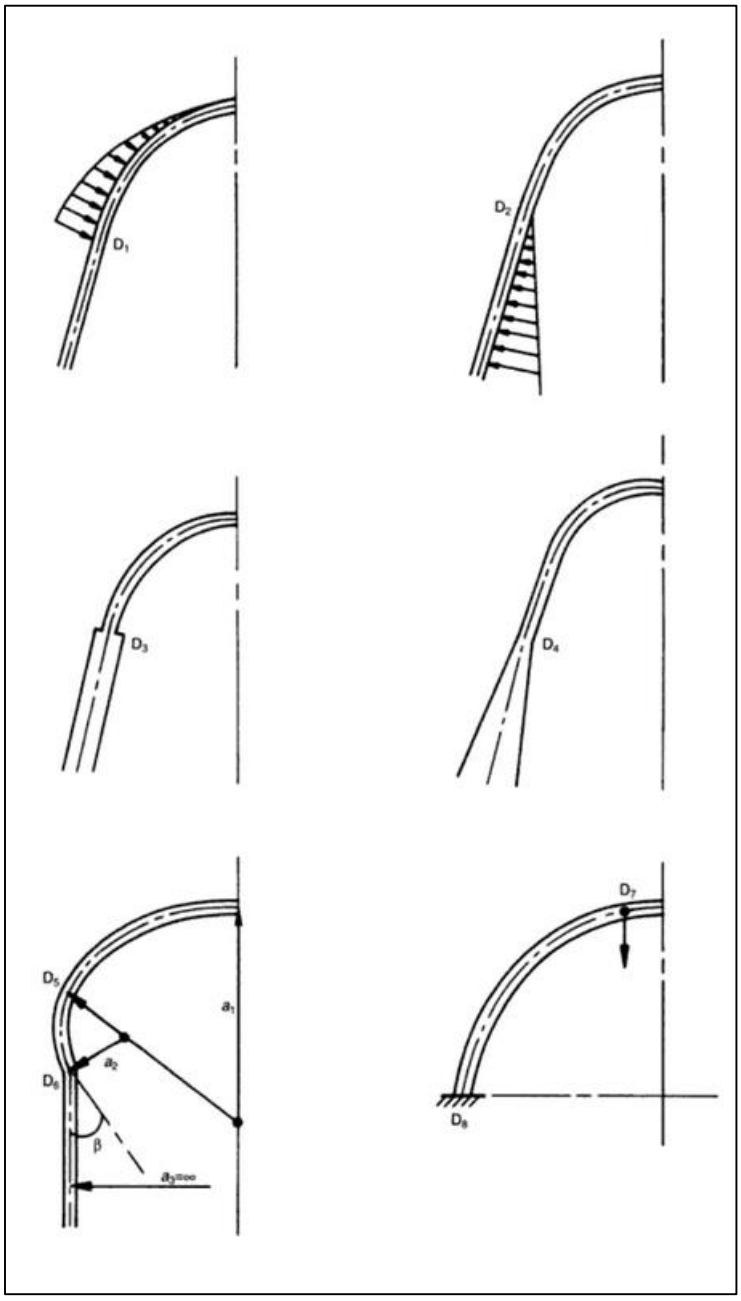

Figure 2-4: Lines of distortion within membrane theory (Zingoni, 1997). "D" refers to a discontinuity. D_1, in the radial loading component; D_2, in the first derivative of the radial loading component; D_3, in shell thickness; D_4, in the first derivative of thickness; D_5, meridional radius of curvature; D_6, meridional slope and meridional radius; D_7, concentrated line load; D_8, support.

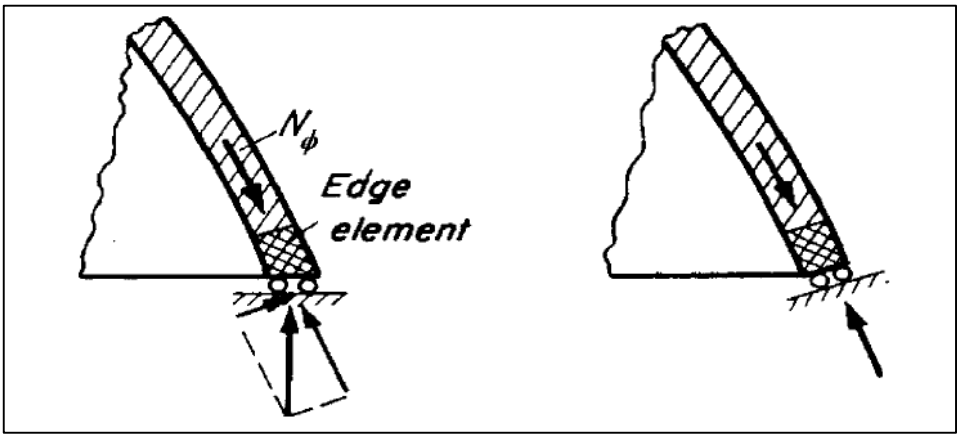

Figure 2-5: Compatibility of boundary conditions (Farnsworth, 1999)

Figure 2-5 shows the physical edge of a shell supported by two different boundary conditions. The support condition on the left is free to move horizontally. However, the reaction force can be resolved into a component which acts normal to the shell surface. This contradicts membrane theory, where there are no forces which act out of plane. The support on the right however only has a reaction which acts in the plane of the shell, along with no moment or shear force, satisfying the assumptions of membrane theory.

2.3 Deformations

In axisymmetrically loaded shells of revolution, the displacements of interest which occur are v, the displacement in the direction of the tangent to the meridian and w, the displacement in the direction normal to the shell midsurface. These displacements are necessary in order to obtain the edge effects by the flexibility method and to evaluate the deflections and distortions of the shell.

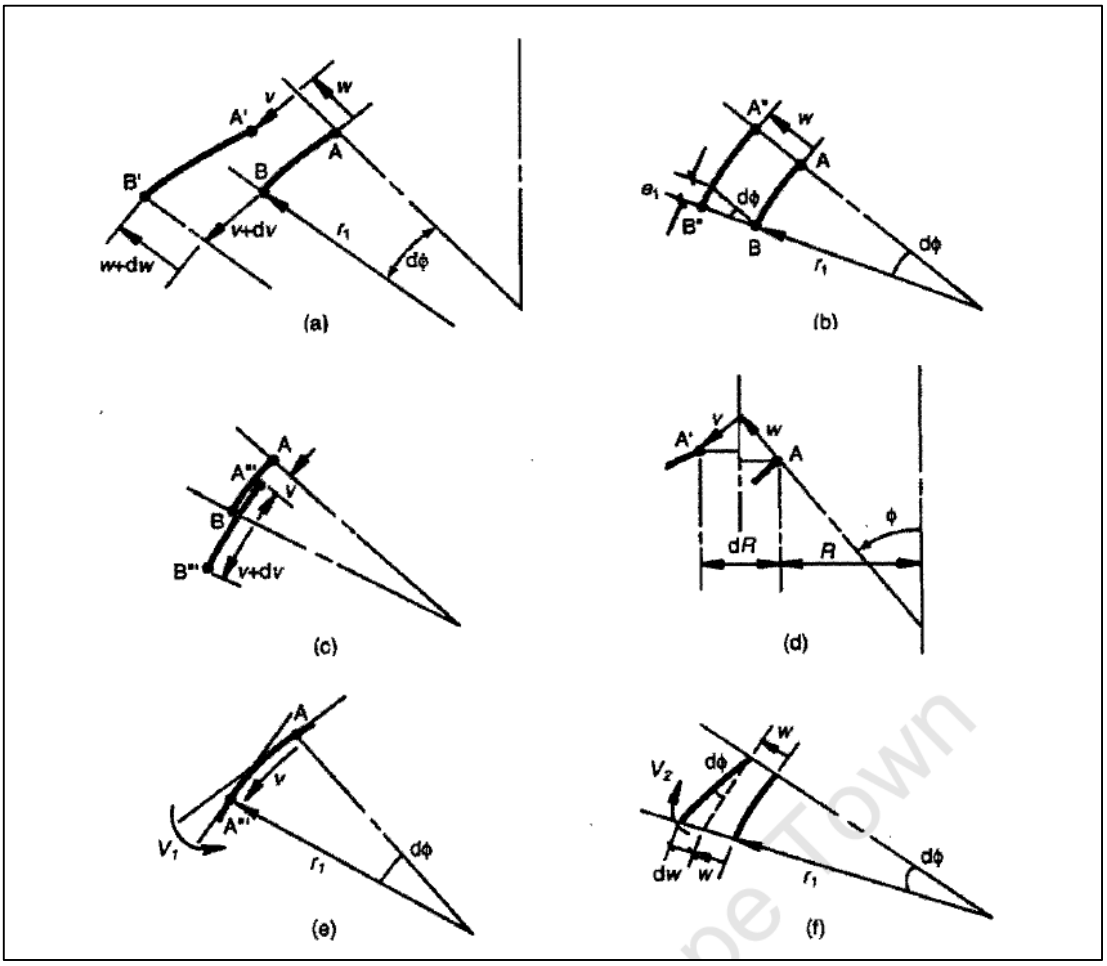

Figure 2-6: Deformation of a line element of an axisymmetrically loaded shell of revolution (Zingoni, 1997)

Figure 2-6 (a) shows line element AB, where the total elongation, e_ϕ, is shown as the addition of e_1 and e_2 given by Figure 2-6(b) and (c) by the radial movement w ($e_1 = wd\phi$) and the difference due to tangential movements A and B, v ($v = dv$).

$$e_\phi = dv + wd\phi \qquad 2\text{-}22$$

However, given that the original length of the line element is equal to $r_1 d\phi$, the meridional strain can be expressed by:

$$\epsilon_\phi = \frac{1}{r_1 d\phi}(dv + w d\phi) = \frac{1}{r_1}\left(\frac{dv}{d\phi} + w\right) \quad 2\text{-}23$$

Examining Figure 2-6(d), the movement of point A to A' causes the radius of the circle of latitude at point A to increase from R to $R + dR$. Consequently, the hoop strain ϵ_θ can be expressed by:

$$\epsilon_\theta = \frac{2\pi(R+dR)-2\pi R}{2\pi R} = \frac{dR}{R} \quad 2\text{-}24$$

It can be seen from Figure 2-6(d) that

$$dR = v\cos\phi + w\sin\phi \quad 2\text{-}25$$

Therefore:

$$\epsilon_\theta = \frac{v\cos\phi + w\sin\phi}{R} = \frac{1}{r_2}(v\cot\phi + w\sin\phi) \quad 2\text{-}26$$

As $R = r_2 \sin\phi$

Equations 2-23 to 2-26 result in:

$$\frac{dv}{d\phi} + w = r_1\epsilon_\phi \quad 2\text{-}27$$

$$v\cot\phi + w = r_2\epsilon_\theta \quad 2\text{-}28$$

Equation 2-27 subtracted from Equation 2-28 yields:

$$\frac{dv}{d\phi} + w = r_1\epsilon_\phi - r_2\epsilon_\phi \quad 2\text{-}29$$

From Hooke's law

$$\epsilon_\phi = \frac{1}{E}(\sigma_\phi - \nu\sigma_\theta) = \frac{1}{Et}(N_\phi - \nu N_\theta) \quad 2\text{-}30$$

$$\epsilon_\theta = \frac{1}{E}(\sigma_\theta - \nu\sigma_\phi) = \frac{1}{Et}(N_\theta - \nu N_\phi) \quad 2\text{-}31$$

And substitution into Equation 2-29 gives:

$$\frac{dv}{d_\phi} - v\cot\phi = \frac{1}{Et}\left[r_1(N_\phi - \nu N_\theta) - r_2(N_\theta - \nu N_\phi)\right]$$

$$= \frac{1}{Et}\left[(r_1 + \nu r_2)N_\phi - (r_2 + \nu r_1)N_\theta)\right] \quad 2\text{-}32$$

Using standard integration yields the result

$$v = \sin\phi\left[\int\left(\frac{1}{\sin\phi}\right)\frac{1}{Et}\left[(r_1 + \nu r_2)N_\phi - (r_2 + \nu r_1)N_\theta\right]d\phi + k\right] \qquad 2\text{-}33$$

Where k is a constant of integration to be determined from a suitable boundary condition.

When v is obtained, it follows that w can be calculated from Equation 2-28 and 2-31

$$w = r_2\epsilon_\theta - v\cot\phi = \frac{r_2}{Et}\left(N_\theta - \nu N_\phi\right) - v\cot\phi \qquad 2\text{-}34$$

However, practically speaking, the horizontal displacement dR, which will now be denoted as δ and the meridional rotation V which are required to be evaluated. Using these expressions, edge effects may be calculated using the flexibility method, which is beyond the scope of this investigation.

Since $\epsilon_\theta = \frac{dR}{R} = \frac{\delta}{R}$, it follows that:

$$\delta = E\epsilon_\theta = (r_2\sin\phi)\epsilon_\theta \qquad 2\text{-}35$$

Using Equation 2-31 to eliminate ϵ_θ, yields:

$$\delta = \frac{1}{Et}(r_2\sin\phi)\left(N_\theta - \nu N_\phi\right) \qquad 2\text{-}36$$

Using Figure 2-6(e) and (f), the meridional rotation may be obtained. When A moves to A'' by an amount v, the tangent at point A rotates anticlockwise by $V_1 = d\phi = \frac{v}{r_1}$. As a result of the differential radial movement at both ends of the line element, a net clockwise rotation is caused by $V_2 = d\phi = \frac{dw}{r_1 d\phi}$. Therefore

$$V = \frac{1}{r_1}\left(v - \frac{dw}{d\phi}\right). \qquad 2\text{-}37$$

Differentiating Equation 2-28 results in

$$\frac{dv}{d\phi}\cot\phi - \frac{v}{\sin^2\phi} + \frac{dw}{d\phi} = \frac{d}{d\phi}(r_2\epsilon_\theta) = \frac{d}{d\phi}\left[\frac{r_2}{Et}(N_\theta - \nu N_\phi)\right] \qquad 2\text{-}38$$

Whilst multiplying Equation 2-32 by $\cot\phi$ results in

$$\frac{dv}{d\phi}\cot\phi - v\cot^2\phi = \frac{\cot\phi}{Et}\left[(r_1 + \nu r_2)N_\phi - (r_2 + \nu r_1)N_\theta\right] \qquad 2\text{-}39$$

Subtraction of these two equations gives

$$v - \frac{dw}{d\phi} = \frac{\cot\phi}{Et}\left[(r_1 + \nu r_2)N_\phi - (r_2 + \nu r_1)N_\theta\right] - \frac{d}{d\phi}\left[\frac{r_2}{Et}(N_\theta - \nu N_\phi)\right] \qquad 2\text{-}40$$

Where after substituting into Equation 2-37 gives:

$$V = \frac{1}{r_1}\left[\frac{\cot\phi}{Et}\left[(r_1 + \nu r_2)N_\phi - (r_2 + \nu r_1)N_\theta\right] - \frac{d}{d\phi}\left[\frac{r_2}{Et}(N_\theta - \nu N_\phi)\right]\right] \qquad 2\text{-}41$$

Chapter 3

Literature review

3.1 Introduction

As mentioned in Section 1.2, the applications and uses for this previously neglected shell of revolution is increasing as technology advances. As applications range from pipe bends to concept space stations, no study has been undertaken with respect to toroidal tanks as a means of liquid containment. This chapter reviews the previous work done on toroidal shells with particular emphasis placed on the statics, dynamics and stability.

3.2 Static analysis of toroidal shells

When investigating the static analysis of thin-walled shells, there are two main theories which are used: the membrane and the bending theory of shells. The membrane theory is discussed in Chapter 2. If the exact state of stress is desired, the bending theory of shells is employed. This theory takes into account extensional and flexural effects and is used in conjunction with membrane theory, as bending stress resultants are incorporated accordingly. Key to both of these theories are the assumptions given by the Kirchhoff-Love hypothesis.

Static analyses are important for the design of toroidal shells as it enables designers to evaluate locations where the stresses within the shell are largest and allowing them to make provision for these expected stresses. Static analyses for circular and elliptic toroidal shells are described below.

3.2.1 Circular toroidal shells

As described by Zingoni (1997) and, for a circular torus of constant thickness, internal constant pressure of $p_r = p$ and where ϕ is measued from the vertical axis of the circular cross section, towards the surface of the outer surface of the torus as viewed from Figure 3-1. The principal radii of curvature are: $r_1 = a$ and $r_2 = \frac{A+a\sin\phi}{\sin\phi}$. Substitution of these parameters into the membrane equations yield:

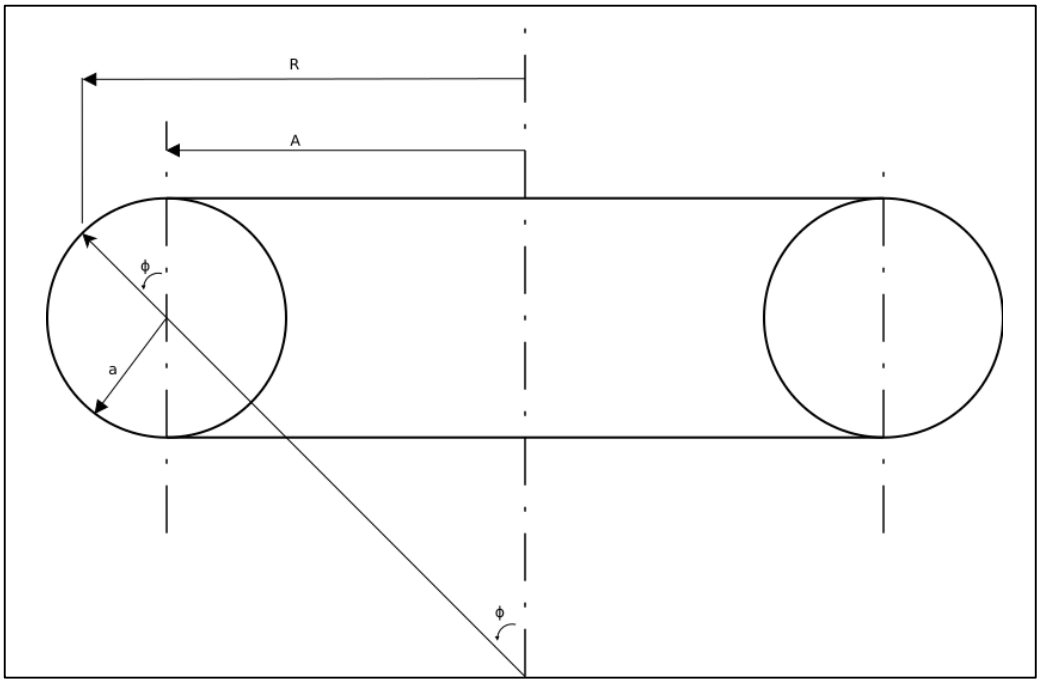

Figure 3-1: Geometry of a circular torus

$$N_\phi = pa\frac{\left(A+\frac{a}{2}\sin\phi\right)}{(A+a\sin\phi)} \quad 3\text{-}1$$

$$N_\theta = \frac{pa}{2} \quad 3\text{-}2$$

ϕ is postitve for the outer surface (from $0 \leq \phi \leq \pi$) and negative for the inner surface ($0 \geq \phi \geq \pi$). For the inner surface of the shell, the above expression for N_θ remains the same. However, N_ϕ becomes:

$$N_\phi = pa\frac{\left(A-\frac{a}{2}\sin\phi\right)}{(A-a\sin\phi)} \quad 3\text{-}3$$

Due to the change in curvature from positive to negative at locations of $\phi = 0$ and $\phi = \pi$, it is expected that bending will occur due to the breakdown of one of the governing assumptions of the membrane theory of shells. This is explained by term outside the square brackets the curvature as $\frac{1}{r_2}$ vanishing as r_2 jumps from $+\infty$ to $-\infty$ from the outer surface to the inner surface respectively, or can be described by a change in the shell curvature, which violates membrane theory. Membrane deformations at these locations confirm this breakdown of the membrane solution.

Enoma et al (2015) analytically solved the problem of circular toroids under hydrostatic pressure. In this case, the loading conditions were changed to account for the linearly varying hydrostatic pressure and boundary conditions were introduced at locations $\phi = \frac{\pi}{2}$ and $\phi = \frac{3\pi}{2}$. Due to the inclusion of boundary conditions, expressions for stress resultants vary, resulting in stress resultants in four different regions obtained. The equations are given below, where O refers to outer surface and i refers to the inner. Subscripts 1 and 2 refer to the region above and below the supports respectively:

$$(N_\phi)_1^O = \frac{\gamma a^2}{6\sin\phi(A+a\sin\phi)}[a(1+(-3+2\cos\phi)\cos^2\phi) - 3A(\phi+(-2+\cos\phi)\sin\phi)] \quad 3\text{-}4$$

$$(N_\theta)_1^O = \frac{\gamma a^2}{6\sin^2\phi}\left[4a(5+4\cos\phi)\sin^4\left(\frac{\phi}{2}\right) + 3A(\phi-\cos\phi\sin\phi)\right] \quad 3\text{-}5$$

$$(N_\phi)_2^O = \frac{\gamma a^2}{6\sin\phi(A+a\sin\phi)}[a(5+(-3+2\cos\phi)\cos^2\phi) - 3A(\pi-\phi-(-2+\cos\phi)\sin\phi)] \quad 3\text{-}6$$

$$(N_\theta)_2^O = \frac{-\gamma a^2}{12\sin^2\phi}[a(1+6\cos\phi+3\cos 2\phi-2\cos 3\phi) + 6A(\pi-\phi-\cos\phi\sin\phi)] \quad 3\text{-}7$$

$$(N_\phi)_1^i = \frac{\gamma a^2}{6\sin\phi(A-a\sin\phi)}[a(-1+2\cos\phi)(1+\cos\phi)^2 + 3A(\phi-\pi+(2+\cos\phi)\sin\phi)] \quad 3\text{-}8$$

$$(N_\theta)_1^i = \frac{\gamma a^2}{6\sin^2\phi}\left[4a(-5+4\cos\phi)\cos^4\left(\frac{\phi}{2}\right) + 3A(\pi-\phi-\cos\phi\sin\phi)\right] \quad 3\text{-}9$$

$$(N_\phi)_2^i = \frac{\gamma a^2}{6\sin\phi(A - a\sin\phi)}\left[a(-5 + (3 + 2\cos\phi)\cos^2\phi) + 3A(\phi + (2 + \cos\phi)\sin\phi)\right] \quad 3\text{-}10$$

$$(N_\theta)_1^i = \frac{-\gamma a^2}{12\sin^2\phi}\left[a(1 - 6\cos\phi + 3\cos 2\phi + 2\cos 3\phi) + 3A(-2\phi + \sin 2\phi)\right] \quad 3\text{-}11$$

From the above expressions, substitution of A=0 results in the membrane solutions and membrane deformations obtained by Zingoni (1997) for a spherical tank loaded hydrostatically, which confirm the validity of the above expressions. A numerical example is shown below for a steel circular toroidal shell with the following properties:

- Young's Modulus, E = 200 GPa
- Poisson's ratio, $\nu = 0.3$
- Constant thickness, t = 0.05m
- Mean radius, A = 30m
- Circular cross-sectional radius, a =15m
- Water with a unit weight, $\gamma = 10\text{kN/m}^3$

The stress resultants are shown over the domain $20° \leq \phi \leq 160°$, due to the poor approximation of the membrane stresses below $\phi = 20°$ and above $\phi = 160°$, as bending occurs at these locations due to the change of curvature of the torus.

As seen from Figure 3-2, for both the inner and outer surface, as the value of ϕ increases for values of $\phi < 90°$, the value of σ_ϕ and σ_θ both increase, indicating that the vessel is in tension from the apex to the location of the support. Discontinuities occur at locations of supports, whilst for the lower half of the tank, the value of σ_θ are in compression at the support and slowly become more tensile as ϕ goes to the bottom of the tank.

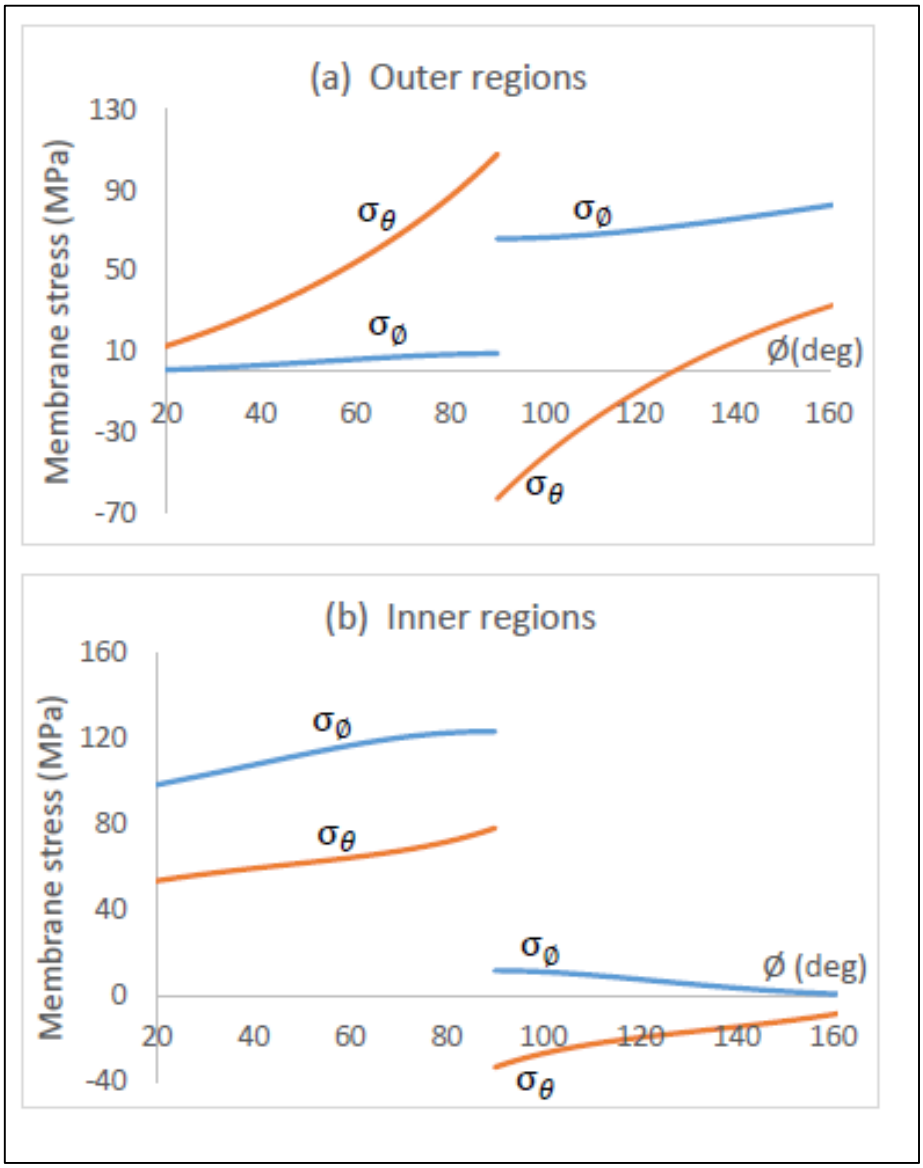

Figure 3-2: Membrane stress resultants for a hydrostatically loaded circular torus (Enoma et al, 2015)

Studies regarding the bending of pressurised toroidal shells have also been investigated, with Wissler (1916) was the first to give solutions to this singularity, by using the power series of $\lambda = \frac{A}{a}$ to the Reissner-Meissner equations of thin shells of revolution. For large

opening ratios, it was found that the series solution would converge rapidly, whilst slowly for smaller ratios. Consequently, it was mainly used for slender torus design, but not often used for engineering applications. Following this, Zhang (1944), obtained an asymptotic solution by using the Reissner-Meissner-Toelke thin shell equation given by:

$$\frac{d^2X}{ds^2} + (i\psi - \phi)X = \tau(s)\sqrt{\frac{r}{h}} \qquad 3\text{-}12$$

Which was transformed into the Bessel's equation:

$$\frac{d^2w}{dz^2} + \frac{1}{z}\frac{dw}{dz} + \left(1 - \frac{p^2}{z^2}\right)w = 0 \qquad 3\text{-}13$$

Where $p = \frac{1}{3}$, resulting in the following solution obtained:

$$w = {}_{\pm\phi}\, C_1 J_{\frac{1}{3}}\left(\pm\sqrt{\pm i}r\right) + {}_{\pm\phi} C_2 H^{(1)}_{\frac{1}{3}}\left(\pm\sqrt{\pm i}r\right) \qquad 3\text{-}14$$

$$r = \int_0^{\phi} \sqrt{\frac{\sin\phi}{1+\frac{\sin\phi}{\lambda}}|d\phi|} \qquad z = \pm\int_0^{\phi} \sqrt{\pm i\psi}|d\psi| \qquad X = \sqrt{\frac{z}{\sqrt{i\psi}}}w \qquad 3\text{-}15$$

According to Ren et al (1999), a few years later, Clark (1950), Novozhilov (1951) and Tumarkin (1959) developed, independent to each other, solutions for the aforementioned singularity, with the exception that instead of the λ used, the elastic bending theory of shells was used for values of μ, whereby $\mu = \frac{\sqrt{12(1-\nu^2)}a^2}{At}$. Large values of μ were used. From these two approaches, the power series was found to converge for large aspect ratios, whilst the asymptotic approach was found two converge for smaller aspect ratios. These approaches were used until Zhenhui (1986) developed a solution which he termed the approximated-asymptotic solution, which is valid for both large and small values of μ, expressed in terms of Airy functions.

These formulations were only first approximations to the homogenous solution. Ruojing (1990) expanded, giving results to higher approximations, whilst still ensuring the accuracy of thin shell theory. The expansions which were developed, were expressed in generalised Airy functions, eliminating the need of Bessel and or Airy functions for the homogenous solution and Lommel functions for the particular solution.

Sun (2010), noted that with these approximations, they were not in closed form, due to the complex governing equations involved. He focussed on slender toroidal shells, in which closed form solutions were obtained. The expressions are:

$$N_\phi = \frac{K}{a}\left(\frac{du}{d\phi} + w\right) \quad 3\text{-}16$$

$$N_\theta = \frac{\mu K}{a}\left(\frac{du}{d\phi} + w\right) \quad 3\text{-}17$$

Where K is the bending stiffness and u and w are given by:

$$u = C_5 \cos\phi + C_6 \sin\phi + \int_\phi p(\xi)\sin(\phi - \xi)d\xi \quad 3\text{-}18$$

$$w = \psi - \frac{du}{d\phi} = \frac{a^2}{K}\left[C_1 - \int_\phi q_1(\xi)d\xi\right] + C_5 \sin\phi - C_6 \cos\phi - \int_\phi p(\xi)\cos(\phi - \xi)d\xi$$

And constants of integration are to be solved using suitable boundary conditions. This was applied to thermal compensation devices. In doing so, a formula constructed by Dahl (1953) was corrected based on the given solution.

Whilst the above literature describes isotropic shells, orthotropic shells under axisymmetric loading have also been investigated when Dieker (1986) as cited by Ren et al. (1999) derived the basic equations using the theory of thin shells. Following which, solutions were obtained for complete toroidal shells under external pressure.

There have also been various nonlinear theories used for obtaining solutions to toroidal shells, with Sanders and Liepins (1963) obtained an asymptotic solution by using nonlinear membrane theory for an internally pressurised torus. The solutions obtained, were for use for a specific range of certain toroidal geometries. According to Ren et al (1999), Yi et al. (1988) used the perturbation method to obtain solutions for both the closed and open toroidal shells with the use of Fourier and power series respectively. Ren (1988) also similarly solved the problem, but obtained an asymptotic solution, assuming that the shells would undergo small deformations, but moderate rotations, similar to the solution obtained by Sanders and Liepins. This is shown by Figure 3-3

below which shows the accuracy of the nonlinear solution when compared to experimental and linear membrane theory respectively.

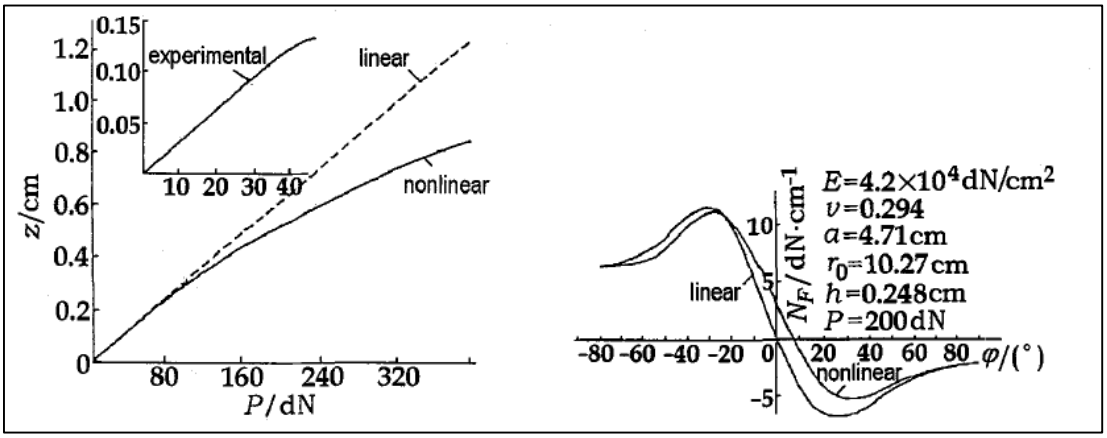

Figure 3-3: A comparison between a) an experimental test and theoretical formulation and b) between linear and nonlinear theory (Ren *et al*, 1988)

3.2.2 Elliptical toroidal shells

In order to properly characterise the elliptic toroid, the geometric aspects of an ellipsoid of revolution is first considered and then extended to the elliptic toroid. The following is adapted from Zingoni (1997). The ellipsoid of revolution is formed by rotating the meridian about the vertical y-axis. The typical cross-section for the aforementioned shell is depicted by Figure 10. It is given by the following equation:

$$\frac{x^2}{a^2}+\frac{y^2}{b^2}=1 \qquad 3\text{-}19$$

It can be seen that the vertical y-axis is the axis of revolution and the x-axis is horizontal and coincident with the meridian bisector and consequently the x-coordinate or a point on the elliptical cross-section is the radius R of a circle of latitude. The origin is taken as the intersection of the x and y axes, resulting in symmetry in both the vertical and horizontal planes. Let the semi major and semi minor axes be denoted by b and a respectively.

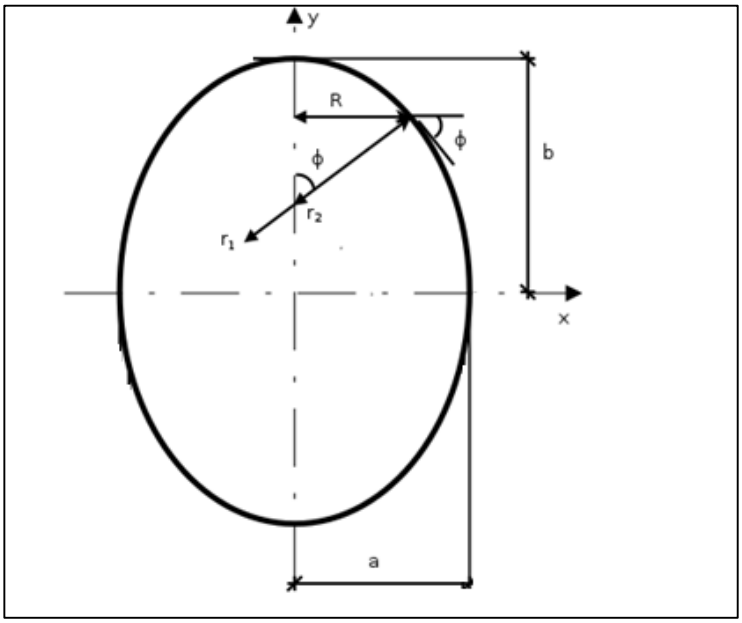

Figure 3-4: Geometry of an ellipsoid of revolution

r_1 is given by the following expression:

$$r_1 = \frac{\left[1+\left(\frac{dy}{dx}\right)^2\right]^{\frac{3}{2}}}{\frac{d^2y}{dx^2}} \quad 3\text{-}20$$

Whilst r_2 can be described as:

$$r_2 = \frac{R}{\sin\phi} = \frac{x}{\sin\phi} \quad 3\text{-}21$$

The coordinates and principal radii of the ellipsoid of revolution may be expressed in terms of the variable ϕ. Rearranging the equation of the meridian in terms of x and allowing y to be the subject of the formula results in:

$$y = \pm\frac{b}{a}\sqrt{a^2 - x^2} \quad 3\text{-}22$$

Differentiating the above equation with respect to x results in the following expression:

$$\frac{dy}{dx} = \pm\frac{b}{a}\frac{x}{\sqrt{a^2-x^2}} \quad 3\text{-}23$$

However, $\frac{dy}{dx}$ is defined in calculus as being the tangent to the meridian at the point in question, from which it is evident from Figure 3-4, the slope of this tangent can be expressed as $\tan\phi$, as ϕ is the angle between the tangent to the meridian and the direction of the x axis. Therefore:

$$\left(\frac{dy}{dx}\right)^2 = \tan^2\phi = \frac{b^2}{a^2}\left(\frac{x^2}{a^2-x^2}\right) \qquad 3\text{-}24$$

Rearranging this in terms of x yields:

$$x^2 = \frac{a^2\tan^4\phi}{b^2+a^2\tan^2\phi} \qquad 3\text{-}25$$

Which leads to:

$$x = \frac{a\tan^2\phi}{(a^2\sin^2\phi+b^2\cos^2\phi)^{\frac{1}{2}}} \qquad 3\text{-}26$$

Substituting this into the equation of the meridian gives y as:

$$y = \pm\frac{b^2\cos^2\phi}{(a^2\sin^2\phi+b^2\cos^2\phi)^{\frac{1}{2}}} \qquad 3\text{-}27$$

The second derivative of y in terms of x is given by:

$$\frac{d^2y}{dx^2} = \pm\frac{ab}{(a^2-x^2)^{\frac{3}{2}}} \qquad 3\text{-}28$$

Substitution of the first and second derivative into the radius of curvature expression yields:

$$r_1 = \frac{[a^2(a^2-x^2)+b^2x^2]^{\frac{3}{2}}}{a^4b} \qquad 3\text{-}29$$

And substitution of x into the above equation leads to the principal radii of curvature:

$$r_1 = \frac{a^2b^2}{(a^2\sin^2\phi+b^2\cos^2\phi)^{\frac{3}{2}}} \qquad 3\text{-}30$$

$$r_2 = \frac{x}{\sin\phi} = \frac{a^2}{(a^2\sin^2\phi+b^2\cos^2\phi)^{\frac{1}{2}}} \qquad 3\text{-}31$$

With the principal radii of curvature obtained, it can be applied to an elliptical torus. Figure 3-5 shows the geometry of an elliptic torus, where it can be observed that this shell of revolution is obtained by taking a closed ellipse and rotating the meridian around an axis of revolution.

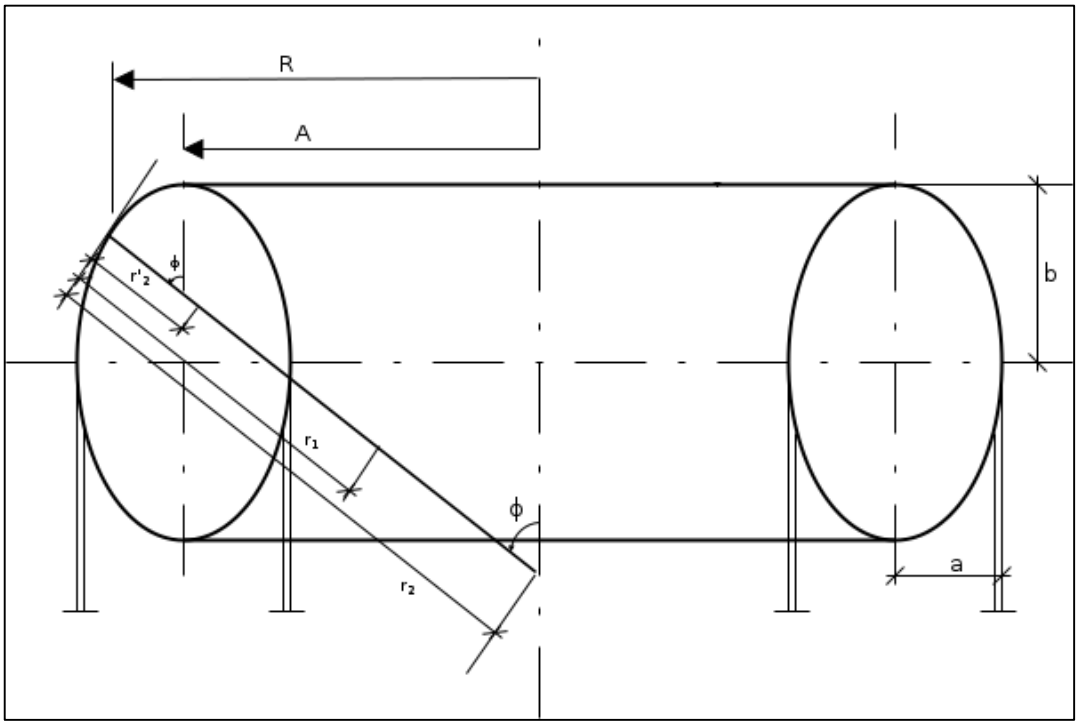

Figure 3-5: Geometry of an elliptic torus

The principal radii of curvature can be obtained from Equation 3-30 and Figure 3-5 as:

$$r_1 = \frac{a^2 b^2}{(a^2 \sin^2 \phi + b^2 \cos^2 \phi)^{\frac{3}{2}}} \quad 3\text{-}32$$

$$r_2 = \frac{A}{\sin \phi} + r_2' = \frac{A}{\sin \phi} + \frac{a^2}{(a^2 \sin^2 \phi + b^2 \cos^2 \phi)^{\frac{1}{2}}} \quad 3\text{-}33$$

Substitution of the above radii, along with $p_r = p$ for a constantly pressurised vessel into Equation 2-21 results in the following expressions:

$$N_\phi = \frac{pa^2}{(a^2\sin^2\phi + b^2\cos^2\phi)^{\frac{1}{2}}}\left[\frac{A(a^2\sin^2\phi + b^2\cos^2\phi)^{\frac{1}{2}} + \frac{a^2}{2}\sin\phi}{A(a^2\sin^2\phi + b^2\cos^2\phi)^{\frac{1}{2}} + a^2\sin\phi}\right] \quad 3\text{-}34$$

$$N_\theta = \frac{pa^2}{b}\left[A\left(\frac{b^2-a^2}{a^2}\right)\sin\phi + \frac{b^2 - \frac{1}{2}(a^2\sin^2\phi + b^2\cos^2\phi)}{(a^2\sin^2\phi + b^2\cos^2\phi)^{\frac{1}{2}}}\right] \quad 3\text{-}35$$

Substituting b=a into the above expressions gives the results for a circular torus, whilst substituting A=0, results in the stress resultants for an ellipsoid of revolution being obtained. As with the circular torus discussed earlier, when $\phi = 0°$ and $\phi = 180°$, a singularity in the solution is reached, with the membrane solution unable to fully capture the behaviour at this point of interest as bending will occur.

Sutcliffe (1971) solved the six first-order differential equations in order to obtain the stress and deflection distributions in internally pressurised elliptical and circular toroidal shells. From the results obtained, it was found that the maximum bending stress in an elliptical torus was substantially greater than those of circular toroidal shells.

Zingoni et al (2015) solved the equatorial bending of prolate elliptical toroidal shells by utilising a semi-elliptic toroid. Approximate bending solutions were obtained in regions adjacent to the horizontal equatorial plane. This was done by taking the semi-elliptic toroid and subjecting the edges by applying uniformly distributed bending moments and shear forces on both the inner and outer edges with an approximate solution to a fourth order differential equation derived from the Reissner-Meissner differential equations, utilising the rapid decay of edge effects and the slow change of curvature at equatorial regions of the toroid. The results were then verified by use of the finite element software, ABAQUS, whereby two noded-axisymmetric shell elements were used, with the difference between the derived and numerical results agreeing with each other, having an error of less than 1%. A sample comparison between the derived expression for a bending moment applied at the outer edge of the torus and the numerical results is shown for a semi-elliptical toroidal shell with the following parameters:

- a = 10m
- b = 20m
- A = 30m
- t = 0.05m

- E = 200 GPa
- $\nu = 0.3$

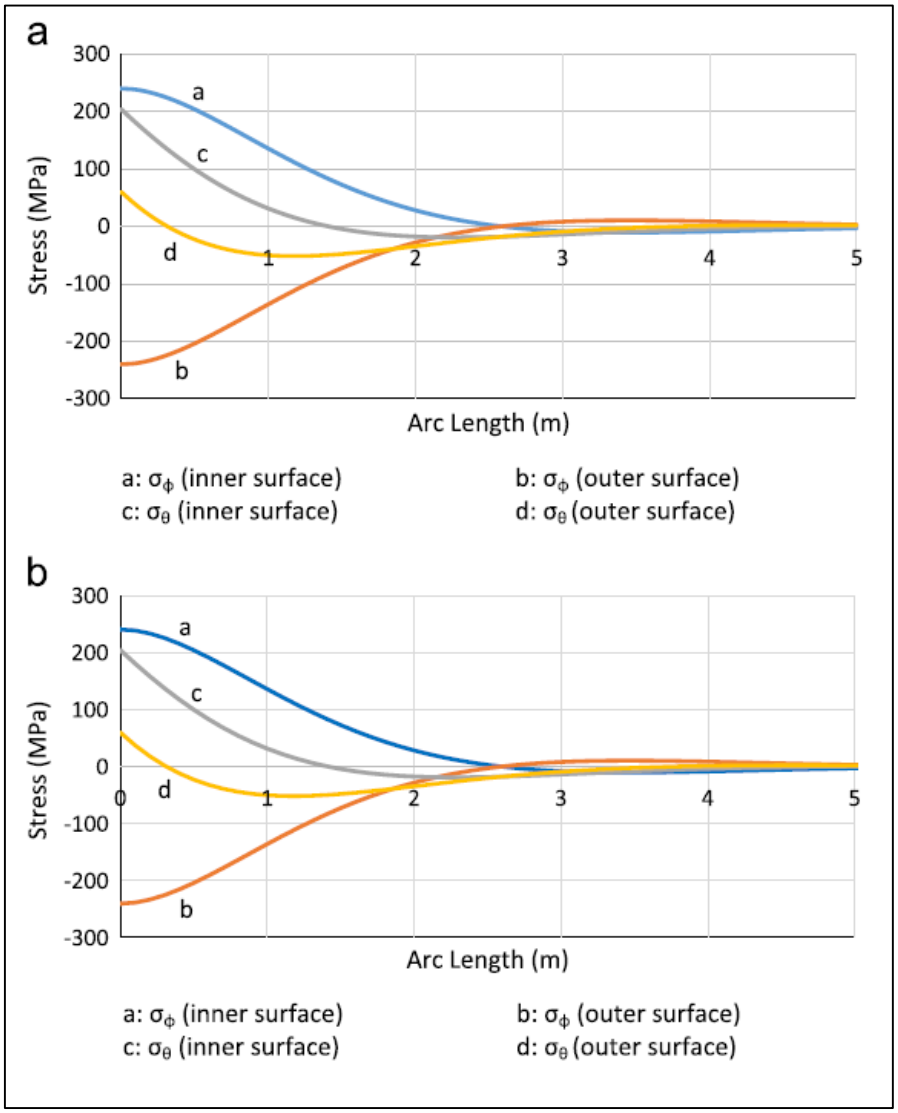

Figure 3-6: A comparison of a) analytical and b) numerical results for the derived expression for an application of a bending moment on the outer edge (Zingoni et al, 2015)

3.2.3 Stress analysis

Zhan and Redekop (2009), performed a stress analysis on metal toroidal tanks with a nozzle, with the intent for designing LPG tanks. These tanks, described as squarish are shown below. A finite element analysis was undertaken using ADINA to investigate the stress concentration around the nozzle. It was discovered that the stress concentration was higher if the nozzle was located at the intrados of the torus, in comparison to placing it at the extrados. The nozzle size and thickness was also investigated and it was concluded that the stress concentration varies largely with the nozzle size and nozzle thickness, compared to the nozzle length, which had little effect.

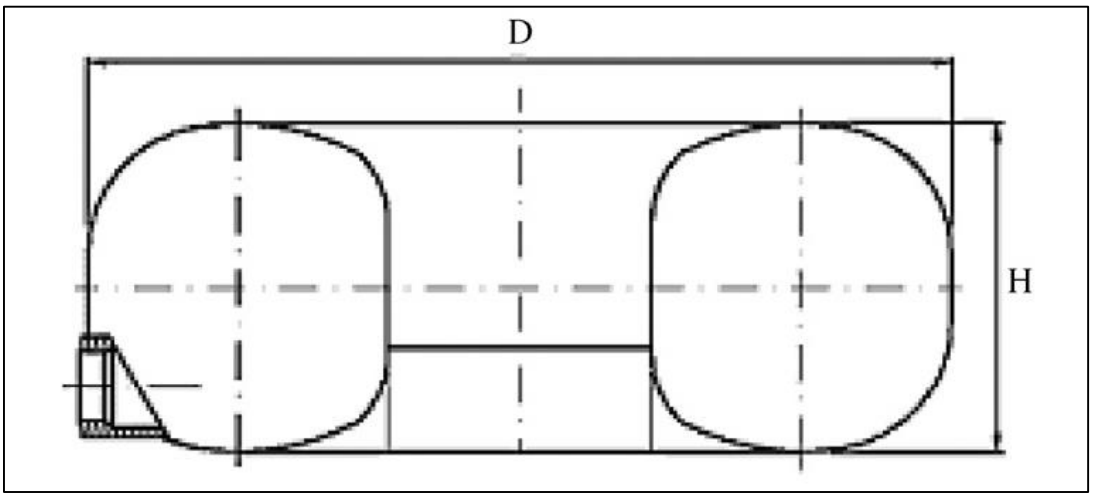

Figure 3-7: Squarish toroidal tank with nozzle (Zhan et al, 2008)

Similarly, Veličković (2007), performed a similar study, with a welded toroidal container used. In this investigation, it was not possible to obtain an analytical solution and a nonlinear finite element analysis was undertaken. The various stresses in each of the components comprising the toroidal container was obtained, whereby it was found that the maximum stresses and strains within the container occurred where the container fitting was welded. However, it was shown that the toroidal container could potentially be loaded with a greater pressure than was originally recommended.

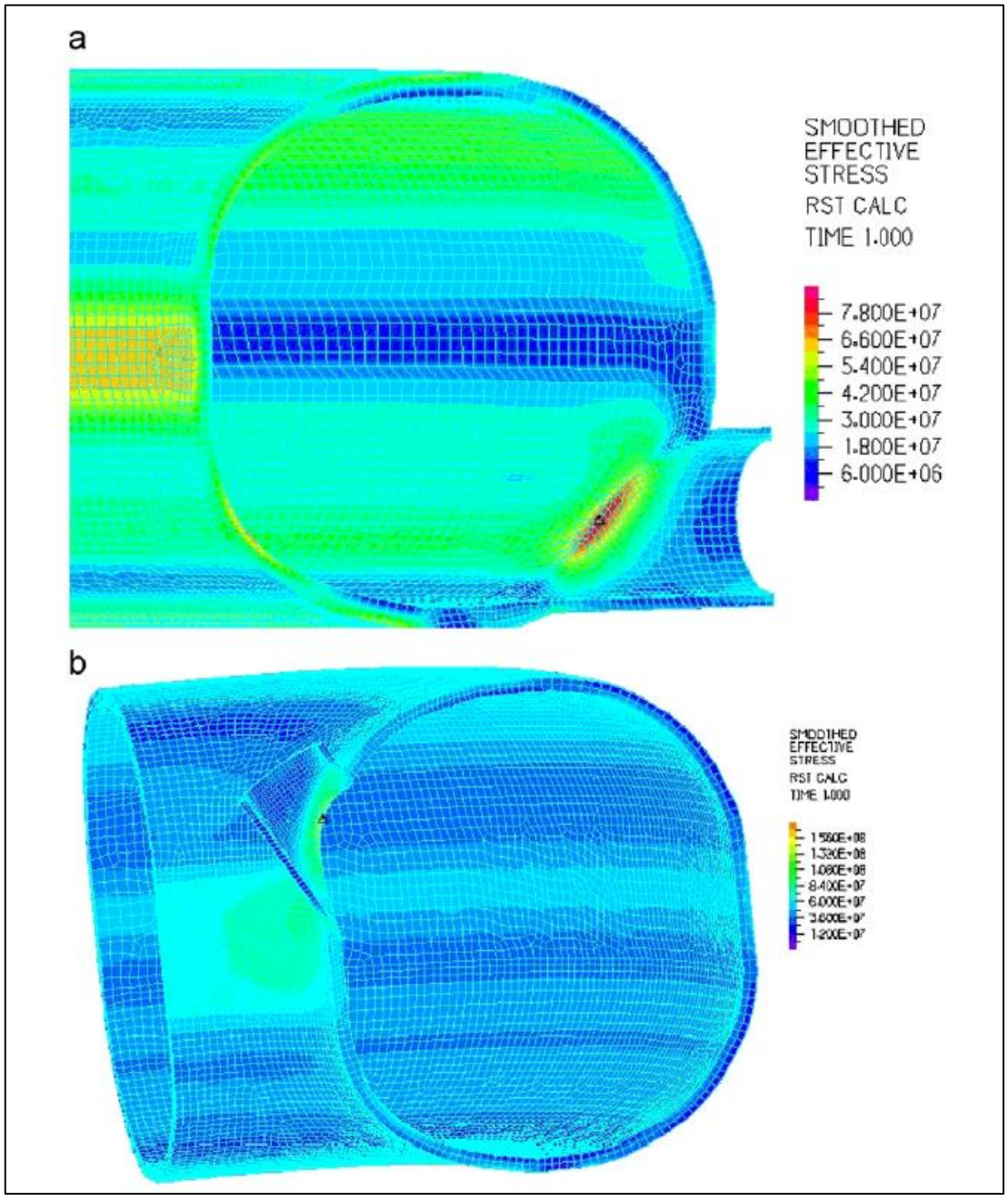

Figure 3-8: The effective stress at the surface of a squarish toroidal tank, with nozzle at (a) extrados and (b) intrados (Zhan *et al*, 2008)

3.2.4 Economical design

Assuming that designers fabricate toroidal shells out of sheet metal, the surface area and volume are essential characteristics which govern the amount of metal used and the volume capacity of the chosen shell. These expressions are well known from multivariate calculus and are given by the following equations for circular and elliptical toroids respectively.

The surface area for a circular torus is given by:

$$S = 4\pi^2 Aa \tag{3-36}$$

And volume:

$$V = 2\pi^2 Aa^2 \tag{3-37}$$

The expression for the surface area of an elliptical torus is:

$$S = 8\pi AaE(e) \tag{3-38}$$

Where $E(e)$ is known as a complete elliptic integral of the first kind and e, the eccentricity is given by:

$$e = \sqrt{1 - \frac{b}{a}} \tag{3-39}$$

The volume of an elliptical toroidal tank is given by:

$$V = 2\pi^2 Aab \tag{3-40}$$

Steele (1965) investigated the weight and volume for toroidal pressure vessels for circular and elliptic cross-sections. According to Vu (2010), Bogomol'nyi and Zhidyaev (1992) used these results to derive an analytical formula for a circular torus to minimise the weight involved.

Vu (2010) used differential equation and particle swarm methods to the design of minimum weight of toroidal shells for internally pressurised vessels and further expanded his research in 2013, by establishing optimum shapes for both elastic and

destruction states. In both of these papers, it was found that using the methods used, material savings in excess of 70% could be reached in certain arrangements.

3.3 Vibration of toroidal shells

Vibrations in toroidal shells will occur when the shell experiences a disturbance about its equilibrium point, resulting in oscillations occurring. There are two types of vibration: forced vibration, which occurs when the object is subjected to a particular frequency or force and free vibration, when an initial force is applied and the object is allowed to vibrate freely.

The free-vibration response of a structure is an imperative characteristic which is required when designing. If the natural frequency of an object is reached, a phenomenon known as resonance occurs, whereby the structure may sway and fail due to the increase in energy. The studies investigated below deal with the free vibration of toroidal shells.

Liepins (1965) was amongst the first to investigate the free vibrations of prestressed toroidal shells. In the investigation, linearised theories of vibrations were used. The finite difference method, along with Gaussian elimination was used to obtain the frequency equation in the form of a matrix from which, trial and error was used to solve the equations. It was found that under high prestressing conditions, the bending stiffness is an important consideration when dealing with vibration of toroidal shells and whilst when prestressing is small, the bending stiffness will increase the natural frequencies substantially. An interesting conclusion drawn from this paper deals with the singularity regarding membrane theory as explained in Section 3.2.1, as it was discovered that the mode shapes would be continuous around these regions where the membrane theory breaks down. Figure 3-9 shows the mode shapes for selected geometries.

Balders and Armenakas (1973) used the basis of the Love-Reissner shell theory to solve the problem of free vibrations for ring stiffened toroidal shells. From this investigation, it was shown that the natural frequencies would increase with an increasing thickness, similar to the findings from Liepins (1965) and a decrease in opening ratio. The effect of

the stiffeners was shown to increase the frequencies, especially for the case of smaller opening ratios.

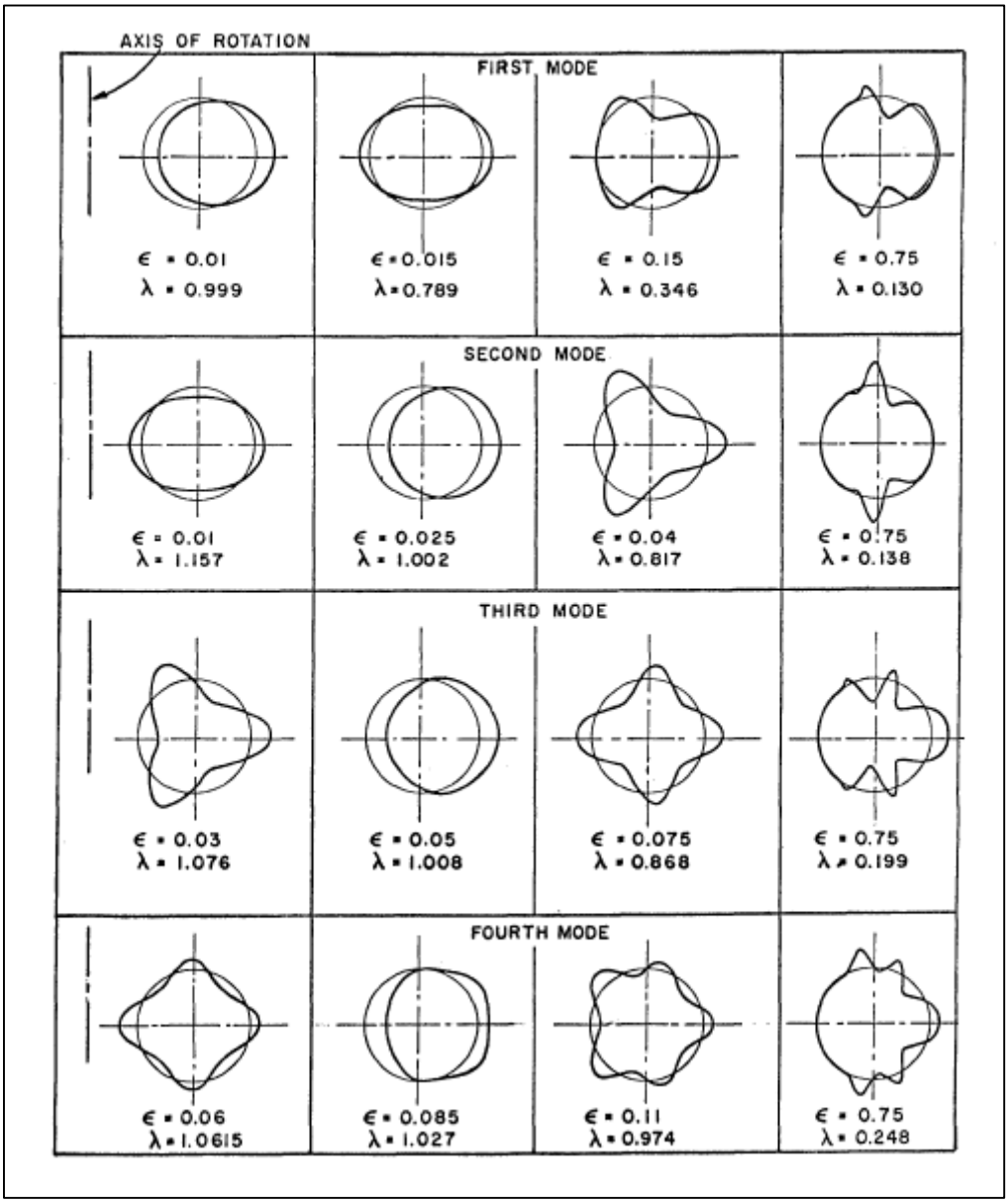

Figure 3-9: Axisymmetric mode shapes, t/R = 0.01 (Liepins, 1965)

Gavelya and Kononenko (1975) used toroidal shells with holes and calculated the natural frequencies and propagating waves by using special matrices, which belong to

the family of Green matrices. Although the method of initial perturbation was not used, it was noticed that the highest value if membrane stresses and moments reached, were obtained at the point of changing curvature, as already established extensively by membrane theory and Liepins (1965).

Kosawada et al (1985) used thin shell theory in order to analyse the natural frequencies of circular toroidal shells. Using the Lagrangian, the equations of motion were solved using a power series expansion and numerically solving the natural frequencies and corresponding mode shapes. Results which were obtained were then compared to Liepins (1965) and Balders and Armenakas (1973) and showed good agreement with the previous studies undertaken.

Whilst all previous studies until this point dealt with circular toroids, Yamada et al (1989) analysed elliptical toroids and their vibration characteristics. Both open and closed toroids were investigated. Using Love's first approximation theory, equations were derived and solved using the transfer matrix method, which proved to be an effective way of solving such problems. Results of the parametric study are shown by Figure 3-10.

Leung and Kwok (1994) obtained the free vibration of toroidal shells in the form of curved pipes using the dynamic stiffness method, where this method could potentially predict and infinite number of natural frequencies. The theory was modelled by the Donnel-Mushtari-Vlasov linear theory of thin shells. Fourier series were used in order to obtain an exact solution and results were numerically verified using the Galerkin method in FEM. Results which were obtained were accurate to those obtained by the numerical models and showed good promise for the use in free vibration studies.

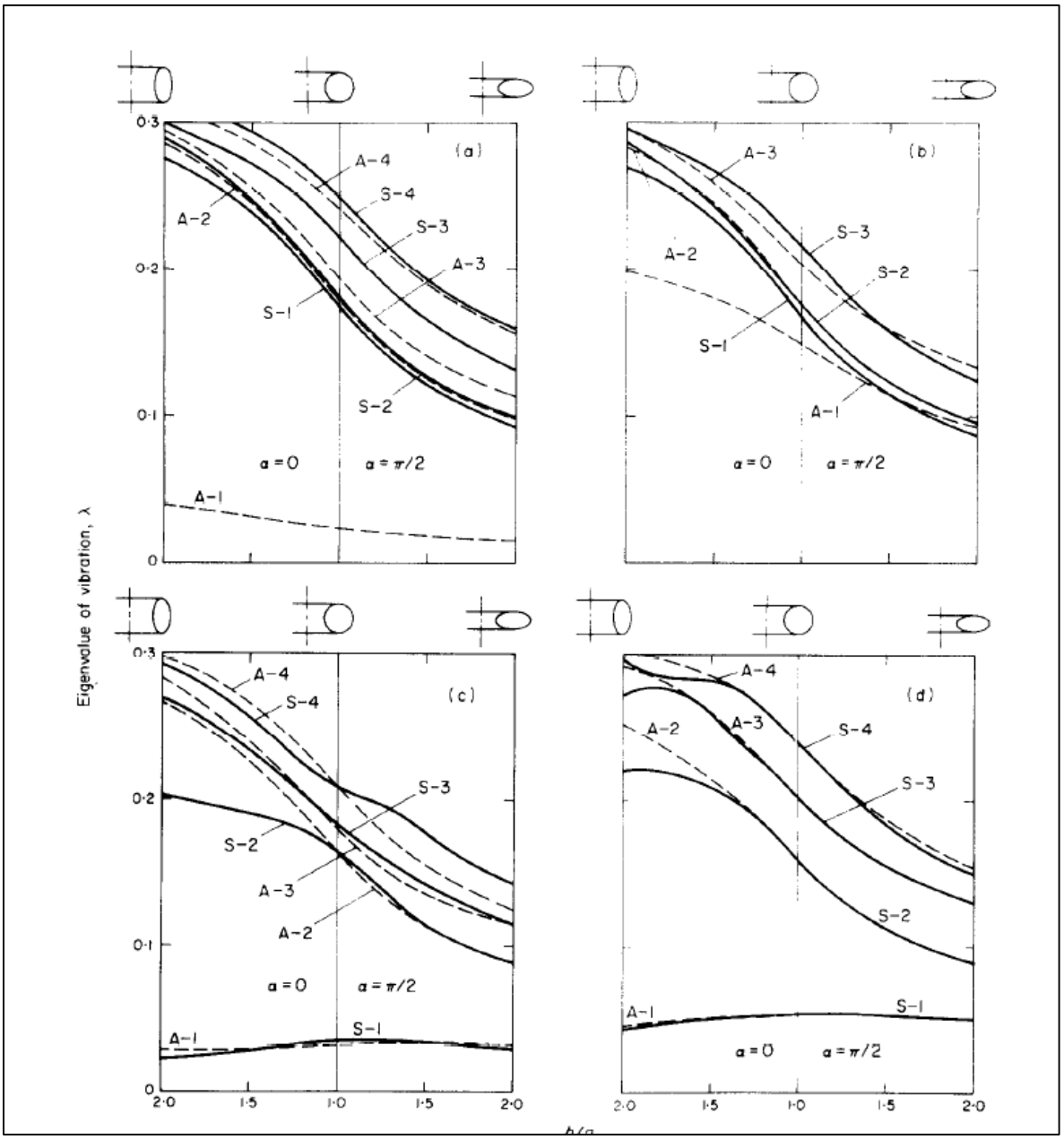

Figure 3-10: Eigenvalues of vibration of toroidal shells with closed elliptical cross-section with ν=0.3, R/A =2.5, t/R = 0.01, (a) n=0, (b) n=1; (c) n = 2; (d) n=3 (Yamada, 1989)

Ming et al (2001) investigated vibrations of elastic circular toroidal shells, by varying different boundary conditions. In this study, the linear Sanders thin shell theory was used. Beam and trigonometric functions were used to describe the motion and

deformation respectively and it was found that given the beam functions satisfying the boundary conditions, the natural frequencies and corresponding mode shapes could be successfully predicted. Results were then verified in ABAQUS, with good agreements occurring between the theory and numerical modelling. Support conditions investigated include simply supported and clamped ends, where it was found that for a simply supported toroidal shell, the lowest natural frequency obtained is due to symmetrical vibration whilst for clamped end conditions, the first few natural frequencies are obtained from antisymmetrical vibration.

Similarly, the linear elastic Sanders theory was used by Huang et al (1997) to obtain natural frequencies and mode shapes for curved pipes, modelled as incomplete toroidal shells. Solutions were verified by using the Mushtari-Vlasov-Donnel theory, as previously investigated by Redekop (1994), as similarly used by Leung and Kwok (1994). The results were then further verified with the use of the FEM software, ANSYS. Thereafter, a parametric study was undertaken, where frequencies and mode shapes are given for various geometries of 90° bends. Zheng and Zhang (2010) used linear Flugge thin shell theory to investigate the natural frequencies of elastic toroidal shells. It was found that in accordance with Ming et al (2001), as long as the circumferential modes were represented by trigonometric functions and meridional modes were represented by beam functions, results could be accurately obtained. This paper also investigated the effects of boundary conditions on the natural frequency, whereby it was found that, for fixed ends, natural frequencies were found to be higher.

Salley and Pan (2001) investigated the modal characteristics of curved pipes using toroidal surfaces. A parametric study was undertaken, using the commercial FEM software MSC/NASTRAN. Geometries which were chosen, were chosen to match industry norms and obtained results were verified by using experimental and numerical data. The bend angle of curved pipes was the focus of the investigation, where it was found that as the bend angle increases, each mode corresponds to a different mode shape. When the wall thickness was increased and reducing the bend radius, an increase in stiffness of modes was shown to occur.

Using the differential quadrature method (DQM), there have been various studies done involving vibration of toroidal shells. DQM is a method used whereby partial derivatives of a function with respect to coordinate direction are expressed as linear weighted sum of all the functional values at all mesh points along that particular direction, as explained by Jiang and Redekop (2002). Vibration investigations in this study were performed for isotropic and for orthotropic thin-walled circular toroidal shells. Results were verified using ADINA. Conclusions drawn from this study show that the DQM and finite element methods agree with each other as natural frequencies and mode shapes found have little error.

Wang (2004) used a variation of the Sanders linear elastic theory of shells, known as the Sanders-Budiansky shell theory, of which according to the author, is one of the best equations for describing the vibration of cylindrical shells. This was used in conjunction with DQM. Orthotropic thin shells were investigated and the effect of having completely free shells and the influence of circumferential line supports were investigated along with stiffening the toroidal shells with rings. Results were then verified using the finite element method, whereby it was found that the DQM method is suitable for use in the determination of vibration, as similarly noted by Jiang and Redekop (2002). It was also shown that the natural frequencies would increase for a toroidal shell that had more stiffeners.

Xu (1999) investigated the vibration of toroidal panels. In this investigation, panels were considered sectioned from various positions for toroidal shells and various methods of obtaining the natural frequencies were obtained. Methods employed were: using a Fourier series approach, the DQM and finite element method. It was found that the Fourier Series method was the most computationally efficient, but the formulation was difficult in comparison to FEM, which little formulation is required, but it took a longer time to compute. A parametric study was undertaken, varying the thickness and boundary conditions, where it was found that decreasing the panel thickness results in lower frequencies obtained, whilst relaxing the boundary conditions results in lower frequencies and changes in mode shapes.

Buchanan and Liu (2005) performed an analysis of the free vibration of thick walled isotopic toroidal shells, whereby the equations of motion and strain displacement equations were derived using toroidal coordinates shown by Figure 3-12. From the

three dimensional equations, assumptions were made in order to reduce the equations to an axisymmetric format, whilst still keeping a three dimensional character of the solution. Following which, this was incorporated into a finite element model and results were verified with previous studies.

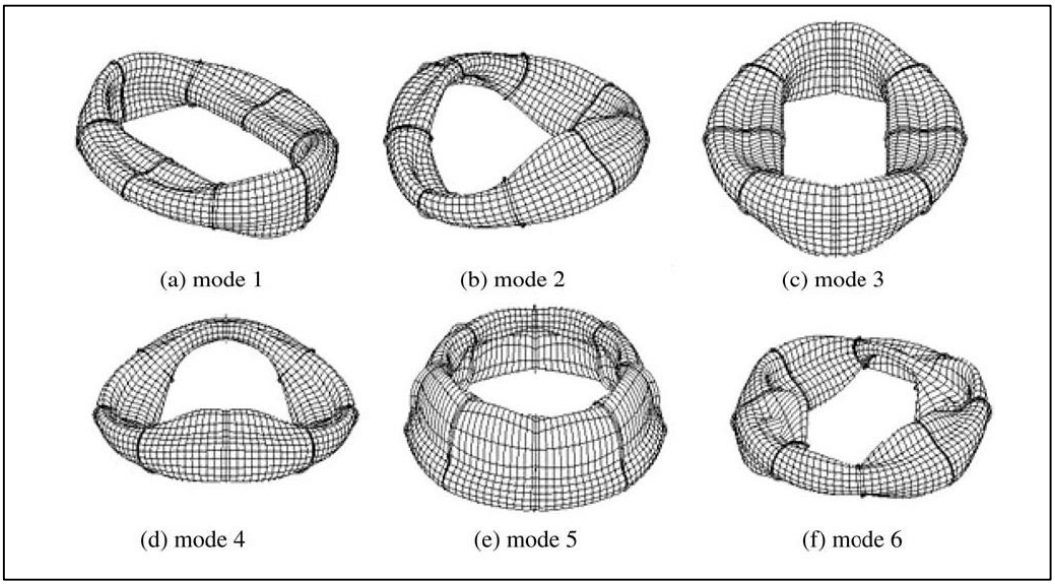

Figure 3-11: Vibration mode shapes for a shell stiffened with 8 rings
(Wang, 2006)

Zhan and Redekop (2008), based on their ovaloid tanks shown above also investigated the free vibration using ADINA. It was shown that from thicknesses, boundary conditions and various materials used for toroidal LPG tanks, that the boundary conditions have the greatest effect on the natural frequency obtained. It was recommended that supports on the inner equator (where $= -\frac{\pi}{2}$) correspond to the lowest natural frequency.

Zhou et al (2010) looked at three-dimensional vibrations of hollow elastic toroidal shells using the variational Ritz procedure, formulating in toroidal coordinates as opposed to polar coordinates and derived equations to calculate natural frequencies. The torus radius ratio and the cross sectional ratio were varied, where it was found that when the

torus radius ratio is varied, the natural frequency is smaller for smaller torus radius ratios.

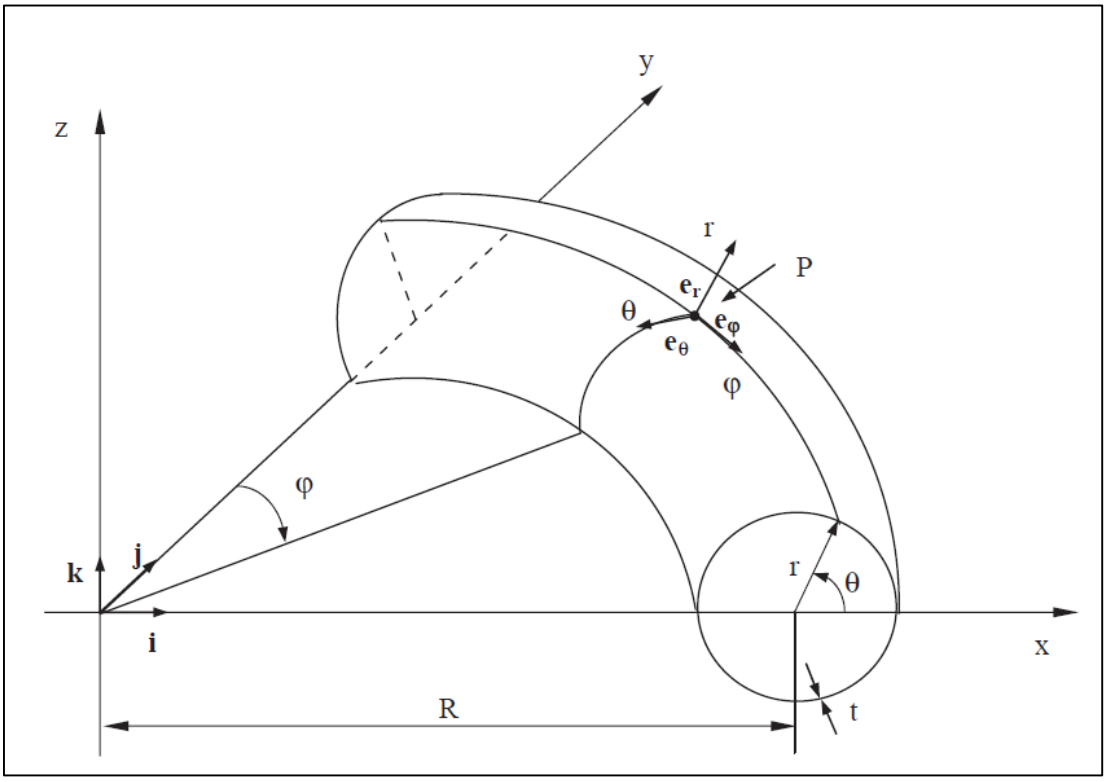

Figure 3-12: Toroidal coordinates (Buchanan and Liu, 2005)

Wang (2011) continued with previous research into vibration of toroidal shells by investigating the natural frequencies of moderately thick and thick toroidal shells. As thin shell theory was not valid, the Timoshenko-Midlin shell theory was used as a method of formulating the vibration equations. This was done due to the inclusion of shear deformation within this theory. Following this, as was done in their 2004 study, the DQM method was used to obtain results. It is interesting to note that this study used shear deformation theory to obtain their results and the results obtained were in agreement with previous studies undertaken.

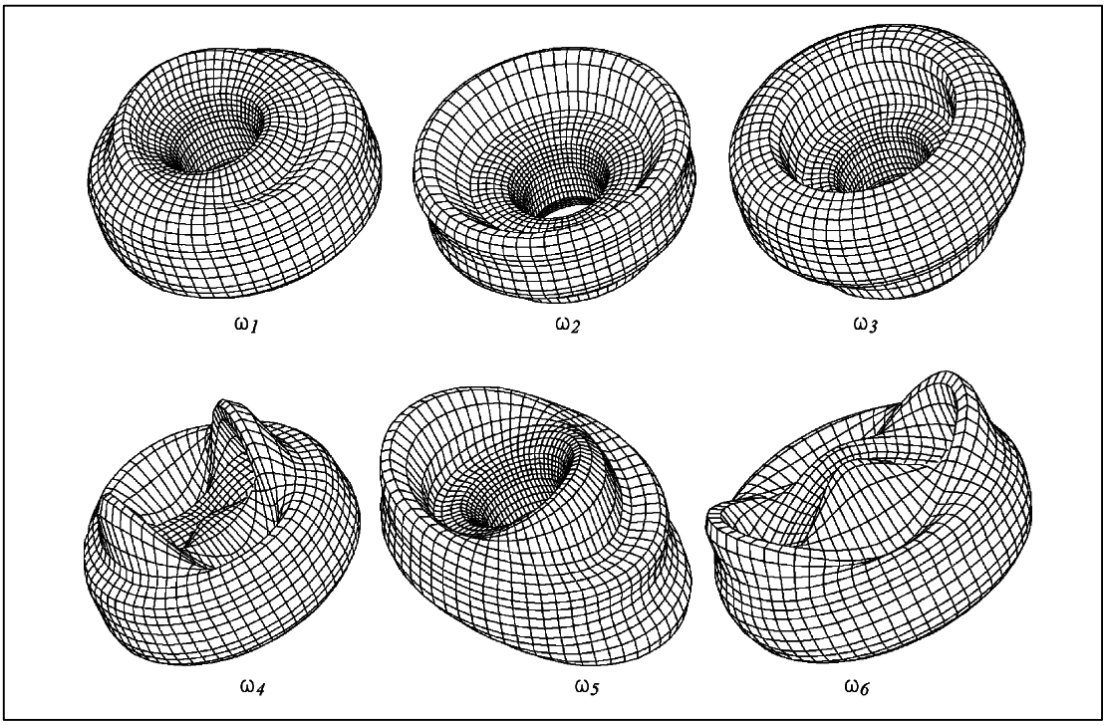

Figure 3-13: Vibration mode shapes for an ovaloid toroidal tank (Zhan et al, 2007)

Tizzi (2015) performed a free vibration analysis of toroidal shells in free space, with the intent of possible future space stations and space applications utilising toroidal shells. Thin shell theory was used in the formulation of the derived equations, but included in this were transverse shear terms. Due to the unique application, multilayer composite angle-ply laminate, with a non-uniform thickness was the material used in this investigation. Using the Rayleigh-Ritz method, the generalised eigenvalue problem was solved and results were verified using Wang and Redekop (2004) and Ming et al (2001).

3.4 Buckling of toroidal shells

Stresses resulting in toroidal shells can either be classified as bending or membrane as discussed above. However, the membrane stiffness is more often than not far greater than the bending stiffness, allowing the shell to absorb a larger amount of membrane

strain energy, than it can bending strain energy. Consequently, if there are compressive stresses throughout the shell resulting in membrane strain energy and there is a path available to convert the membrane strain energy to bending strain energy, buckling will occur.

Buckling is also an essential aspect to consider when designing toroidal shells as it generally occurs with little prior indication and extents of the associated damage may be extremely severe. A comprehensive static analysis will help identify the critical areas of buckling, as buckling will occur around locations of high compressive stress. Studies reviewed in this section are categorised into buckling investigations undertaken for external and internal loading respectively.

3.4.1 External pressure

External pressure is widely regarded as the more likely applied loading which could cause buckling within toroidal shells. Sobel and Flugge (1967) explain that when their investigation was done, very little research had been undertaken on shells of revolution which had a varying Gaussian curvature. According to them and Ren et al (1999), Machnig (1963) was the first to successfully investigate buckling of toroidal shells. In his study, buckling of both axisymmetric and asymmetrical modes were studied and it was concluded that axisymmetric buckling modes would give the more critical pressure. The method in which the solutions was obtained used a perturbation technique to solve a system of equations. Furthermore, Sobel and Flugge (1967) state that Koiter (1964) reviewed this investigation and commented that power series expansion which was used would break down for toroidal shells for shells with small opening ratios.

Sobel and Flugge (1967) were the first to solve the stability problem for toroidal shells experiencing uniform external pressure. This paper is considered to be one of the seminal works in the stability of toroidal shells. The equations of buckling were solved with the use of series expansions, occurring in both the meridional and circumferential directions, essentially utilising a precritical membrane state. Equations were solved for both symmetric and axisymmetric modes and a parametric study was performed, with reasonable toroidal geometries investigated. Figure 3-15 shows the design curves illustrated in their study.

At the same time, Hutchinson (1967) investigated the post-buckling behaviour of toroidal shell segments, varying different loading conditions applied. Koiter's general theory of initial post buckling behaviour was used as the basis of the derived solution, where the results are based on linear buckling analyses. In their study, it was found that similarly to classic buckling, the post buckling behaviour and imperfections encountered were strongly dependent on the principal radii of curvature. However, due to the changing curvature of toroidal shells, surfaces which correspond to anticlastic and synclastic surfaces were considered separately.

Fishlowitz (1970) who was one of the first to perform an experimental investigation into the buckling of toroidal shells. 8 toroidal shells were constructed using a plastic material consisting of Versamid 140 resin and Epon 828 resin, with a Young's modulus of approximately 314000 psi (2.1×10^6 Pa). The shells which were fabricated were of a wide variety geometrically. Once results were obtained, they were compared to the previous work investigated by Sobel and Flugge and Bushnell, where it was found that the Bushnell analysis was in favour of the experimental results, whilst the Sobel and Flugge analysis only agreed with half of the shells. Figures from left to right show the deformation from the original shape to collapse.

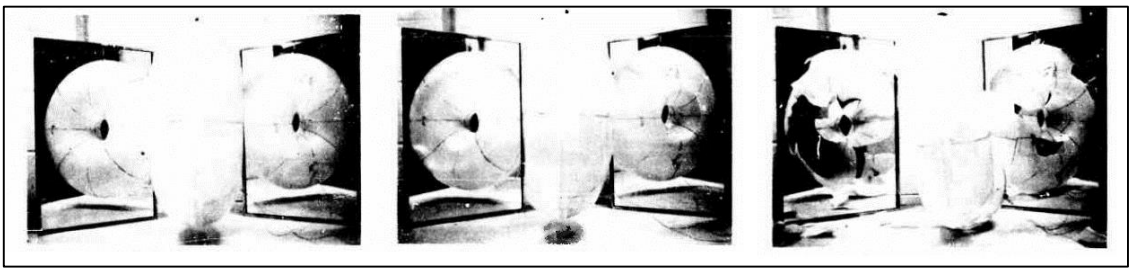

Figure 3-14: Buckling of a toroidal shell under external pressure (Fishlowitz, 1970)

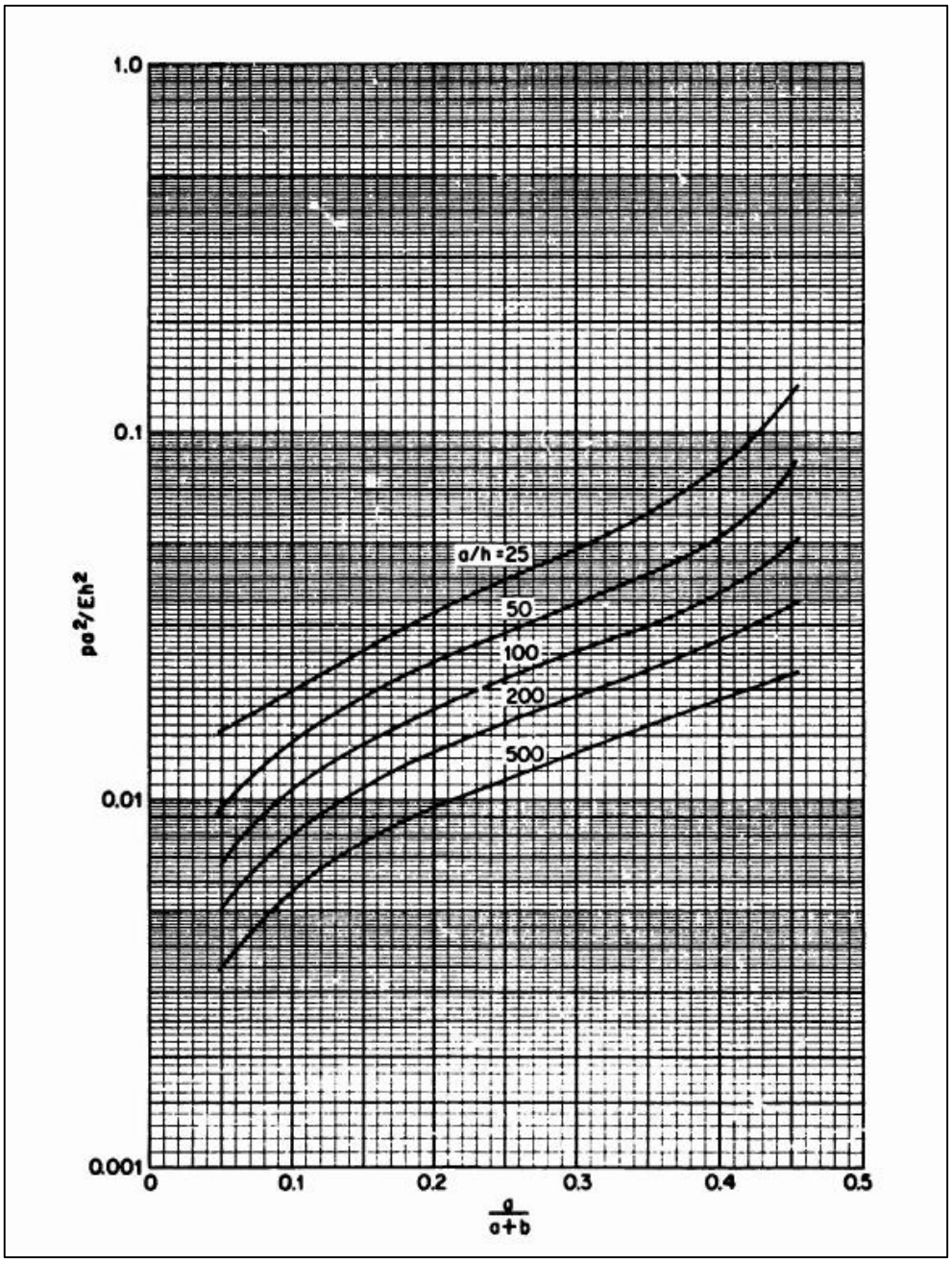

Figure 3-15: Buckling coefficients for toroidal shells under uniform external pressure (Sobel and Flugge, 1967)

Galletly and Galletly (1996) used BOSOR5, the shell buckling program based on variational differences to investigate buckling of complex toroidal shells. The application

researched was a series of submersible pipes containing gaseous oxygen. Various configurations of toroidal pipes were considered with external pressure on the surface in addition to the axial load caused at the connection of segments. The results obtained were compared by the use of the following expression:

$$p_{cr} = 0.92E\left(\frac{1}{L}\right)\left(\frac{t}{R_c}\right)^{\frac{3}{2}} \quad 3\text{-}41$$

Which represents the buckling pressure when the ends of a cylindrical shell are simply supported. It was found that the results were conservative, as the above expression gave calculations which were approximately three-quarters of the numerical pressures.

Blachut and Jaiswal (2000) further expanded on investigating the buckling effects of externally pressurised toroidal shells and studied the buckling resistance of geometrically perfect and imperfect complete steel toroidal shells. A parametric study was done, varying over a range of geometries, boundary conditions and material properties and both elliptical and circular toroidal shells were investigated. ABAQUS was used to numerically model the various shells. It was found that elliptical shells will potentially be stronger than their circular counterparts the geometry with the largest load carrying capacity was identified. With regards to imperfections in toroidal shells, it was shown that the buckling pressure for such a case would be sensitive to the presence of any imperfection. This work was then expanded on, as Blachut (2004) undertook another parametric study, although with the exception of composite toroidal pressure hells being tested. The material used was a carbon fibre reinforced plastic (CFRP) whereby it was shown that decreasing the aspect ratio from prolate to oblate elliptic toroidal shells corresponds to a decrease in buckling pressure.

Wang et al (2006) ADINA to investigate the buckling pressures of stiffened toroidal shells. In this study, meridional ring stiffeners and equatorial lines of supports were varied. Results presented show that the influence of buckling firstly increases the buckling pressure in comparison to unstiffened toroidal shells and furthermore, it is preferable to use a more “light” rings than a fewer amount of “heavy” rings. Lastly, it was shown that using either inner or outer line supports will alter the buckling pressures experienced.

3.4.2 Internal pressure

Galletly (1998) explains that buckling of toroidal shells due to internal pressure is a very rare case indeed. It was thought to be just a theory, until in 1956, an internally pressurised torisphere based in the United States had failed, due to at the time unknown reasons. Once it was examined, it was concluded that elastic buckling due to internal pressure was the cause of failure and this was further confirmed by experimental results. Following this, studies were undertaken involving the stability of toroidal shells due to internal pressure. Galletly (1998), due to the lack of experimental data available, created numerical models in order to solve the problem of elastic buckling of ordinary steel elliptical toroidal shells. Two independent shell buckling programs, BOSOR5 and INCA were used to model the torus and associated internal pressure. A variety of geometries were investigated and a parametric study varies the aspect ratio, the thickness and the ratio of minor and major axes of mostly prolate elliptical toroidal shells. Included in this were circular toroidal shells, where no buckling was found, due to hoop strains being tensile. As expected it was shown that as the elliptical cross-section becomes slenderer, the buckling pressure experienced would decrease. A sample curve from this investigation is shown by Figure 3-16, where k is defined as the aspect ratio.

Combescure and Galletly (1999) further extended the previous study by examining the plastic buckling of internally pressurised elliptical toroidal shells. The same methodology as applied in their previous investigation was employed, where it was found that for more circular prolate toroids, the plastic buckling pressures were substantially lower, but as the torus became slenderer, with the aspect ratio was equal to 2.5, the plastic and elastic buckling pressure experienced were approximately the same. Also investigated were the effects due to initial imperfections, where it was shown that for internally pressurised elliptic toroidal shells, the presence of imperfections has no effect on the bucking pressure.

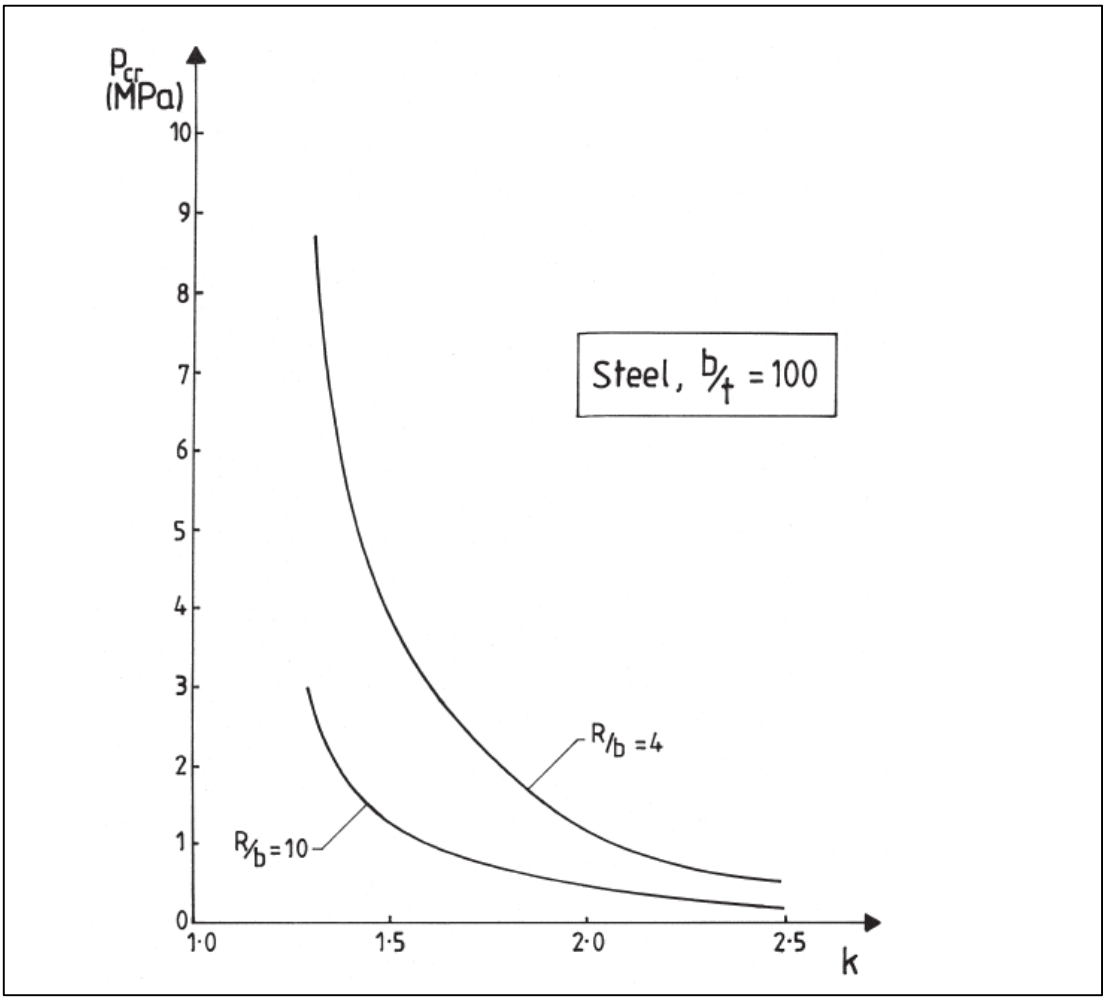

Figure 3-16: Internal buckling pressure for steel toroids (Galletly, 1999).

Whilst the previous studies investigated pressure, Redekop et al (1999) examined the stability of a toroidal shell subjected to fluid loading. The Budiansky shell stability theory was applied and extended to toroidal coordinates and developed using the DQM. Results were compared with FEM analyses of the same problem and the applicability of the DQM, as with vibration, was shown to be an efficient way of calculating buckling pressures. A similar study was undertaken by Redekop (2005), with the DQM and Budiansky shell theory used to determine the buckling pressure of orthotropic thin

circular toroidal shells. The modulus ratio, E_1/E_2 was shown to influence the buckling pressures considerably in comparison to changing the boundary conditions.

Zhan and Redekop (2008), as mentioned above, also investigated the buckling and collapse or ovaloid toroidal tanks. Various shell sizes, thicknesses, materials and support conditions were varied and simulations were done using ADINA. Calibration of the model was achieved using the results achieved by Galletly (1998). Results obtained indicate that increasing the thickness of the toroidal tanks results in higher buckling pressures achieved and the relationship was nonlinear between thickness and pressures. When boundary conditions were varied, it was shown that the location of boundary conditions had little effect on buckling pressure. This is in contrast with the vibration of the same tank, where it was shown that the boundary conditions have the greatest effect on the buckling pressures obtained.

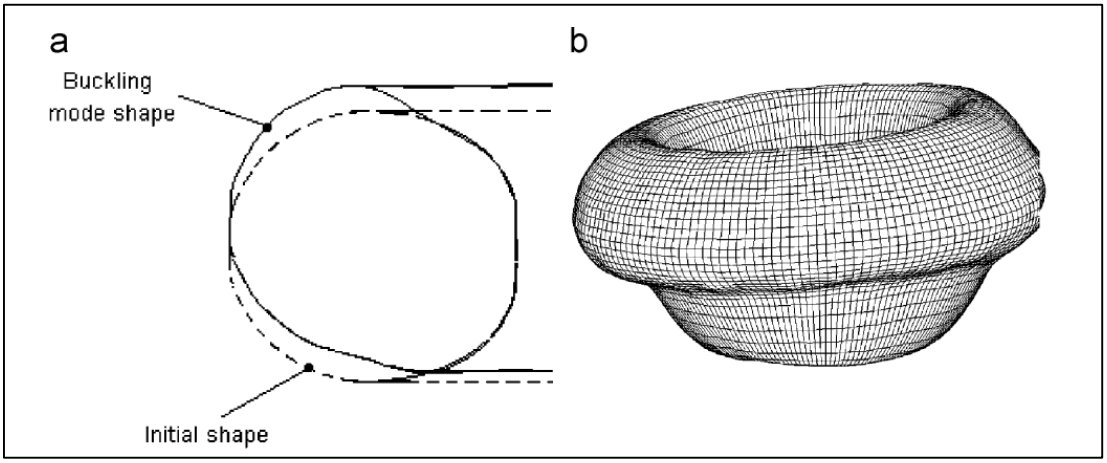

Figure 3-17: Buckling of an ovaloid tank (a) cross-sectional view and (b) mode shape (Zhan & Redekop, 2008)

3.5 Statement and scope of research

This literature review has covered the statics, dynamics and stability of both circular and elliptical toroidal shells. Emphasis has been placed on the static analysis, where derivation and application of membrane theory has been shown.

The summary of the previous research reviewed shows that the statics, dynamics and stability of toroidal shells has primarily been focussed on pressurised vessels. However, a recent paper from Enoma et al (2015), shows that there is much more research to be done in investigating the potential of toroidal shells as a means for liquid containment.

This study explores the membrane stresses of both elliptical and circular toroidal shells, loaded hydrostatically. Owing to the complex geometry of toroidal shells, the aspect and opening ratios of prolate, oblate and circular toroidal shells are varied. The findings of this research aim to provide structural designers with expressions to calculate the membrane stresses and to design toroidal tanks to their specifications.

3.6 Objectives of this investigation

The objectives of this research are as follows:

- To derive expressions for the meridional and hoop stress resultants for elliptical toroidal shells
- To investigate the sensitivity of the membrane stress resultants to a change in the aspect and opening ratio for circular and elliptical toroidal shells
- To give practical recommendations to designers for a range of toroidal shells

3.7 Research methodology

Toroidal shell structures have a complex geometry associated with them, due to the number of variables involved. The membrane stress expressions, apart from providing an indication of the location of membrane stresses, may be used in future studies to obtain approximate solutions, along with various other applications. The procedure followed in this investigation is as follows:

- The expressions are to be derived using the equations for membrane theory, once the necessary geometric and loading preliminaries have been determined.

- The derived expressions will then be verified using the finite element analysis software ADINA, where both meridional and hoop stresses can be validated for accuracy.

- Once the expressions have been verified, a parametric study examining the membrane stresses for prolate, oblate and circular toroidal shells, where the expression has already been derived by Enoma et al (2015), will be investigated.

- Numerical comparisons for practical sizes of hydrostatically loaded toroidal shells will be compared and practical recommendations given.

Chapter 4

The finite element method

4.1 Introduction to the finite element method

The finite element method at its core, is simply the approximation of a differential equation. Consequently, it is a method of analysis, with many ranges spanning over numerous fields. In its simplest form, it is a region described as a continuum where it is discretized into smaller, specified geometric shapes which are known as “elements” (Govender, 2013). Each of these elements is interconnected by nodes, which exist on the vertices of each element. Relevant data is inputted to construct the model which leads to a set of equations. As these equations are then solved, various outputs are given by the approximations at each node.

In finite element analysis, there are three stages: pre-processing, processing or analysis and post-processing.

In pre-processing, a model is constructed where the object is defined, along with loading and geometric preliminaries. However, with the advent of CAD, geometrical aspects of finite element models may be constructed externally and imported into the relevant software.

The processing, or analysis phase, is where the model created in the pre-processing phase is solved. This is done by solving a system of equations which may vary, depending on the desired result and application.

The final stage is the post-processing phase. In post-processing, the various results are now presented. These results are application dependent and can vary from stress distributions to modal shapes. Roylance (2001) indicates that in the infancy of FEA, the results would be reams of paper with various values, but with the advent of commercial software and enhanced graphic capabilities, visual results are often shown.

4.2 Basic finite element formulation

A good example to illustrate the finite element problem is shown by the 1D elastic bar as follows. The well-known example is taken from Fish and Belytschko (2007), using the Galerkin Method. An overview of the formulation is as follows:

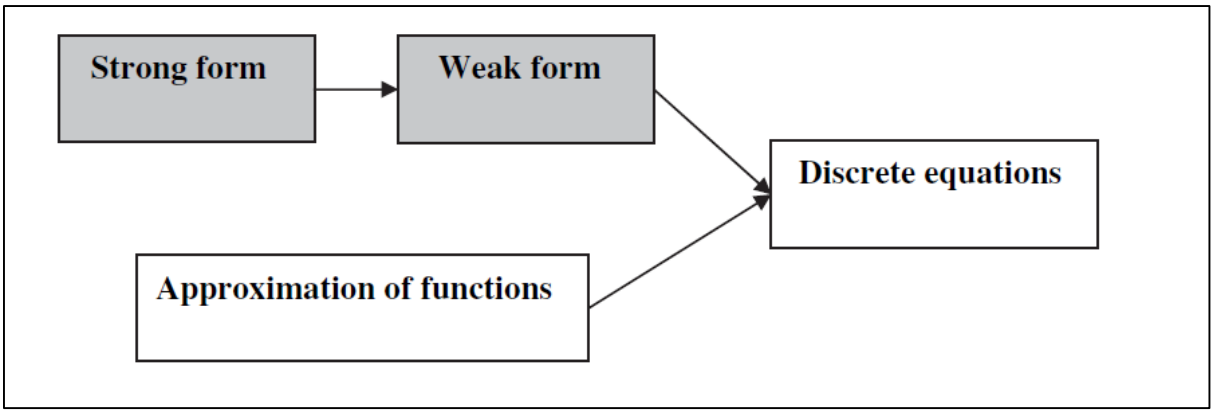

Figure 4-1: An overview of the finite element formulation (As adapted from Fish and Belytschko, 2007)

4.2.1 Strong form

The strong form, which is comprised of the governing equations for the model, for a one-dimensional elastic bar is derived as follows:

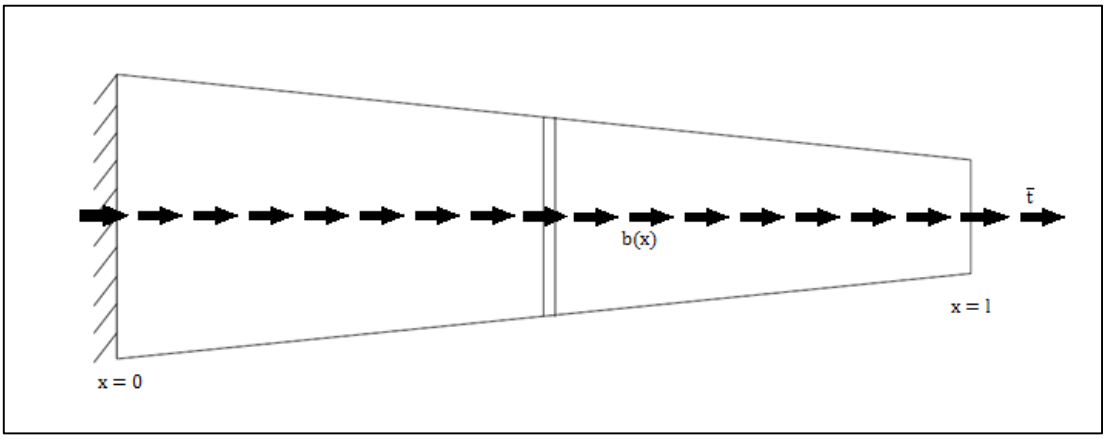

Figure 4-2: A 1D elastic bar

Consider a one-dimensional linear elastic bar, with a variable cross-section fixed at one end and prescribed loads applied at the ends of the bar, whereby the aim is to find the stress, $\sigma(x)$ and displacement, $u(x)$, as a result from the strain, $\varepsilon(x)$. The bar is also subjected to a body force denoted by $b(x)$.

The following assumptions are made:

1. The bar must be in static equilibrium
2. The bar obeys Hooke's law
3. The displacement field must be compatible
4. It must satisfy the strain-displacement equation

In order to obtain the governing differential equation, a slice is taken on a segment of the bar:

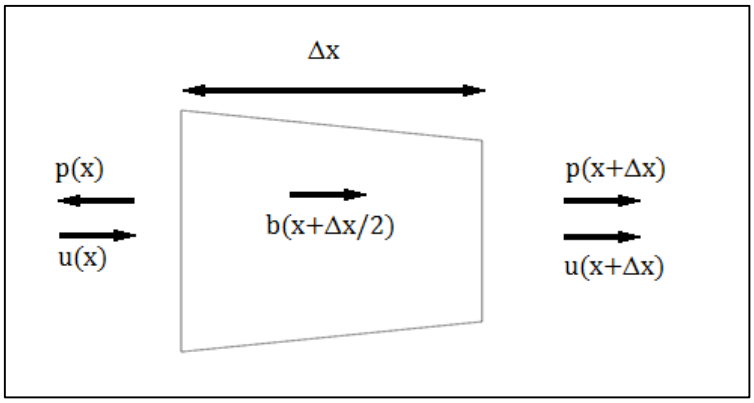

Figure 4-3: A slice of the 1D elastic bar

Summing the forces on the bar and dividing by Δx, the following is obtained:

$$\frac{p(x+\Delta x)-p(x)}{\Delta x} + b(x+\frac{x}{2}) = 0 \qquad 4\text{-}1$$

Applying the limit as $\Delta x \to 0$, it results in the following equation:

$$\frac{dp(x)}{dx} + b(x) = 0 \qquad 4\text{-}2$$

Making use of the definitions of stress, strain and Hooke's law:

$$\sigma(x) = \frac{p(x)}{A(x)}, \qquad \varepsilon(x) = \frac{du}{dx} \qquad \text{and} \qquad \sigma(x) = E(x)\varepsilon(x)$$

And substituting the relationships into Equation 4-1 gives:

$$\frac{d}{dx}\left(AE\frac{du}{dx}\right) + b = 0, \qquad 0 < x < l \qquad 4\text{-}3$$

However, this second-order ordinary differential equation needs boundary conditions to be solved which, for this example are:

$$\sigma(l) = \left(E\frac{du}{dx}\right)_{x=l} = t \quad \& \qquad u(0) = 0$$

4.2.2 Weak form

The weak form is an alternate configuration of the strong form in integral form, whereby the governing conditions are "relaxed" in order to solve the problem. The weak form

makes use of the test function, $w(x)$, from which a trial solution, which Fish and Belytchko (2007) define as "a set of admissible solutions that satisfy certain conditions", may be formulated.

Taking the governing equations and traction boundary condition, multiplying it by the test function and integrating over the domain results in the following equations:

$$\int_0^l w\left[\frac{d}{dx}\left(AE\frac{du}{dx}\right)+b\right]dx = 0 \qquad \forall w,$$
$$\left(wA\left(E\frac{du}{dx}-\bar{t}\right)\right)_{x=l} = 0 \qquad \forall w \tag{4-4}$$

Applying integration by parts to Equation 4-4 gives:

$$wAE\frac{\mathrm{du}}{\mathrm{dx}}\Big|_0^l - \int_0^l \frac{\mathrm{dw}}{\mathrm{dx}}AE\frac{\mathrm{du}}{\mathrm{dx}}\mathrm{d}x + \int_0^l wb\mathrm{d}x = 0 \qquad \forall w \tag{4-5}$$

Letting all weight functions satisfy $w(0) = 0$ and evaluating the above equation yields:

$$(wA\sigma)_{x=l} - (wA\sigma)_{x=0} - \int_0^l \frac{\mathrm{dw}}{\mathrm{dx}}AE\frac{\mathrm{du}}{\mathrm{dx}}\mathrm{d}x + \int_0^l wb\mathrm{d}x = 0 \qquad \forall w \tag{4-6}$$

And from Equation 4-6 above, the first term is equal to the boundary condition and the second term vanishes, since the weight function was constructed with $w(0) = 0$. With this, the weak form can now be laid out as follows:

Find $u(x)$ among the smooth functions that satisfy $u(0) = \bar{u}$ such that

$$\int \frac{dw}{dx}AE\frac{du}{dx} = (wA\bar{t})_{x=l} + \int_0^l wbdx \quad \forall w \; with \; w(0) = 0 \tag{4-7}$$

4.2.3 Approximation functions

In order to approximate a solution to the finite element problem, approximation functions are required. A polynomial of varying orders may be used to express the approximation in the formulated element with regards the values at each node. The simplest version of an approximation can be represented by a straight line of the expression:

$$N_i^e = a + bx \tag{4-8}$$

For this example, the Lagrange polynomial is used and satisfies the conditions:

$$N_1^e(x_1) = 1; N_1^e(x_2) = 0$$

$$N_2^e(x_1) = 0; N_2^e(x_2) = 1$$

The shape function will therefore be:

$$\boldsymbol{N}^e = [N_1^e \quad N_2^e] = \frac{1}{x_2 - x_1}[x_2^e - x \quad x - x_1^e] \tag{4-9}$$

And its derivative:

$$\boldsymbol{B}^e = \left[\frac{dN_1^e}{dx} \quad \frac{dN_2^e}{dx}\right] = \frac{1}{x_2 - x_1}[-1 \quad 1] \tag{4-10}$$

4.2.4 Discrete equations

Using the arbitrariness of the weight function and trial functions as defined earlier, the weight functions and trial solutions may be approximated by:

$$w(x) \approx \boldsymbol{N}(x)\boldsymbol{w}$$

$$u(x) \approx \boldsymbol{N}(x)\boldsymbol{d}$$

Similarly, the derivatives of the weight and trial functions are:

$$\frac{dw}{dx} \approx \boldsymbol{B}(x)\boldsymbol{w}$$

$$\frac{du}{dx} \approx \boldsymbol{B}(x)\boldsymbol{d}$$

However, the trial solution must satisfy the essential boundary condition and similarly, the test function must vanish at this location.

Substituting into Equation 4-7 gives per element:

$$\sum_{e=1}^{n_{el}} \boldsymbol{w}^{eT} \left\{ \int_{x_1^e}^{x_2^e} \underbrace{\boldsymbol{B}^{eT} A^e E^e \boldsymbol{B}^e \mathrm{d}x \boldsymbol{d}^e}_{\boldsymbol{K}^e} - \int_{x_1^e}^{x_2^e} \underbrace{N^{eT} b \mathrm{d}x}_{\mathbf{f}_{\Omega^e}} - \underbrace{\left(N^{eT} A^e t\right)_{x=l}}_{\mathbf{f}_{\Gamma^e}} \right\} = 0 \qquad 4\text{-}10$$

From the above equation, matrices crucial to the finite element formulation have been defined. These are, the stiffness matrix, $\mathbf{K}$ and the force matrix, $\mathbf{f}$, where $\mathbf{f}$ is comprised of the body force exerted over the domain, Ω and at the prescribed location, Γ. Global matrices are:

$$\boldsymbol{K} = \sum_{e=1}^{n_{el}} \boldsymbol{L}^{eT} \boldsymbol{K}^e \boldsymbol{L}^e$$

$$\boldsymbol{f} = \sum_{e=1}^{n_{el}} \boldsymbol{L}^{eT} \boldsymbol{f}^e$$

Where $\mathbf{L}$ are the gather matrices used to assemble the global matrices. Summing the above equations gives:

$$\boldsymbol{w}^T(\boldsymbol{K}\boldsymbol{d} - \boldsymbol{f}) = 0 \qquad \forall w, \text{except } w(0) = 0 \qquad 4\text{-}11$$

A residual, $\mathbf{r}$, is then introduced which is defined as:

$$\boldsymbol{r} = \boldsymbol{K}\boldsymbol{d} - \boldsymbol{f} \qquad 4\text{-}12$$

From which the set of resulting equations may then be solved by use of a suitable solution procedure such as the partition method, where known displacements and corresponding components from the force and stiffness matrix are partitioned, where by the displacements of the system may be solved using linear algebra.

4.3 Types of elements

Depending on the problem encountered, there are various elements which may be applied in the finite element method, where the ABAQUS user manual (2012) states that there are five aspects of an element which describe its behaviour. These aspects are:

- Family
- Degrees of freedom
- Number of nodes
- Formulation
- Integration

The different families of elements are shown by Figure 4-4, whereby each family of elements corresponds to a certain geometry and application. Related to the family of elements are the degrees of freedom of each element, which are the variables calculated during processing. Nodes are an important characteristic of each element, as other degrees of freedom are calculated during analysis at these locations, in addition to defining the geometry. Formulation of an element refers to the fundamental theory which characterises the behaviour of an element whilst integration refers to the numerical method to evaluate the integrals encountered within the formulation of the element.

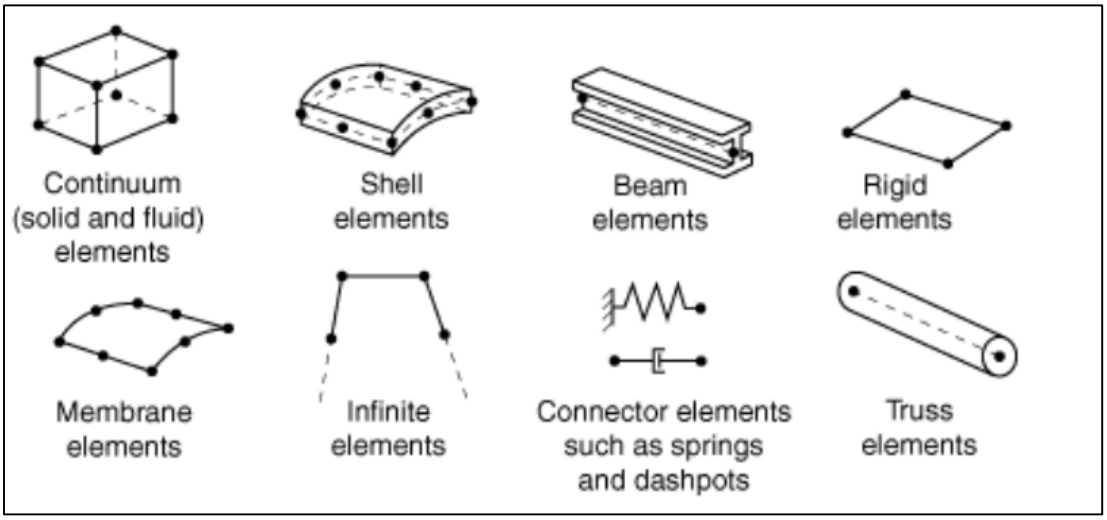

Figure 4-4: Families of elements (ABAQUS user manual, 2012)

As toroidal shells are investigated in this study, shell elements are required in order to accurately capture the geometry of the structure. There are two types of shell elements available in ADINA. These elements are: the conventional shell element and the axisymmetric shell element. Both these elements have pros and cons attached to them and are discussed below.

4.4 Axisymmetric and conventional shell elements

Conventional shell elements are formulated in ADINA as a three-dimensional continuum element by applying the last two Kirchhoff-Love assumptions as discussed in Section 1.2, whereby these assumptions made can be applied to model both thick and thin shells. There are also options to use 4 to 32 noded shells, depending on the application. Shell elements may have 6 degrees of freedom attached, which correspond to the three degrees of translation and rotation. ADINA integrates these elements by either applying Gaussian integration or the Newton-Cotes method. However, the computational cost attached to these elements are often very expensive which leads to the use of the axisymmetric shell element.

In ADINA, the axisymmetric shell element is considered to be a special case of the iso-beam element. It is defined as a 2-dimensional element, with three degrees of freedom per node. An illustration of the typical axisymmetric shell element is shown below by Figure 4-5.

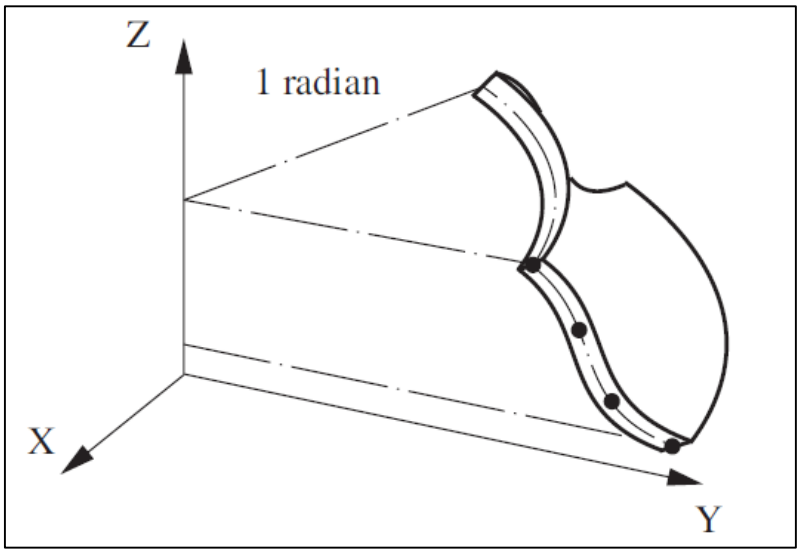

Figure 4-5: The axisymmetric shell element (ADINA user manual, 2012)

The axisymmetric shell element has the distinct advantage of having the meridional and hoop stress and strain components included in its formulation, allowing for comparison

between the derived expressions and the numerical model. The ADINA user manual states that the numerical integration for the axisymmetric shell element is performed in the r-s plane, which corresponds to the plane along the shells midsurface and in the direction normal to the shell, resulting in a far more computationally efficient model, especially for thin shells. Only one radian is modelled as shown by the above Figure.

Due to the nature of the problem, where an axisymmetric shell is experiencing axisymmetric loading, the axisymmetric shell element is favoured over the conventional shell element for two main reasons. The first is due to the computationally cheaper formulation of the element whilst the second is due to the ability of the axisymmetric shell element to give the exact meridional and hoop stresses, instead of stresses in three dimensions which occur within the conventional shell.

4.5 Verification of ADINA models

As mentioned in Section 4.4 above, the axisymmetric shell element in ADINA is theoretically suitable for use for verification of analytical membrane solutions of asymmetrically loaded shells. In order to ensure that the method used to create models in ADINA is sufficiently accurate, the analytical solution of an ordinary pressurised ellipse and a hydrostatically loaded spherical tank is compared to the corresponding ADINA model to ensure that the methods of modelling the respective geometrical, loading and support conditions are suitable for later use within this investigation.

4.5.1 Internally pressurised elliptical torus

The equations for an internally pressurised elliptical torus are shown by Equations 3-34 and 3-35. An ADINA model is created with 100 axisymmetric elements with the following geometric and loading conditions:

- $A = 30\text{m}$
- $a = 10\text{m}$
- $b = 20\text{m}$
- $t = 0.05\text{m}$
- $p = 1000$ Pa (constant internal pressure)

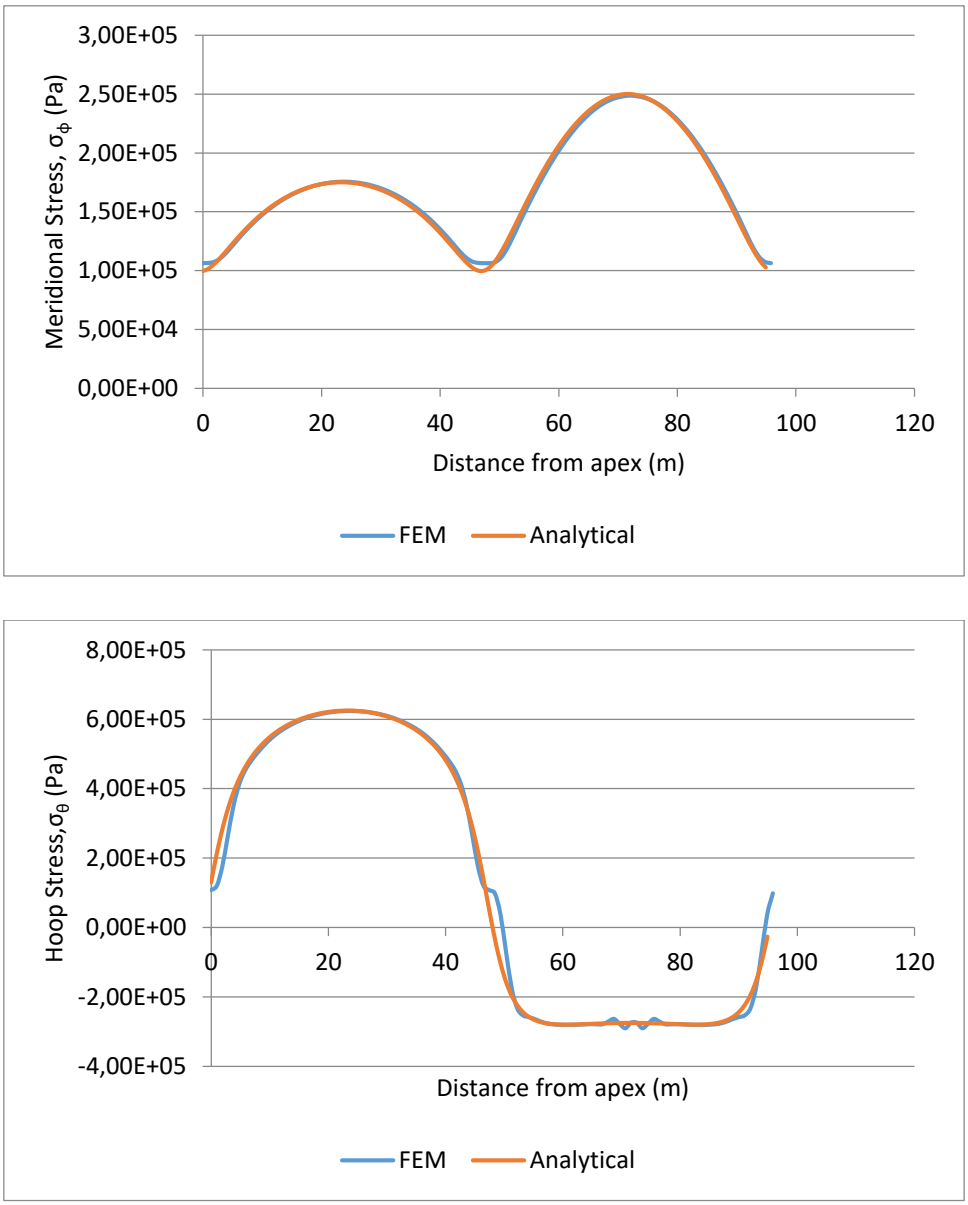

Figure 4-6: Numerical and analytical comparison for an internally pressurised elliptical torus

As it can be shown by the above Figure, there is consistent agreement between the numerical and analytical solutions for the internally pressurized. Discrepancies between the solutions occur at locations corresponding to the top and bottom of the elliptical

torus, where a change in curvature occurs and the consequent breakdown of the membrane solution. However, apart from these locations, the error is negligible, indicating that the model created on ADINA can suitably simulate the geometric aspects of the elliptical torus.

4.5.2 Hydrostatically loaded spherical tank

The spherical tank has the same support and loading conditions of the hydrostatically loaded elliptical torus. It is assumed that a support occurs at a location corresponding to equatorial circle of latitude. Equations for the spherical tank are given by the following:

For $0 \leq \phi \leq \frac{\pi}{2}$:

$$N_\phi = \frac{\gamma a^2}{6}\left(\frac{1-\cos\phi}{1+\cos\phi}\right)(1+2\cos\phi) \qquad 4\text{-}13$$

$$N_\theta = \frac{\gamma a^2}{6}\left(\frac{1-\cos\phi}{1+\cos\phi}\right)(5+4\cos\phi) \qquad 4\text{-}14$$

And for $\frac{\pi}{2} \leq \phi \leq \pi$:

$$N_\phi = \frac{\gamma a^2}{6}\left(\frac{5-5\cos\phi+2\cos^2\phi}{1-\cos\phi}\right) \qquad 4\text{-}15$$

$$N_\theta = \frac{\gamma a^2}{6}\left(\frac{1-7\cos\phi+4\cos^2\phi}{1-\cos\phi}\right) \qquad 4\text{-}16$$

An ADINA model is created with 100 axisymmetric shell elements. The hydrostatic loading of the tank is modelled by creating a surface function within ADINA. The tank has the following properties:

- a = 10m
- t = 0.1m
- γ = 10E3 N/m^3
- E = 200 GPa
- $\nu = 0.3$

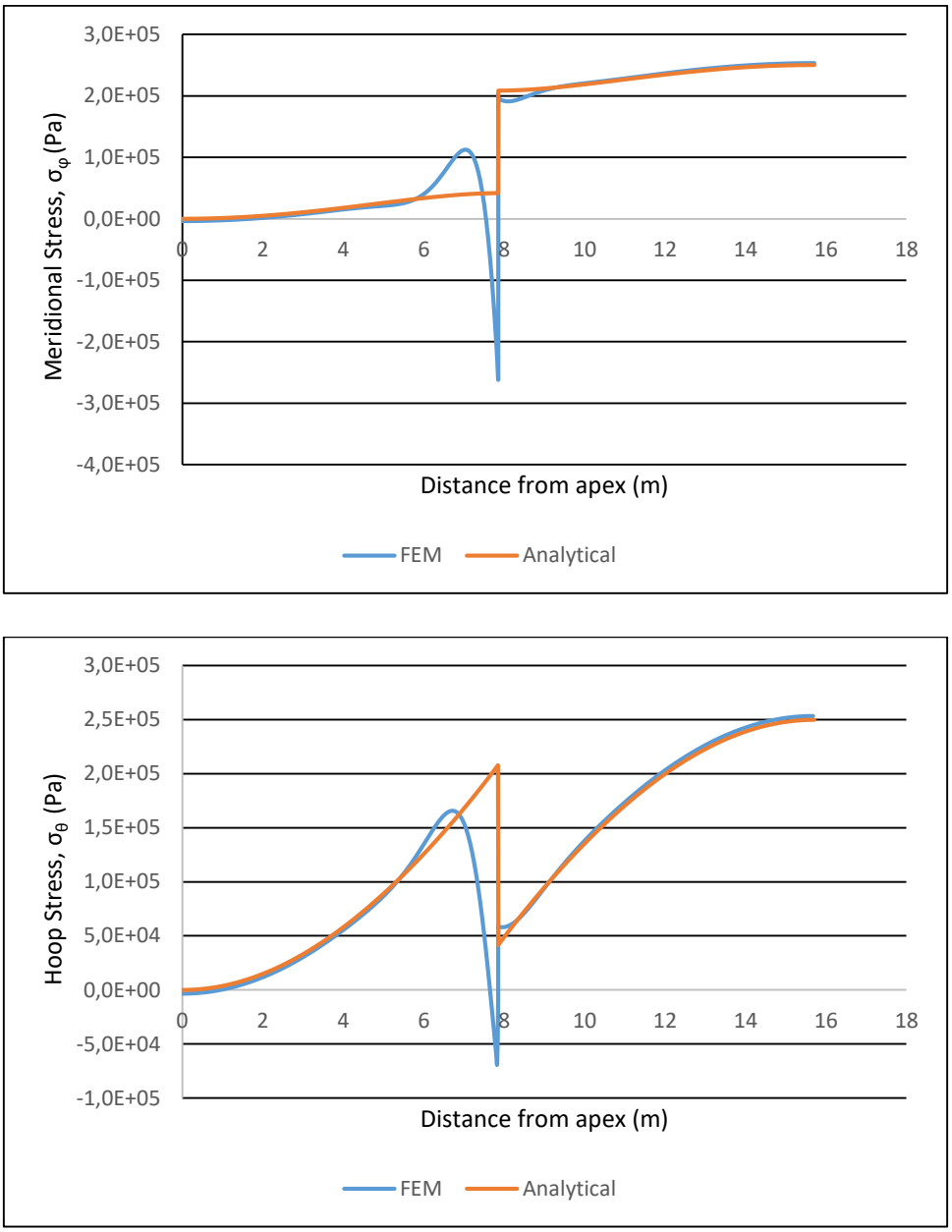

Figure 4-7: Numerical and analytical comparison for a hydrostatically loaded spherical tank

The numerical and analytical solutions have excellent agreement with each other, with the exception to this occurring at the presence of the support – a location where a

breakdown of the membrane hypothesis is expected to occur. However, at locations which are sufficiently far from the support, the difference between solutions is negligible. Consequently, the loading and support conditions of the above model, in conjunction with the geometric aspects of the internally pressurized elliptical torus, can provide an accurate estimation of the membrane stresses at locations sufficiently far away from the change in curvature and supports.

Chapter 5

Theoretical results

5.1 Introduction

This chapter derives the meridional and hoop stresses for hydrostatically loaded elliptic toroidal shells. This is done by examining the geometric and loading preliminaries of the structure and applying them into the governing equations of membrane theory, where the necessary expressions are obtained. Following this, the derived expressions are verified against numerical models constructed on ADINA.

5.2 Geometric aspects

Consider an ellipse with a semi major and semi minor axes of a and b respectively which is symmetrical about the x-axis. If this ellipse were rotated around the vertical axis of revolution, the elliptical toroidal shell would be formed. Figure 5-1 shows the meridional cross-section of a hydrostatically loaded elliptical torus.

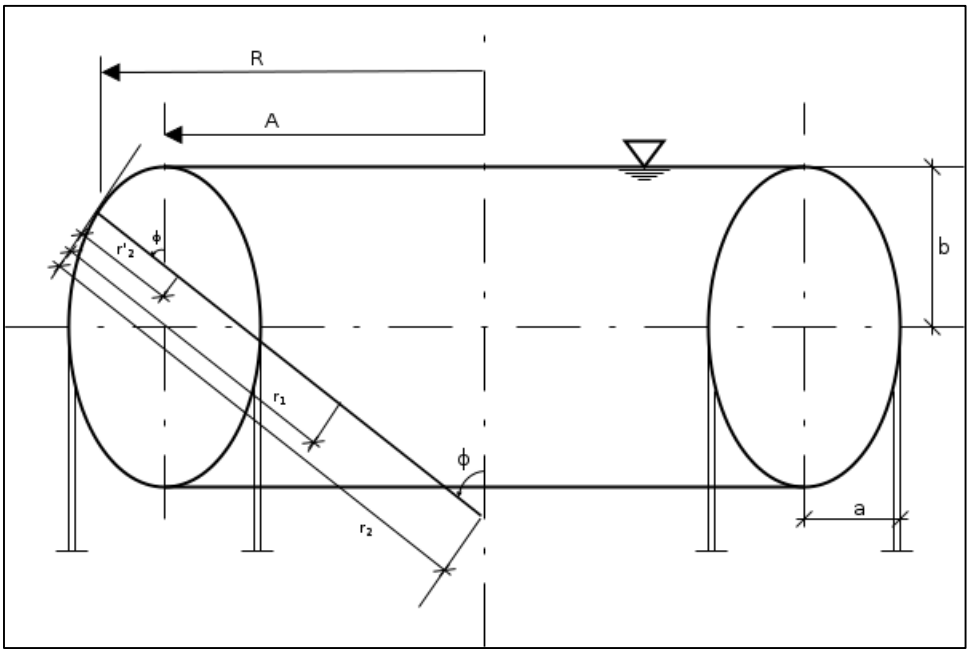

Figure 5-1: A meridional cross-section of the hydrostatically loaded elliptical torus

The angle ϕ is measured from the vertical axis of the cross-section towards the outer surface of the torus. Consequently, ϕ is positive for the outer surface of the torus, where the Gaussian curvature is positive ($0 \leq \phi \leq \pi$), whilst for the inner surface, which has negative Gaussian curvature, ϕ is negative ($0 \geq \phi \geq -\pi$).

As shown previously by Equation 3-32, the principal radii of curvature are:

$$r_1 = \frac{a^2 b^2}{(a^2 \sin^2 \phi + b^2 \cos^2 \phi)^{\frac{3}{2}}} \tag{5-1}$$

$$r_2 = \frac{A}{\sin \phi} + r_2' = \frac{A}{\sin \phi} + \frac{a^2}{(a^2 \sin^2 \phi + b^2 \cos^2 \phi)^{\frac{1}{2}}} \tag{5-2}$$

5.3 Loading preliminaries

Assuming that the shell is completely filled with liquid of weight γ per unit volume, the depth of the liquid at a given y-coordinate will be:

$$d = b - y \tag{5-3}$$

However, as shown by Section 3.2.2, as y is a function of ϕ, a positive coordinate is given for values of $0 < \phi < \frac{\pi}{2}$ and $0 > \phi > -\frac{\pi}{2}$, whilst a negative y-coordinate is given for $\frac{\pi}{2} < \phi < \pi$ and $-\frac{\pi}{2} > \phi > -\pi$. This leads to the development of the loading component p_r, which is the load per unit area of the shell midsurface, in the direction of the normal to the shell midsurface.

This leads to:

$$d = b - \frac{b^2 \cos^2 \phi}{(a^2 \sin^2 \phi + b^2 \cos^2 \phi)^{\frac{1}{2}}} \qquad 5\text{-}4$$

Therefore, the loading component p_r is given by:

$$p_r = \gamma d = \gamma \left(b - \frac{b^2 \cos^2 \phi}{(a^2 \sin^2 \phi + b^2 \cos^2 \phi)^{\frac{1}{2}}} \right) \qquad 5\text{-}5$$

As the hydrostatic pressure exerted purely acts perpendicular to the shell, the loading components p_θ and p_ϕ, the load per unit area of the shell midsurface in the hoop and meridional directions respectively are zero. Hydrostatic pressure is a distributed loading, varying linearly with depth as evident from the above expressions. The membrane theory of shells of revolution can accurately describe the state of stress within the shell provided that the loading and the shell geometry vary smoothly, continuously and not too rapidly. Consequently, the membrane solution obtained is expected to be adequate throughout the shell, with the exception of the top and bottom of the elliptical cross-section whereby the Gaussian curvature of the shell changes signs and the shell is supported respectively.

5.4 Substitution into membrane solution

Substitution of Equations 5-1, 5-2 and 5-5 into Equation 2-21 leads to:

$$r_1 r_2 (p_r \cos\phi - p_\theta \sin\phi)\sin\phi =$$

$$\left(\frac{a^2 b^2}{(a^2\sin^2\phi + b^2\cos^2\phi)^{\frac{3}{2}}}\right)\left(\frac{A}{\sin\phi} + \frac{a^2}{(a^2\sin^2\phi + b^2\cos^2\phi)^{\frac{1}{2}}}\right)\gamma\left(b - \frac{b^2\cos^2\phi}{(a^2\sin^2\phi + b^2\cos^2\phi)^{\frac{1}{2}}}\right)\cos\phi sin\phi$$

5-6

Which when multiplied out yields:

$$\gamma\left(\frac{Aa^2b^2}{\sin\phi(a^2\sin^2\phi + b^2\cos^2\phi)^{\frac{3}{2}}} + \frac{a^4b^2}{(a^2\sin^2\phi + b^2\cos^2\phi)^2}\right)\left(b\cos\phi\sin\phi * \frac{b^2\cos^2\phi}{(a^2\sin^2\phi + b^2\cos^2\phi)^{\frac{1}{2}}}\right)$$

5-7

Which after factoring out γ, the above term can further be shown by the 4 expressions, $\boxed{A}, \boxed{B}, \boxed{C}, \boxed{D}$:

$$\underbrace{\frac{Aa^2b^3\cos\phi\sin\phi}{\sin\phi(a^2\sin^2\phi + b^2\cos^2\phi)^{\frac{3}{2}}}}_{\boxed{A}} + \underbrace{\frac{a^4b^3\cos\phi\sin\phi}{(a^2\sin^2\phi + b^2\cos^2\phi)^2}}_{\boxed{B}}$$

$$-\underbrace{\frac{Aa^2b^4\cos^2\phi\sin\phi}{\sin\phi(a^2\sin^2\phi + b^2\cos^2\phi)^2}}_{\boxed{C}} - \underbrace{\frac{a^4b^3\cos^2\phi\sin\phi}{(a^2\sin^2\phi + b^2\cos^2\phi)^{\frac{5}{2}}}}_{\boxed{D}}$$

Integrating each expression separately:

$$\int \boxed{A}\, d\phi =$$
$$a^2Ab^3\int \frac{\cos\phi}{(a^2\sin^2\phi + b^2\cos^2\phi)^{\frac{3}{2}}}\, d\phi \qquad 5\text{-}8$$

Let $u = \sin\phi$.

Therefore: $\frac{du}{d\phi} = \cos\phi$

Which leads to:

$$a^2Ab^3\int\frac{1}{(a^2u^2+b^2(1-u^2))^{\frac{3}{2}}}du \qquad 5\text{-}9$$

Simplifying the above:

$$a^2Ab^3\int\frac{1}{(u^2(a^2-b^2)+b^2)^{\frac{3}{2}}}du \qquad 5\text{-}10$$

The above equation requires a trigonometric substitution to solve. The book, CRC Standard Mathematical Tables and Formulae: Sec 5.4.5 is used:

$$\int(a+bx^n)^P dx \rightarrow \frac{x(a+bx^n)^{P+1}}{a} \qquad \text{with n(p+1)+1} = 0$$

Consequently, the following result is obtained with the following substitutions of $a = b^2, b = a^2 - b^2, x = u, n = 2$ and $P = \frac{3}{2}$:

$$\frac{u}{b^2((u^2(a^2-b^2)+b^2)^{\frac{1}{2}}} \qquad 5\text{-}11$$

And substituting $u = \sin\phi$ and multiplying by constants yields:

$$\frac{Aa^2b\sin\phi}{(a^2\sin^2\phi+b^2\cos^2\phi)^{\frac{1}{2}}} \qquad 5\text{-}12$$

Which, with the exception of an additional b, which is evident due to the loading component, in the numerator, the above expression is the exact term found by Zingoni (1997).

$$\int\boxed{B}\,d\phi = \int\frac{a^4b^3\cos\phi\sin\phi}{(a^2\sin^2\phi+b^2\cos^2\phi)^2}d\phi \qquad 5\text{-}13$$

Which, after simplifying constants out:

$$a^4b^3\int\frac{\cos\phi\sin\phi}{(a^2\sin^2\phi+b^2\cos^2\phi)^2}\,d\phi \qquad 5\text{-}14$$

Let $u = \sin\phi$

Therefore: $\frac{du}{d\phi} = \cos\phi$

Which leads to:

$$a^4b^3 \int \frac{u}{(a^2u^2+b^2(1-u^2))^2}\, du \qquad 5\text{-}15$$

And rewritten as:

$$a^4b^3 \int \frac{u}{(u^2(a^2-b^2)+b^2)^2}\, du \qquad 5\text{-}16$$

Using Table of integrals, Section 2.124:

$$\int \frac{x}{z_2^m} dx = -\frac{1}{2b(m-1)z_2^m}$$

Whereby $z_2^m = a + bx^2$ and subsequently $a = b^2, b = a^2 - b^2, x = u,$ and $m = 2$. This yields:

$$-\frac{1}{2(a^2-b^2)(a+bx^2)} \qquad 5\text{-}17$$

Substituted back results in:

$$\int \boxed{B}\, d\phi = \frac{a^4b^3}{2(a^2-b^2)(a^2\sin^2\phi+b^2\cos^2\phi)} \qquad 5\text{-}18$$

Which as before, is similar to the term involved in the constant pressurised elliptic torus, with the exception of the additional b in the numerator which is a consequence due to the loading component.

$$\int \boxed{C}\, d\phi = -\int \frac{Aa^2b^4\cos^2\phi\sin\phi}{\sin\phi(a^2\sin^2\phi+b^2\cos^2\phi)^2} d\phi \qquad 5\text{-}19$$

Substituting out constants:

$$-Aa^2b^4 \int \frac{\cos^2 \phi}{(a^2 \sin^2 \phi + b^2 \cos^2 \phi)^2} d\phi \qquad 5\text{-}20$$

Rearranging the denominator by multiplying by $\frac{\cos^2 \phi}{\cos^2 \phi}$ and simplifying gives:

$$-Aa^2b^4 \int \frac{\sec^2 \phi}{(a^2 \tan^2 \phi + b^2)^2} d\phi \qquad 5\text{-}21$$

Substitution of $u = \tan \phi$

Therefore: $\frac{du}{d\phi} = \sec^2 \phi$ gives:

$$-Aa^2b^4 \int \frac{1}{(a^2 \mathrm{u}^2 + b^2)^2} d\phi \qquad 5\text{-}22$$

The reduction formula from CRC Standard Mathematical Tables and Formulae: Sec 5.4.5 is used, with temporarily removing constants:

$$\int \frac{dx}{(a+bx^2)^m} = \frac{2m-3}{2a(m-1)} \int \frac{1}{(a+bx^2)^{m-1}} dx + \frac{x}{2a(m-1)(a+bx^2)^{m-1}}$$

Where $a = b^2, b = a^2, x = u,$ and $m = 2$

This yields:

$$\frac{1}{2b^2} \underbrace{\int \frac{1}{a^2u^2+b^2} du}_{\boxed{C_1}} + \frac{u}{2b^2(a^2u^2+b^2)} \qquad 5\text{-}23$$

Where the second term of the above expression can be substituted back as:

$$\frac{\tan \phi}{2b^2(a^2 \tan^2 \phi + b^2)} \qquad 5\text{-}24$$

And solving for C_1:

$$\int \frac{1}{a^2u^2+b^2}\,du \qquad 5\text{-}25$$

Substituting $v = \frac{au}{b}$, which results in

$$\frac{dv}{du} = \frac{a}{b}$$

And leads to:

$$\frac{1}{ab}\int \frac{1}{v^2+1}\,dv$$

Which is the well-known identity for

$$\frac{1}{ab}\int \arctan v$$

Substituting back gives:

$$\frac{1}{2ab^3}\arctan\left(\frac{a\tan\phi}{b}\right) \qquad 5\text{-}26$$

Plugging in constants and rewriting the solved integral gives:

$$\int \boxed{C}\,d\phi = -\frac{Aab}{2}\text{Arctan}\left(\frac{a\tan\phi}{b}\right) - \frac{Aa^2b^2\sin\phi cos\phi}{2(a^2\sin^2\phi+b^2\cos^2\phi)} \qquad 5\text{-}27$$

Lastly,

$$\int \boxed{D}\,d\phi = \int \frac{a^4b^4\cos^2\phi\sin\phi}{(a^2\sin^2\phi+b^2\cos^2\phi)^{\frac{5}{2}}}\,d\phi \qquad 5\text{-}28$$

Factoring constants out:

$$a^4b^4\int \frac{\cos^2\phi\sin\phi}{(a^2\sin^2\phi+b^2\cos^2\phi)^{\frac{5}{2}}}\,d\phi \qquad 5\text{-}29$$

Letting $u = \cos\phi$

Therefore: $\frac{du}{d\phi} = -\sin\phi$

This leads to:

$$-a^4b^4 \int \frac{u^2}{(a^2+u^2(b^2-a^2))^{\frac{5}{2}}} d\phi \qquad 5\text{-}30$$

CRC Standard Mathematical Tables and Formulae: Sec 5.4.5 is used:

$$\int (cx)^m (a+bx^n)^P dx \rightarrow \frac{(cx)^{m+1}(a+bx^n)^{p+1}}{ac(m+1)}$$

For $m + np + n + 1 = 0$ & $m + 1 \neq 0$

Where $a = a^2, b = b^2 - a^2, x = u,\ n = 2$ and $P = 1$ results in:

$$\frac{-a^4b^4u^3}{3a^2(a^2+u^2(b^2-a^2))^{\frac{3}{2}}} \qquad 5\text{-}31$$

Which after substituting back gives:

$$\frac{a^2b^4\cos^3\phi}{3(a^2\sin^2\phi+b^2\cos^2\phi)^{\frac{3}{2}}} \qquad 5\text{-}32$$

Putting together the results from $\boxed{A} - \boxed{D}$ gives

$$N_\phi = \frac{(a^2\sin^2\phi+b^2\cos^2\phi)^{\frac{1}{2}}}{A\sin\phi((a^2\sin^2\phi+b^2\cos^2\phi)+a^2\sin^2\phi)}\left[\frac{Aa^2b\sin\phi}{(a^2\sin^2\phi+b^2\cos^2\phi)^{\frac{1}{2}}} - \frac{a^4b^3}{2(a^2-b^2)(a^2\sin^2\phi+b^2\cos^2\phi)} - \frac{Aab}{2}\text{Arctan}\left(\frac{a\tan\phi}{b}\right) - \frac{Aa^2b^2\sin\phi cos\phi}{2(a^2\sin^2\phi+b^2\cos^2\phi)} + \frac{a^2b^4\cos^3\phi}{3(a^2\sin^2\phi+b^2\cos^2\phi)^{\frac{3}{2}}} + C\right] \qquad 5\text{-}33$$

Where C is a constant of integration which is obtained from a suitable boundary condition. When $\phi = 0$, it follows that the denominatior of the term outside the bracket is undefined and hence, the term within the square brackets must be 0 in order to satisfy the expression. This results in the following constant obtained:

$$C_1 = \frac{a^4 b}{2(a^2 - b^2)} + \frac{a^2 b}{3} \qquad 5\text{-}34$$

The expression for the top half of the toroid is therefore:

$$N_\phi = \frac{(a^2 \sin^2\phi + b^2 \cos^2\phi)^{\frac{1}{2}}}{A \sin\phi((a^2 \sin^2\phi + b^2 \cos^2\phi) + a^2 \sin^2\phi)} \left[\frac{A a^2 b \sin\phi}{(a^2 \sin^2\phi + b^2 \cos^2\phi)^{\frac{1}{2}}} - \frac{a^4 b^3}{2(a^2 - b^2)(a^2 \sin^2\phi + b^2 \cos^2\phi)} - \frac{Aab}{2} \text{Arctan}\left(\frac{\tan\phi}{b}\right) - \frac{A a^2 b^2 \sin\phi cos\phi}{2(a^2 \sin^2\phi + b^2 \cos^2\phi)} + \frac{a^2 b^4 \cos^3\phi}{(a^2 \sin^2\phi + b^2 \cos^2\phi)^{\frac{3}{2}}} + \frac{a^4 b}{2(a^2 - b^2)} + \frac{a^2 b}{3} \right] \qquad 5\text{-}35$$

Similarly, for the bottom half of the tank, as $\phi \to \pi$, the term within the square brackets must vanish, this leads to the value of C_2:

$$C_2 = \frac{a^4 b}{2(a^2 - b^2)} - \frac{a^2 b}{3} \qquad 5\text{-}36$$

And:

$$N_\phi = \frac{\gamma(a^2 \sin^2\phi + b^2 \cos^2\phi)^{\frac{1}{2}}}{A \sin\phi((a^2 \sin^2\phi + b^2 \cos^2\phi) + a^2 \sin^2\phi)} \left[\frac{A a^2 b \sin\phi}{(a^2 \sin^2\phi + b^2 \cos^2\phi)^{\frac{1}{2}}} - \frac{a^4 b^3}{2(a^2 - b^2)(a^2 \sin^2\phi + b^2 \cos^2\phi)} - \frac{Aab}{2} \text{Arctan}\left(\frac{\tan\phi}{b}\right) - \frac{A a^2 b^2 \sin\phi cos\phi}{2(a^2 \sin^2\phi + b^2 \cos^2\phi)} + \frac{a^2 b^4 \cos^3\phi}{(a^2 \sin^2\phi + b^2 \cos^2\phi)^{\frac{3}{2}}} + \frac{a^4 b}{2(a^2 - b^2)} - \frac{a^2 b}{3} \right] \qquad 5\text{-}37$$

With N_ϕ known, it can be substituted into Equation 2-13 and the corresponding value of N_ϕ is determined to be:

$$N_\theta = \left(\frac{A}{\sin\phi} + \frac{a^2}{(a^2 \sin^2\phi + b^2 \cos^2\phi)^{\frac{1}{2}}} \right) \left(\frac{\gamma b \left((a^2 \sin^2\phi + b^2 \cos^2\phi)^{\frac{1}{2}} - b \cos^2\phi \right)}{(a^2 \sin^2\phi + b^2 \cos^2\phi)^{\frac{1}{2}}} - \frac{N_\phi (a^2 \sin^2\phi + b^2 \cos^2\phi)^{\frac{3}{2}}}{a^2 b^2} \right) \qquad 5\text{-}38$$

The above expressions are equally as valid for the inner half of the toroidal shell, although it should be noted that the angle ϕ for this region is valid for $0 \geq \phi \geq -\pi$.

5.5 Verification of the derived expression

The derived expression unfortunately may not be verified against the circular toroidal shell under hydrostatic loading, as derived by Enoma et al (2015), due to the presence of two terms within the expression which have the denominator of $(a^2 - b^2)$. In a circular toroidal shell, the semi major and semi minor axes are equal to each other, resulting in the above expressions being divisible by zero, which is not possible.

Due to this constraint, the finite element analysis software ADINA is used as a method of verification against the analytical example. Axisymmetric shell elements with three degrees of freedom per node were used, which subsequently meant that the geometry modelled was a section of the toroidal shell, constructed in the +YZ of the ADINA model space. A spatial function was created in order to capture the behaviour of hydrostatic loading and boundary conditions were employed at locations corresponding to $\phi = \frac{\pi}{2}$ and $\phi = -\frac{\pi}{2}$. A sufficiently large number of elements were used in order to ensure that the mesh was fine, resulting in reasonably accurate stresses obtained. A sample input file can be found in Appendix A.

A numerical example with the derived expressions has the following characteristics:

- A = 30m
- b = 20m
- a = 10m
- E = 200 GPa
- $\nu = 0.3$
- t = 0.05m
- $\gamma = 10\text{kN/m}^3$

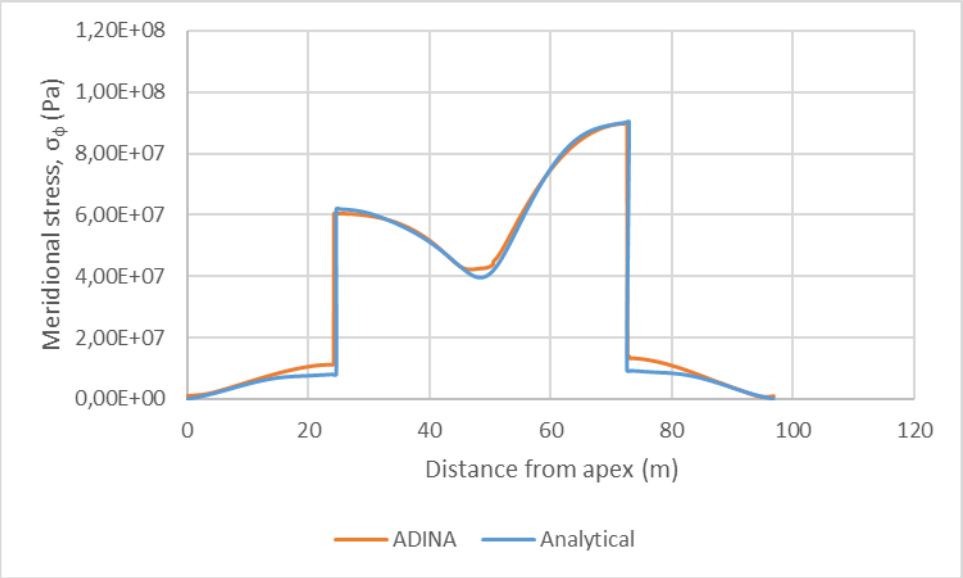

Figure 5-2: A comparison between analytical and numerical results for the meridional stress, N_ϕ

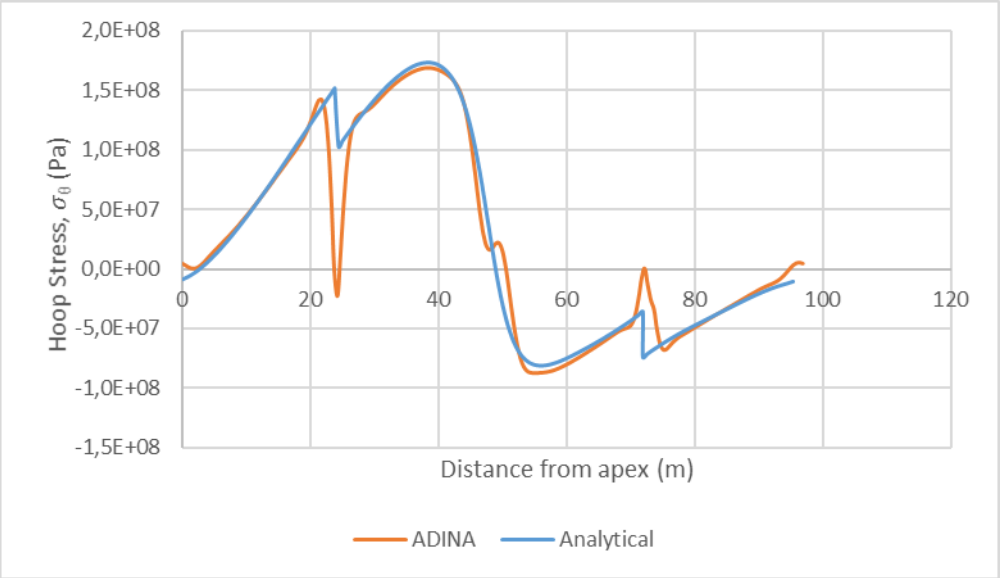

Figure 5-3: A comparison between analytical and numerical results for the hoop stress, N_θ

As it is shown by the above charts, the analytical solution is compared to the numerical results. There is excellent agreement between the analytical expression and the finite

element model, for both values of N_ϕ and N_θ. Discrepencies for both charts occur at the presence of three locations, which correspond to $\phi = 0$ and $\phi = \pi$, where a change in curvature occurs and at the location of $\phi = \frac{\pi}{2}$, which corresponds to the position of the supports. Membrane theory, as discussed in Chapter 2, cannot accurately describe the behaviour at these locations, which accounts for these differences. It is therefore recommended that the membrane theory be used to estimate the state of stress away from the apex and bottom of the tank and sufficiently far away from the supports.

Chapter 6

Parametric results for toroidal shells

6.1 Introduction

This chapter deals with the various membrane stresses experienced within elliptical and circular toroidal shells. Both prolate, oblate and circular elliptical toroidal shells are investigated using the formulae derived in Chapter 5 and by Enoma et al (2015), whereby charts detailing the effects of the aspect ratio $\frac{b}{a}$ and the opening ratio $\frac{A}{a}$ are investigated. A wide range of practical geometries are explored. An organogram is shown below illustrating the types of toroidal shells and the geometries investigated. Tables 6-1 and 6-2 show the parameters varied and Figures 6-1 and 6-2 graphically show an organogram of the parameters, along with the definitions of different cross-sections respectively

Table 6-1: Variation of opening ratios used

Opening Ratios varied						
1.5	2	2.5	3	5	7.5	10

Table 6-2: Variation of aspect ratios varied for elliptical toroidal shells

Type of shell	Aspect ratio (b/a) varied					
Prolate	1.25	1.5	1.75	2	2.25	2.5
Oblate	0.8	0.66	0.57	0.5	0.44	0.4

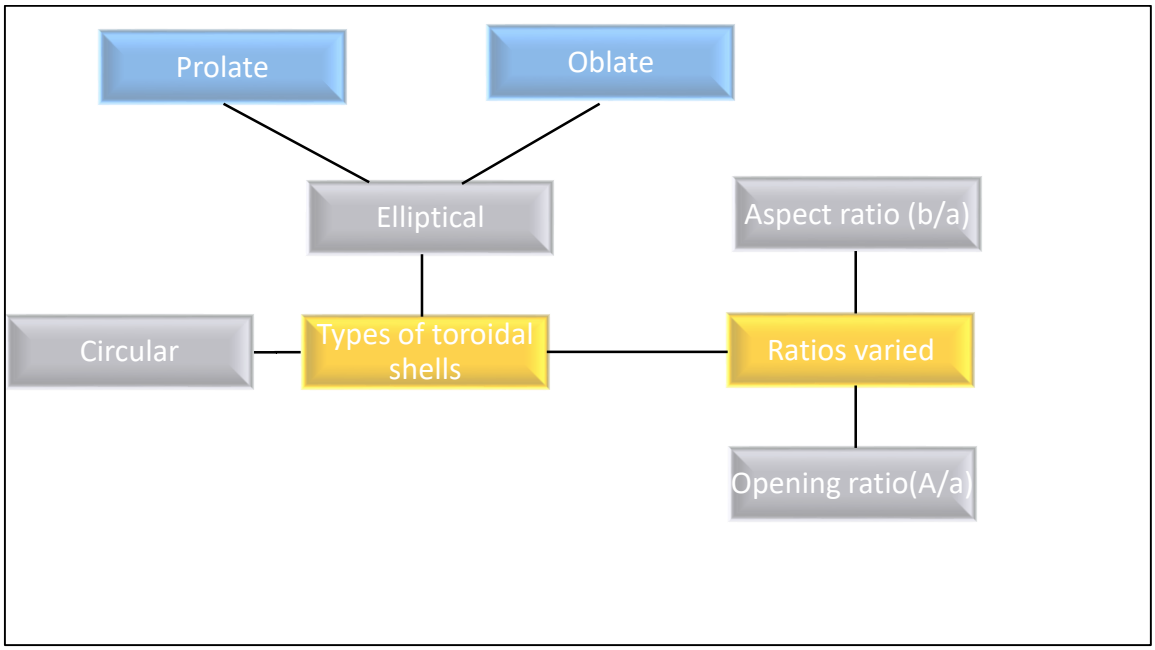

Figure 6-1: An illustration of the design parameters

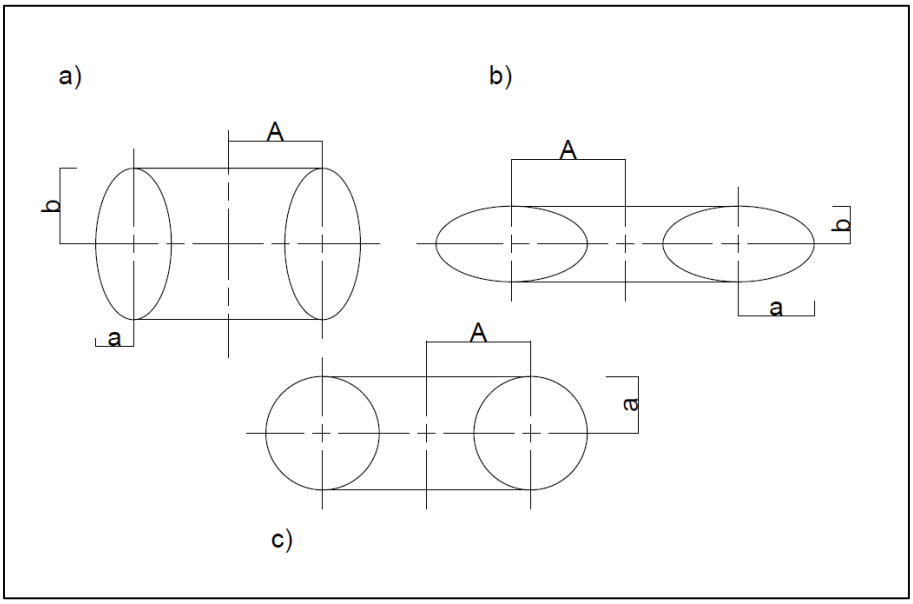

Figure 6-2: The various toroidal shells investigated. a) prolate elliptical, b) oblate elliptical and c) circular

6.2 Prolate elliptical toroidal shells

As discussed above, the outer $0° \leq \phi \leq \pi$ and inner $0° \geq \phi \geq \pi$ surfaces are computed separately and in this section, a numerical example, in addition to the membrane stress resultant parametric study defined above for prolate elliptical toroidal shells is performed.

6.2.1 Outer surface

6.2.1.1. Numerical example

A numerical example is shown by Figure 6-3 and Figure 6-4 below. A relatively large, prolate toroidal shell, fabricated from steel with the following properties $E = 200\text{GPa}$ and $\nu = 0.3$ and a constant thickness is assumed. The tank has the following geometric characteristics: $A = 30\text{m}$, $b = 20\text{m}$ and $a = 10\text{m}$ and is assumed to be filled with water, having a unit weight of $\gamma = 10\text{kN/m}^3$. Supports are considered to be placed at the equatorial circle of latitude, which corresponds to $\phi = \frac{\pi}{2}$, to ensure that support reactions would be tangential to the shell midsurface. A variation of the membrane stress from $\frac{2\pi}{18} \leq \phi \leq \frac{16\pi}{18}$ (which corresponds to the angle between $20°$ and $160°$) is examined, due to the breakdown of the membrane solution because of the change of Gaussian curvature at locations of $\phi = 0°$ and $\phi = \pi$.

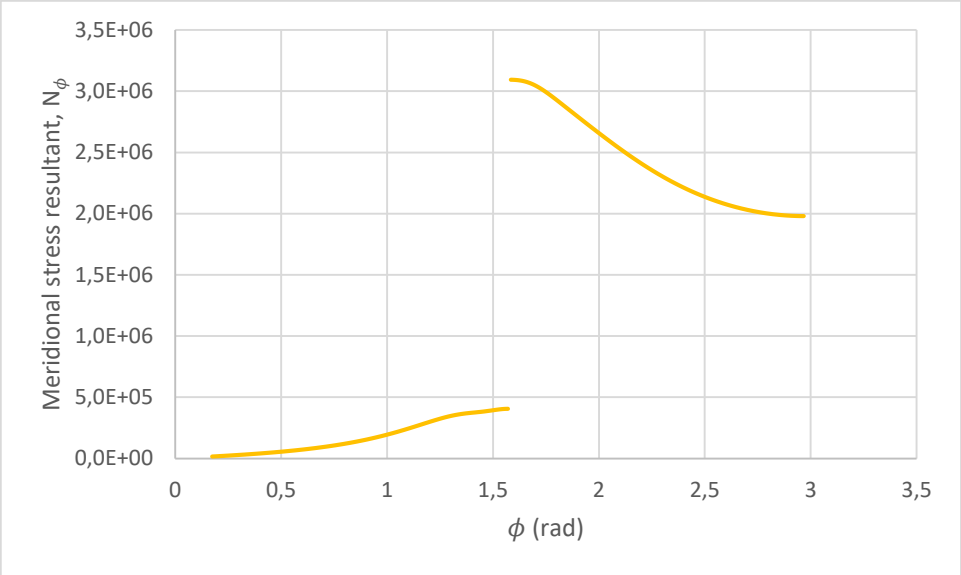

Figure 6-3: Meridional stress resultant, N_ϕ for the outer surface of a prolate elliptic toroidal shell for A=30, a=10 and b=20m

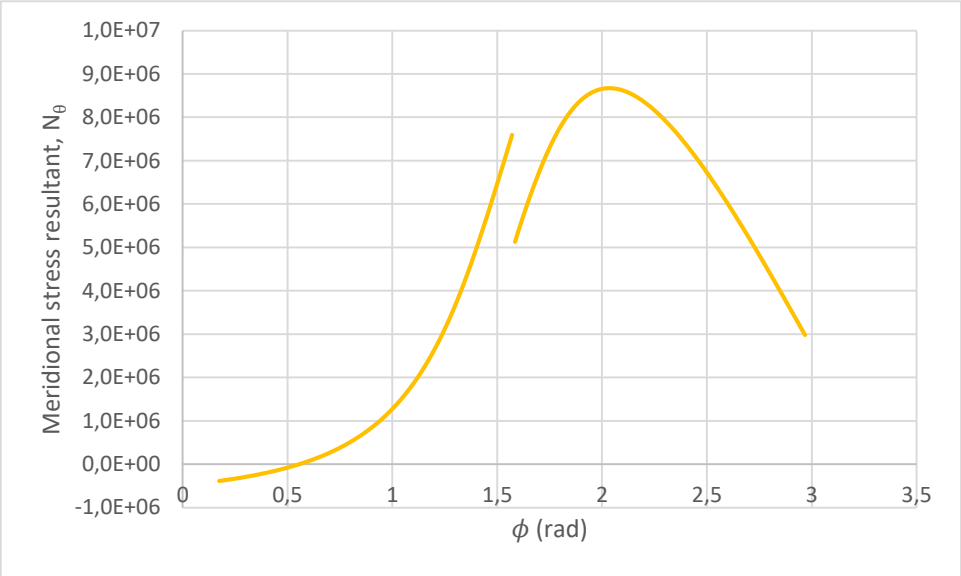

Figure 6-4: Hoop stress resultant, N_θ for the outer surface of a prolate elliptic toroidal shell with the above parameters

As it can be seen from Figure 6-3, the distribution of the meridional stress resultant for a prolate elliptic toroidal shell is in tension throughout. As ϕ increases from the apex of the shell, the value of N_ϕ increases with increasing values of ϕ. A discontinuity occurs at the location of $\phi = \frac{\pi}{2}$, which can be explained numerically by the different expression used for the upper and lower halves of the tank, implying that bending effects occur at this location. On the lower half as the tank, as ϕ tends to the bottom, the value of the meridional stress resultant remains in tension, although decreases at a rate greater than the rate of increase for the upper half of the tank.

Similarly, the hoop stress resultant is primarily in tension throughout for the outer half of the prolate elliptical toroidal tank, where it is observed that as ϕ increases from the apex of the vessel, the numerical value of N_θ increases sharply until ϕ reaches the location of the support. Following from the support, after the discontinuity, there is a small decrease in the circumferential stress resultant, until a maximum peak is reached at the location of $\phi \approx 2$. After this peak, as one moves to the bottom of the outer surface of the tank, the hoop stress resultant decreases.

6.2.1.2. Variation of opening ratio

The opening ratio is varied for a fixed aspect ratio of $\frac{b}{a} = 2$ as shown by the below Figure 6-5 and Figure 6-6. Opening ratios are varied according to Table 6-1. For the parameters investigated, the value of a is taken as 1m and the value of γ is taken as 1N/m^3

Examining Figure 6-5, for a given aspect ratio, changing the opening ratio of the torus has a minimal effect on the stress resultants experienced in the upper-outer half of the tank $0° \leq \phi < \frac{\pi}{2}$ as the value of N_ϕ varies very little, indicating that this region is not critical when examining the stresses occurring throughout the toroidal shell. However, the lower half of the outer surface of the shell does not display the same trend as it can be seen that the meridional stress resultant will increase for a larger opening ratio, although as the value of $\frac{A}{a}$ increases, the effect of the increase in the meridional stress resultant is smaller than when compared to lower opening ratios.

Figure 6-6 shows how for a given aspect ratio, the hoop stress resultant varies with a change in the opening ratio. Both the upper and lower regions of the outer surface of the prolate toroidal elliptic tank show that an increase in the opening ratio corresponds to an increase in the value of N_θ. However, it should be noted that unlike for Figure 6-5, as the opening ratio remains small and varied in small increments, the meridional stress resultant increases less than for larger increases of values of $\frac{A}{a}$.

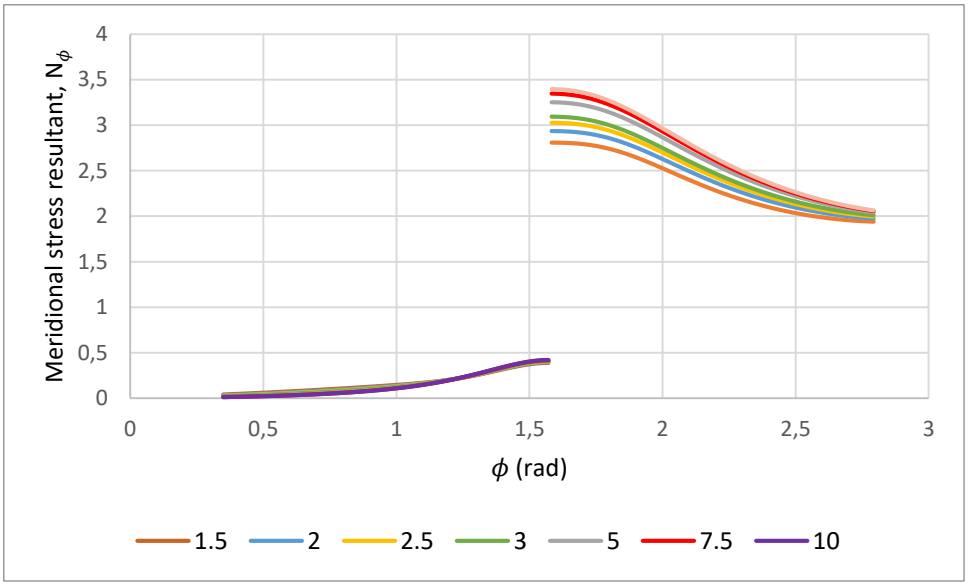

Figure 6-5: Meridional stress resultant, N_ϕ for a fixed aspect ratio of $\frac{b}{a} = 2$ and varying opening ratios for the outer surface of a prolate elliptical torus

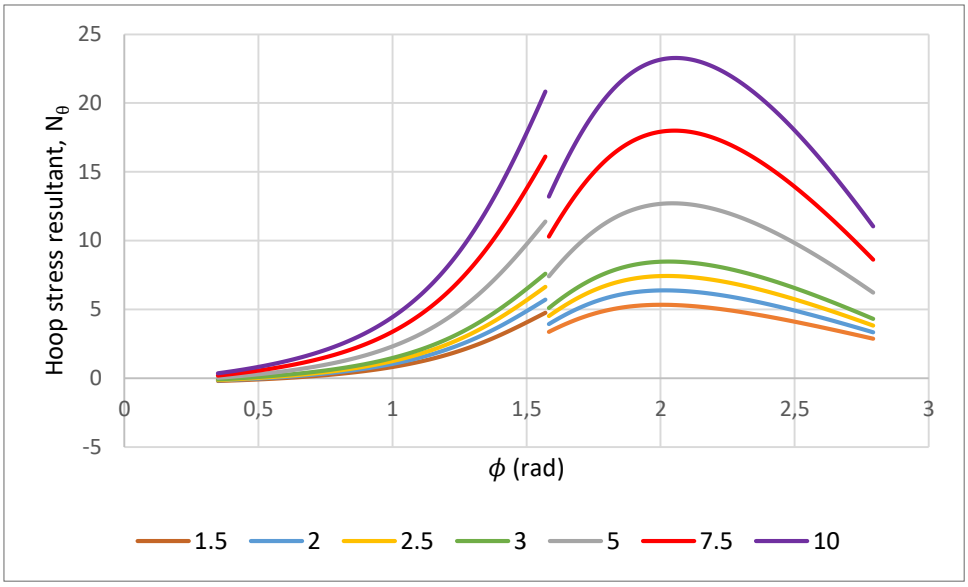

Figure 6-6: Hoop stress resultant, N_θ for a fixed aspect ratio of $\frac{b}{a} = 2$ and varying opening ratios for the outer surface of a prolate elliptical torus

6.2.1.3. Variation of aspect ratio

Figure 6-7 and Figure 6-8 show the variation of the aspect ratio for the outer surface of prolate elliptical toroidal shells for a fixed opening ratio of $\frac{A}{a}$=3. As mentioned above, the value of a is taken as 1m and the value of γ is taken as 1N/m^3.

Examining Figure 6-7, it can be seen that a change in the aspect ratio for a prolate elliptical toroidal shell induces a change the meridional stress resultants experienced for a given aspect ratio. For the upper half of the outer surface, as ϕ increases, not much variation is experienced for values of N_ϕ, except for a slight increase as ϕ tends to the support. However, for the lower half of the tank, it is evident that the larger the aspect ratio is, the greater the corresponding meridional stress resultant will be. The increase in the stress resultant is seen primarily at locations of ϕ just beyond the support and as ϕ increases to the bottom of the tank, the values of N_ϕ converge.

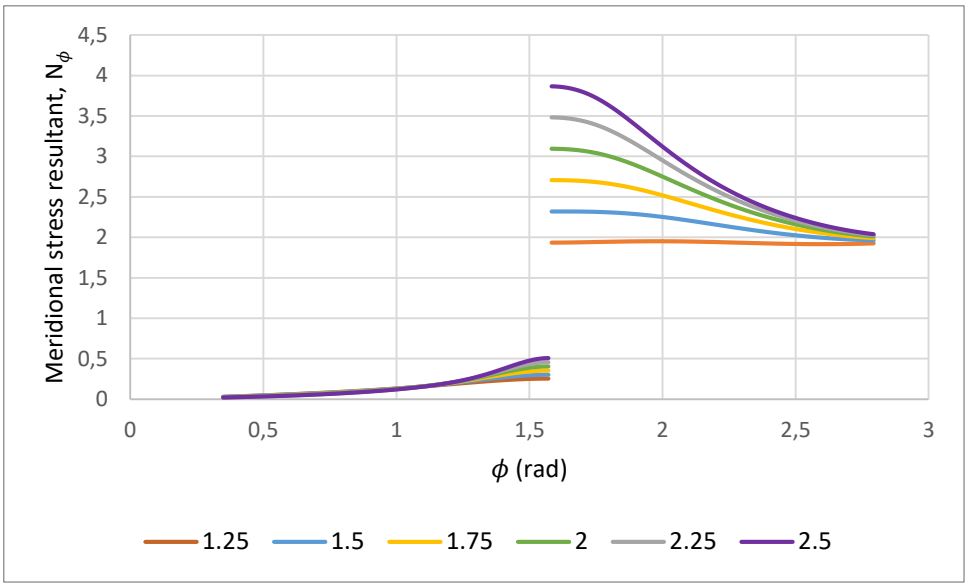

Figure 6-7: Meridional stress resultant, N_ϕ for a fixed opening ratio of $\frac{A}{a} = 3$ and varying aspect ratios for the outer surface of a prolate elliptical torus

Similarly, to the values of N_ϕ, for a given opening ratio, an increase in the aspect ratio for the outer surface of a prolate elliptical shell primarily corresponds to an increase in the circumferential stress resultant experienced. An exception to this occurs within the upper half of the outer surface, where a larger aspect ratio will for values of ϕ up to 1.1rad, be lesser than smaller aspect ratios, but after this point, will result in a larger hoop stress. Examining the lower half of the vessel, it can be seen that the greater the aspect ratio, the greater the value of N_θ. Although, an interesting trend observed, is that the location of the peak hoop stress is shifted lower down the vessel of the tank as the aspect ratio is increased, unlike for the variation of the opening ratio for a fixed aspect ratio, where it remained at a constant location. As ϕ tends to the bottom of the tank, the values of N_θ appear to converge.

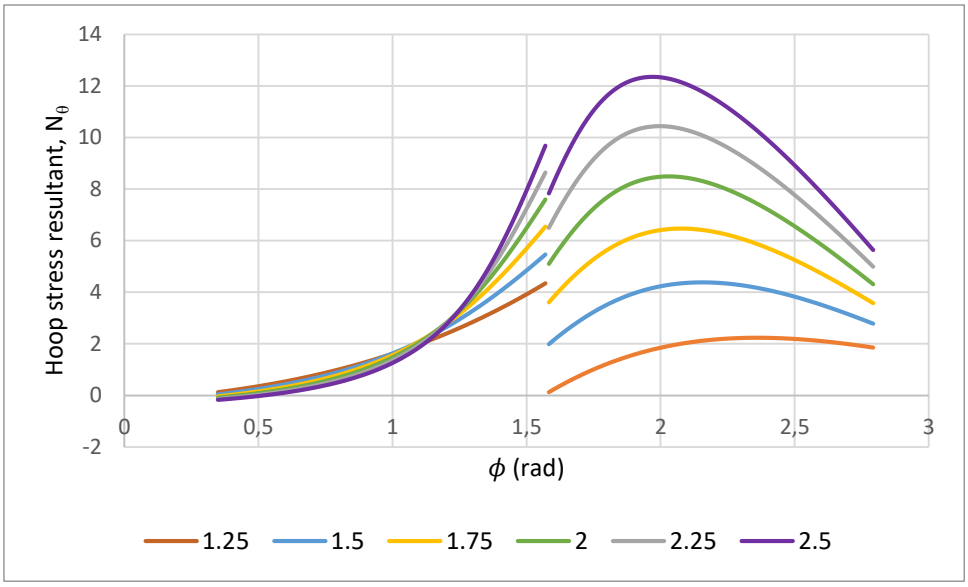

Figure 6-8: Hoop stress resultant, N_θ for a fixed opening ratio of $\frac{A}{a} = 3$ and varying aspect ratios for the outer surface of a prolate elliptical torus

6.2.2 Inner surface

6.2.2.1. Numerical example

The inner surface is characterised by $0° > \phi > \pi$ and the same parameters used for the outer surface for the prolate shell in 6.2.1.1 are used. Results for the numerical example of the inner surface are shown by Figure 6-9 and 6-10.

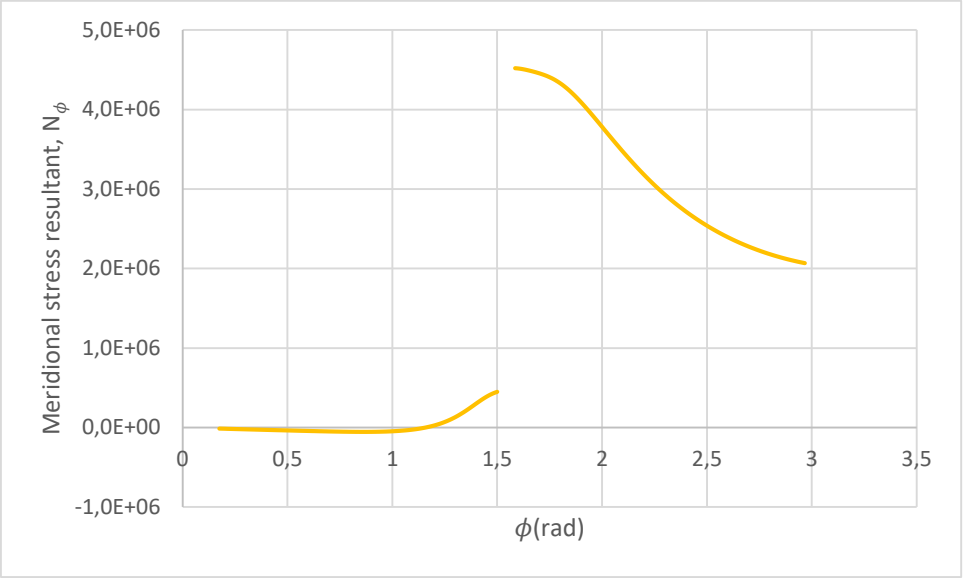

Figure 6-9: Meridional stress resultant for the outer surface of a prolate elliptic toroidal shell for A=30, a=10 and b=20m

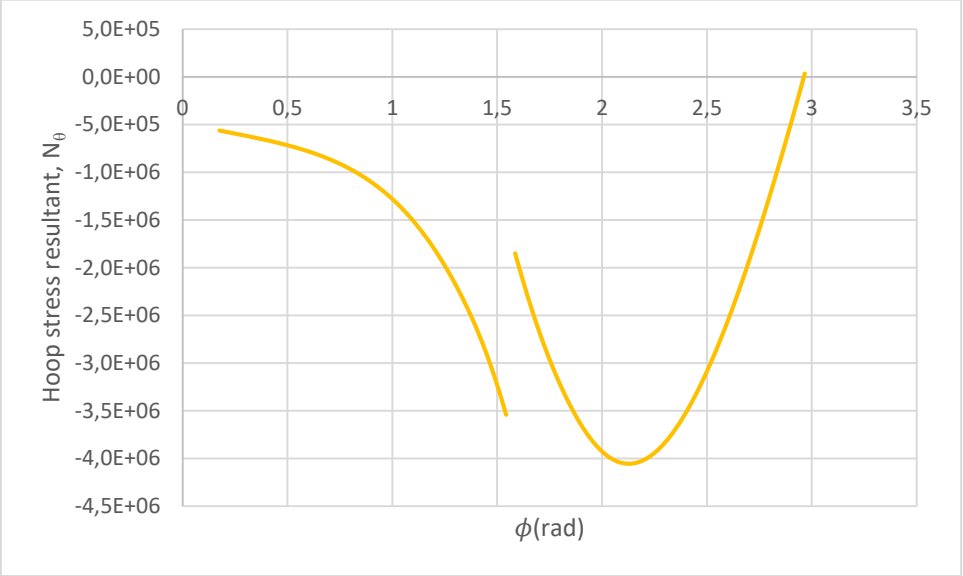

Figure 6-10: Hoop stress resultant for the outer surface of a prolate elliptic toroidal shell for A=30, a=10 and b=20m

As seen from the above charts, the stress resultants for both the meridional and hoop directions differ quite substantially for the inner surface of the torus in comparison to the outer surface. The value of N_ϕ is primarily in a low state of compression for the upper-inner region of the vessel, although becomes tensile as ϕ tends towards the support. For values of ϕ as one moves further down the tank, the meridional stress resultant decreases from large values occurring just after the location of the support. It is interesting to note that for the numerical example computed above, larger values of N_ϕ occur for the lower regions of the inner surface than the outer surface of the tank.

Whilst values of N_θ for the outer surface are primarily in tension, the inner surface does not follow suit, as for the entire domain investigated, the hoop stress resultant is in compression throughout. As one moves from the apex of the tank to the location of the interior support, the value of N_θ increases in compression. Values of ϕ after the support correspond to a slightly lower hoop stress, until a maximum compressive peak is reached, following which the value of N_θ has a lesser compressive stress resultant as one moves to the bottom of the tank. The profile of the shape in Figure 6-10 is almost a mirror image of Figure 6-4, although the magnitude of hoop stresses experienced is far greater for the outer surface of the tank than the inner.

6.2.2.2. Variation of opening ratio

The opening ratio is varied for a fixed aspect ratio of $\frac{b}{a} = 2$ as shown by the below Figures. Opening ratios are varied according to Table 6-1. For the parameters investigated, the value of a is taken as 1m and the value of γ is taken as 1N/m^3

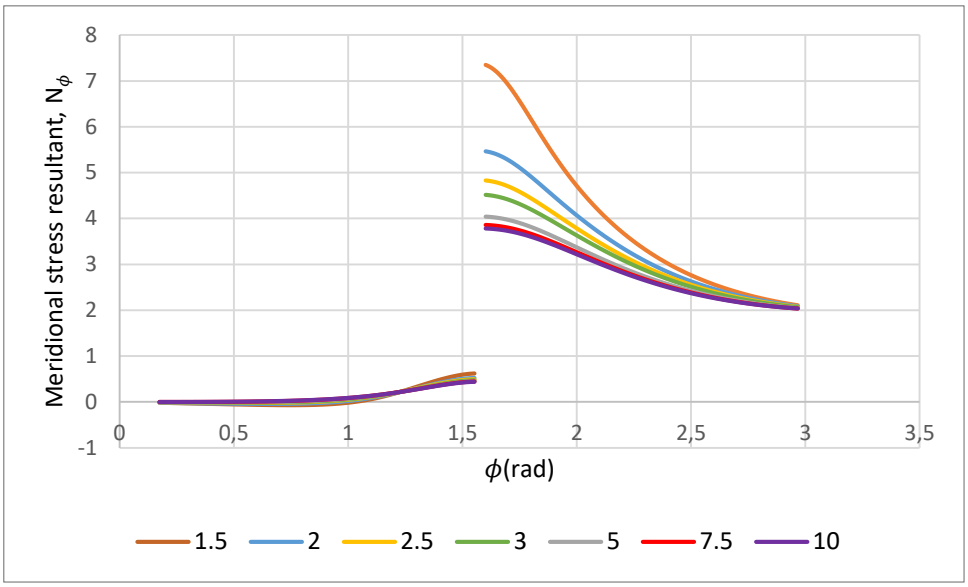

Figure 6-11: Meridional stress resultant, N_ϕ for a fixed aspect ratio of $\frac{b}{a} = 2$ and varying opening ratios for the inner surface of a prolate elliptical torus

Similarly to Figure 6-5, it can be inferred that for the upper half of the inner surface of the prolate tank, there is little variance in the meridional stress resultant experienced for a fixed aspect ratio and a variation of the opening ratio. However, unlike the outer surface of the vessel, the lower the opening ratio, the higher the meridional stress resultant experienced. As discussed in the numerical example for the inner surface above, the value of the meridional stress is greater for the inner surface than for the outer surface. Consequently, it is imperative that designers take this relationship into consideration, as a decrease in the opening ratio corresponds to higher values of N_ϕ for the outer-lower region of the shell.

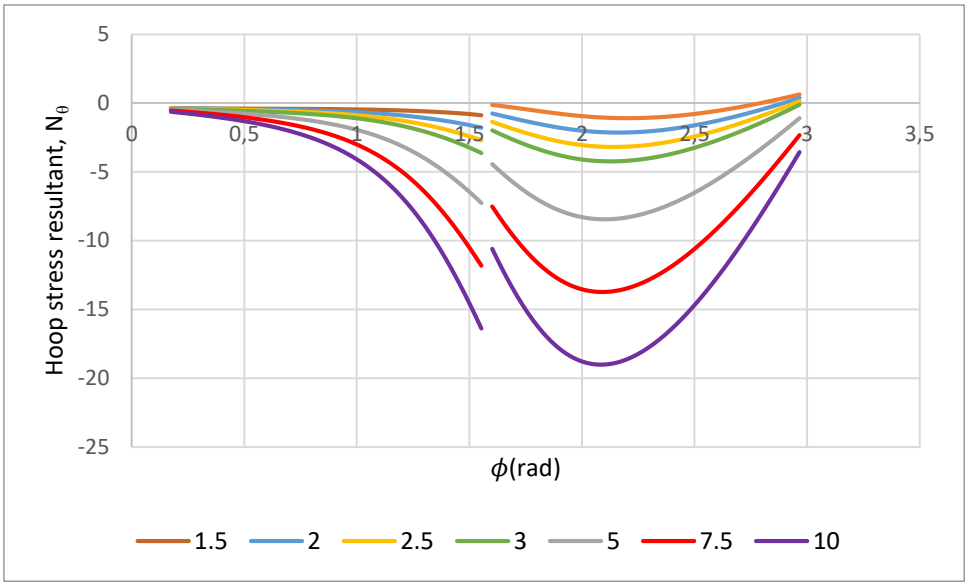

Figure 6-12: Hoop stress resultant, N_θ for a fixed aspect ratio of $\frac{b}{a} = 2$ and varying opening ratios for the inner surface of a prolate elliptical torus

For the hoop stresses within the inner surface, an increase in the opening ratio corresponds to an increase in the compressive values of N_θ, as similarly described for the outer surface of the tank in Figure 6-6. Compressive peaks occur sufficiently far away from the inner support and occur around the same location of ϕ for the given aspect ratio.

6.2.2.3. Variation of aspect ratio

Figure 6-13 and Figure 6-14 show the variation of the aspect ratio for the inner surface of prolate elliptical toroidal shells for a fixed opening ratio of $\frac{A}{a}$=3. The value of a and γ are taken as 1m and 1N/m^3 respectively.

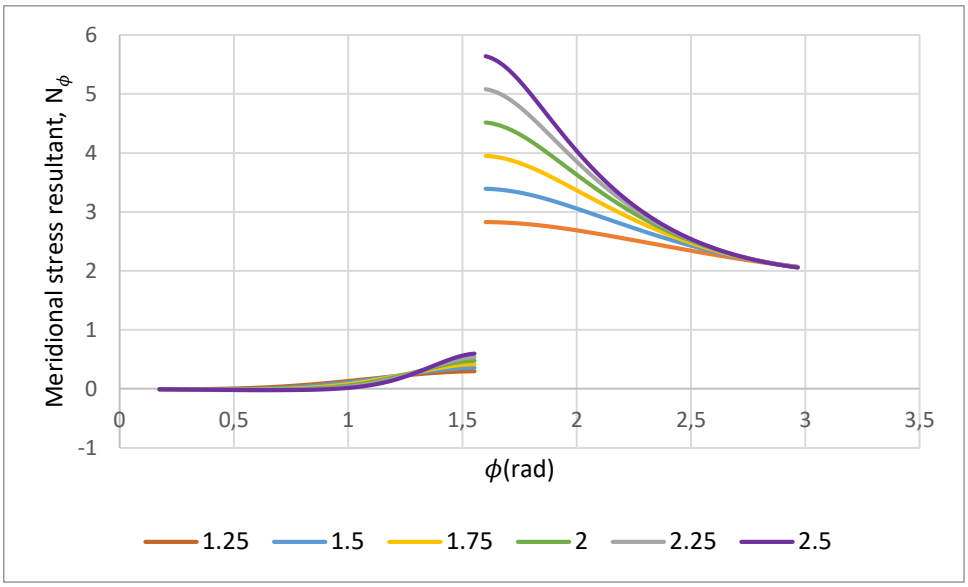

Figure 6-13: Meridional stress resultant, N_ϕ for a fixed opening ratio of $\frac{A}{a} = 3$ and varying aspect ratios for the inner surface of a prolate elliptical torus

The effect of the opening ratio has little effect on the meridional stress distribution for the upper-inner segment of the tank as shown above. There is little variation between values of N_ϕ for the upper half of the tank. The lower half of the tank, however, shows that an increase in the aspect ratio corresponds to an increase in the value of N_ϕ, although as ϕ tends to the lower region of the inner surface, the meridional stress resultants converge.

The hoop stress resultant for the inner surface of the prolate elliptical toroidal tank is however very different to the previous cases examined. As expected, for the upper-inner portion of the shell, an increase in the aspect ratio corresponds to an increase in the value of N_θ. However, for the lower region of the tank, a similar trend follows, with the exception that as the aspect ratio is decreased sufficiently small, the value of N_θ changes from compression to tension. Also, linked to this is that as the aspect ratio becomes smaller, the maximum compressive stress experienced for the hoop stress resultant profile occurs within the upper region of the inner surface of the tank.

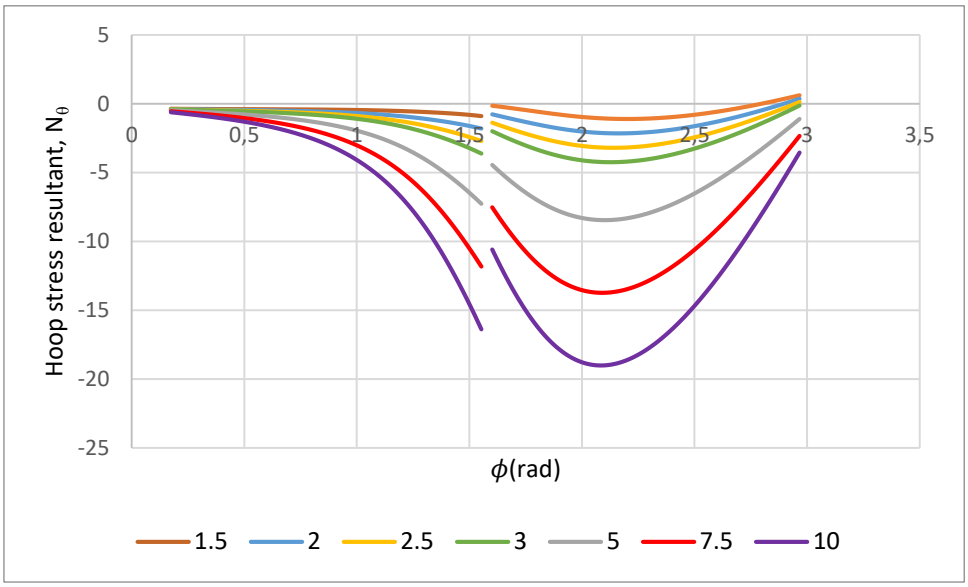

Figure 6-14: Hoop stress resultant, N_θ for a fixed opening ratio of $\frac{A}{a} = 3$ and varying aspect ratios for the inner surface of a prolate elliptical torus

6.3 Oblate toroidal shells

This sections deals with the membrane stresses of oblate toroidal shells. Similarly, as was done with the prolate toroidal shells, numerical examples and a variation of the opening and aspect ratios are considered for both the inner and outer surfaces of the torus are investigated.

6.3.1 Outer surface

6.3.1.1. Numerical example

A numerical example is shown by Figure 6-15 and Figure 6-16 below. A relatively large, oblate toroidal shell, fabricated from steel with the following properties $E = 200\text{GPa}$ and $\nu = 0.3$ and a constant thickness is assumed. The tank has the following geometric characteristics: $A = 30\text{m}$, $b = 10\text{m}$ and $a = 20\text{m}$ and is assumed to be filled with water, having a unit weight of $\gamma = 10\text{kN/m}^3$.

Examining Figure 6-3 in comparison to Figure 6-15, it is immediately evident that the meridional stress profile is vastly different between the two. For the outer surface of oblate toroidal shells, the tank is in tension for all values of ϕ examined. The upper region gradually decreases in tension as the location of the support is reached, whilst the lower half of the tank has the meridional stress resultant increasing with increasing ϕ and the maximum value of N_ϕ occurring at the lowest location of the shell investigated. This indicates that for the membrane solution, there may be large stresses occurring at this location, which is not present for the prolate shell.

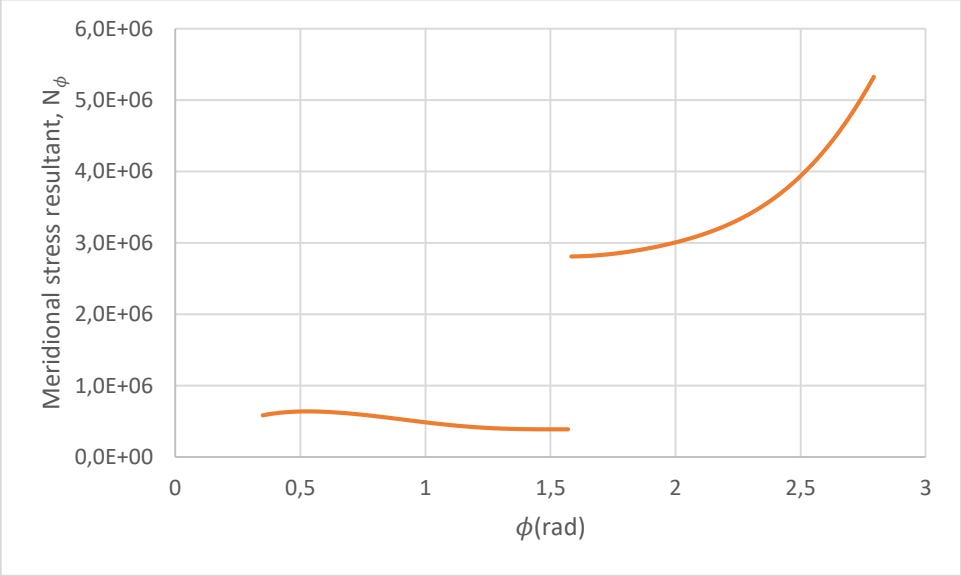

Figure 6-15: Meridional stress resultant, N_ϕ for the outer surface of an oblate elliptic toroidal shell for A=30, a=20 and b=10m

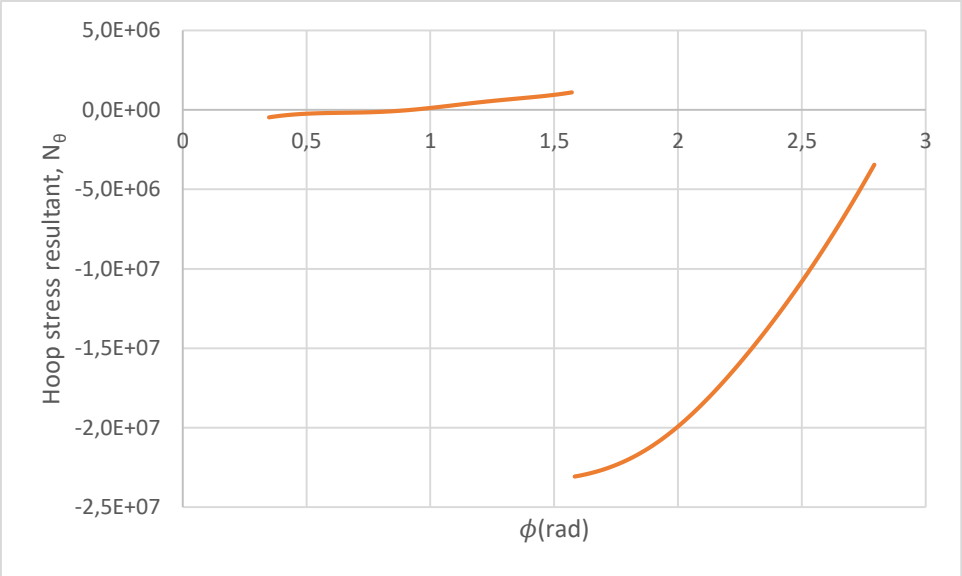

Figure 6-16: Hoop stress resultant, N_θ for the outer surface of an oblate elliptic toroidal shell for A=30, a=20 and b=10m

The hoop stress resultant profile is also substantially different to its prolate counterpart. For the upper region of the outer surface, the circumferential stress is negligible in comparison with the lower half of the tank, although it is noted that as ϕ increases, there is a corresponding increase in the value of N_θ. The lower half of the tank is however completely in compression, although as ϕ moves from the location of the support to the bottom of the tank, the magnitude of the compressive stress decreases. This can be contrasted with the hoop stress resultant profile for a prolate elliptical toroidal shell, where the value of N_θ is in tension throughout the outer surface.

6.3.1.2. Variation of opening ratio

The opening ratio is varied for a fixed aspect ratio of $\frac{b}{a} = 0.5$ as shown by the below Figures. Opening ratios are varied according in the same manner as previously investigated. For the parameters investigated, the value of a is taken as 1m and the value of γ is taken as 1N/m^3.

As seen from Figure 6-17, it can be seen that for a fixed aspect ratio and varying the opening ratio, there is little effect on the meridional stress profile of the outer surface of the oblate torus. For the upper region of the tank, there is no variation in the meridional

stress resultant as ϕ increases to the location of the support. As one moves down the outer surface of the tank after the support, it can be seen that an increase in the opening ratio corresponds to an increase in the value of N_ϕ.

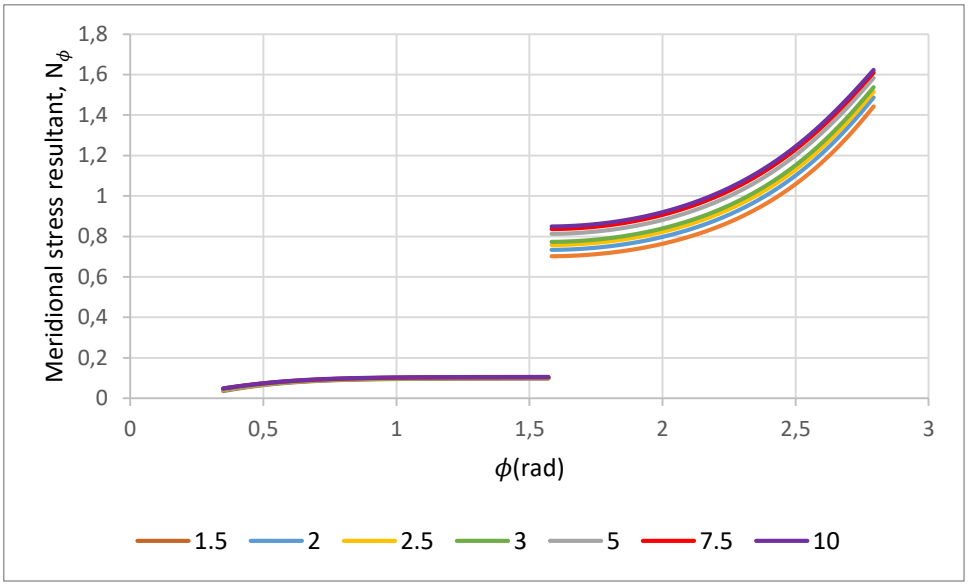

Figure 6-17: Meridional stress resultant, N_ϕ for a fixed aspect ratio of $\frac{b}{a}$=0.5 and varying opening ratios for the outer surface of an oblate elliptical torus

For a fixed aspect ratio, the hoop stress resultant does not vary substantially for the upper region of the outer surface of the oblate toroidal tank, although it is noted that the larger opening ratio corresponds to a slightly larger stress resultant experienced for this portion of the shell. Similarly, for the lower portion of the outer surface of the vessel, for an increase in the opening ratio, a corresponding increase in N_θ is experienced. Although, it is noted that the larger the opening ratio, the value of N_θ will be increased proportionally.

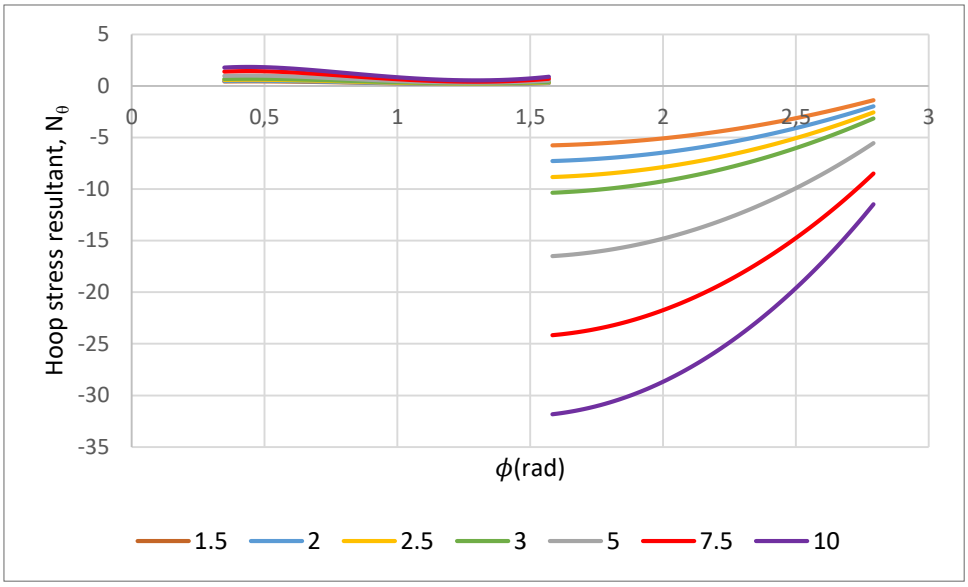

Figure 6-18: Hoop stress resultant, N_θ for a fixed aspect ratio of $\frac{b}{a}$=0.5 and varying opening ratios for the outer surface of an oblate elliptical torus

6.3.1.3. Variation of aspect ratio

Figure 6-13 and Figure 6-14 show the variation of the aspect ratio for the inner surface of oblate elliptical toroidal shells for a fixed opening ratio of $\frac{A}{a}$=3. The value of a and γ are taken as 1m and 1N/m^3 respectively.

For the upper region of the outer surface of an oblate toroidal shell, a decrease in the aspect ratio for a fixed opening ratio corresponds to a slight increase in the magnitude of N_ϕ. This increase becomes more apparent as ϕ increases to the location of the support. Similarly, for the outer-lower portion of the tank, a decrease of the aspect ratio results in an increase of the tensile stress, although as ϕ tends to the bottom of the tank, the value of N_ϕ converges.

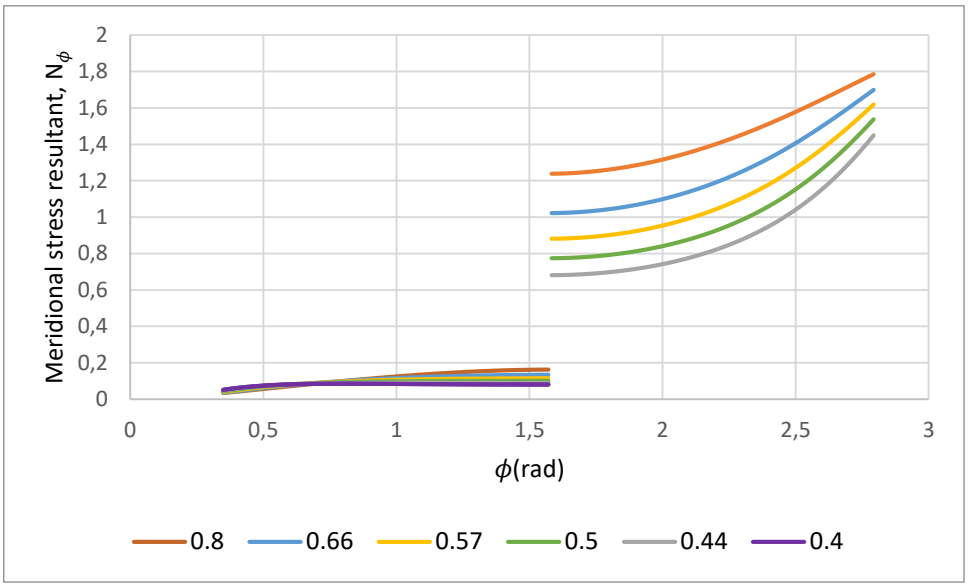

Figure 6-19: Meridional stress resultant, N_ϕ for a fixed opening ratio of $\frac{A}{a}$=3 and varying aspect ratios for the outer surface of an oblate elliptical torus

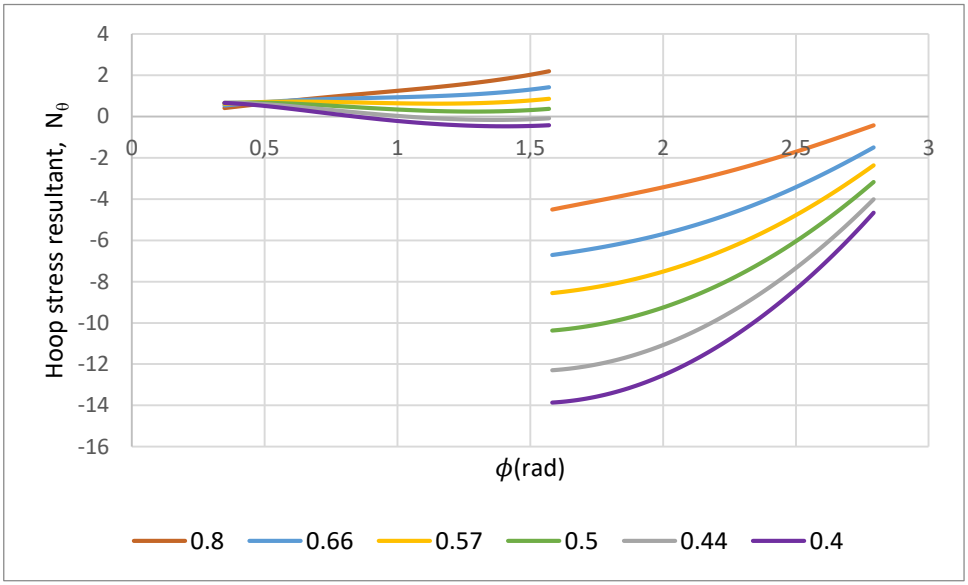

Figure 6-20: Hoop stress resultant, N_θ for a fixed opening ratio of A/a=3 and varying aspect ratios for the outer surface of an oblate elliptical torus

Figure 6-20 demonstrates the effects of a change in the aspect ratio for a fixed opening ratio for the outer surface of an oblate elliptic torus. For the upper-outer region of the tank, it is shown that for large aspect ratios, or as the oblate cross-section tends to a circular one, the hoop stress resultant is positive and becomes more and more tensile as ϕ increases. However, as the aspect ratio decreases and ϕ increases, the intial tensile stress becomes more compressive as ϕ increases towards the support. Examining the lower region of the vessel, a decrease in the aspect ratio results in higher compressive hoop stresses experienced.

6.3.2 Inner surface

6.3.2.1. Numerical example

The inner surface is characterised by $0° > \phi > \pi$ and the same parameters used for the outer surface for the prolate shell in 6.3.1.1 are used. Results are shown by Figure 6-21 and Figure 6-22.

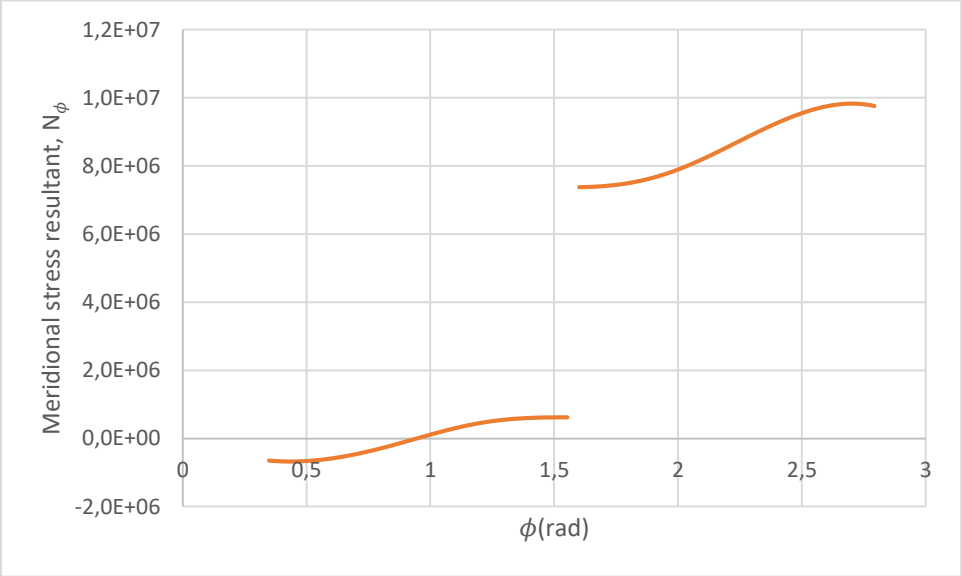

Figure 6-21: Meridional stress resultant, N_ϕ for the inner surface of an oblate elliptic toroidal shell for A=30, a=20 and b=10m

As seen from the above chart, at a distance sufficiently far from the top of the vessel, the meridional stress resultant of the tank is originally in compression, but as ϕ increases,

becomes more tensile as ϕ moves towards the supports. The same trend is followed of the lower half of the inner surface of the tank, whereby the tensile stress increases with increasing ϕ. As was found for the prolate numerical example in Section 6.2, the magnitude of the meridional stress is greater at the inner surface of the shell than the outer.

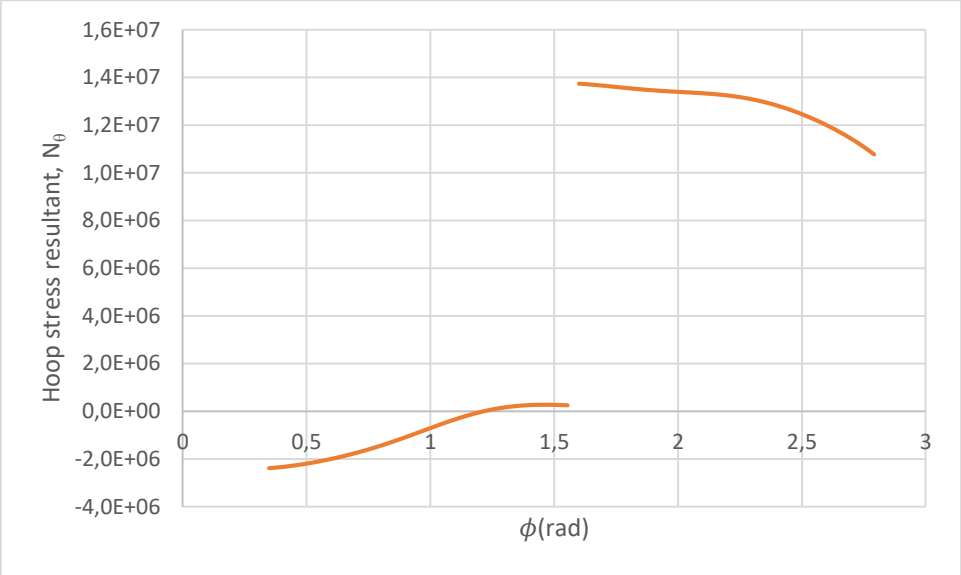

Figure 6-22: Hoop stress resultant, N_θ for the inner surface of an oblate elliptic toroidal shell for A=30, a=20 and b=10m

For the inner surface of the oblate shell, the hoop stress resultant is initially in compression for low values of ϕ, but as ϕ increases towards the support, the value of N_θ becomes tensile in nature. The lower half of the tank is completely in tension, decreasing as ϕ increases to the bottom of the vessel. This is contrasted to the prolate elliptic torus, which experiences compression in the lower-inner region.

6.3.2.2. Variation of opening ratio

The opening ratio is varied for a fixed aspect ratio of $\frac{b}{a} = 0.5$ as shown by the below Figures. Opening ratios are varied according to Table 6-1. Parameters are taken at unity.

Similarly, to the results presented for the outer surface, there is little effect on meridional stress resultants for the upper region of the inner surface of the tank for a fixed aspect ratio and a change in the opening ratio. However, interestingly enough, the meridional stress distribution for the lower region of the tank decreases with an increase in the aspect ratio. Similar results were found for the same case for prolate elliptical toroidal shells, indicating that designers who wish to constrain the stresses by limiting the opening ratio are required to be aware of this occurrence.

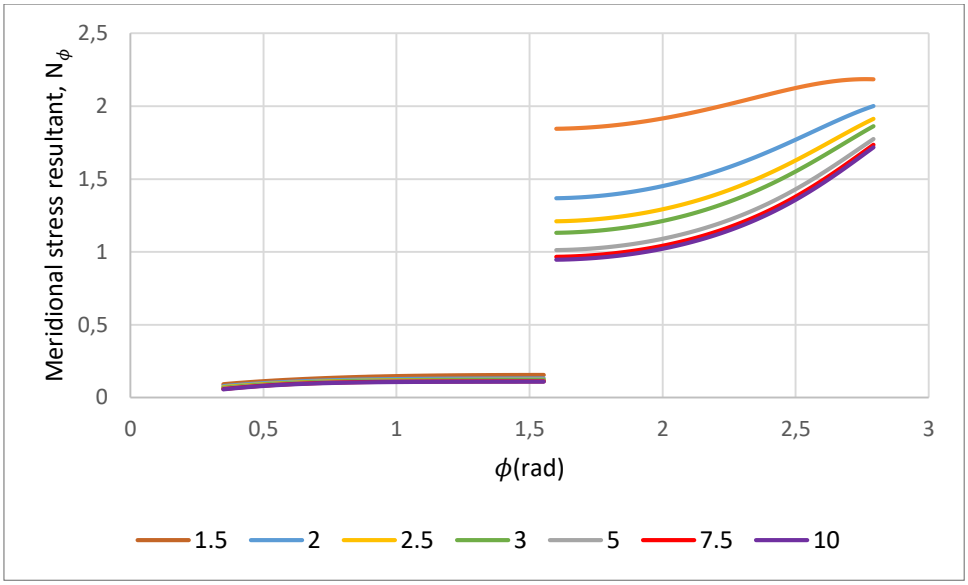

Figure 6-23: Meridional stress resultant, N_ϕ for a fixed aspect ratio of b/a=0.5 and varying opening ratios for the inner surface of an oblate elliptical torus

For a given aspect ratio and varying the opening ratio, the hoop stress resultant for the inner-upper region of the tank has little variation occurring. The lower segment, however shows that an increase in the opening ratio corresponds to a proportional increase of the stress experienced in the shell.

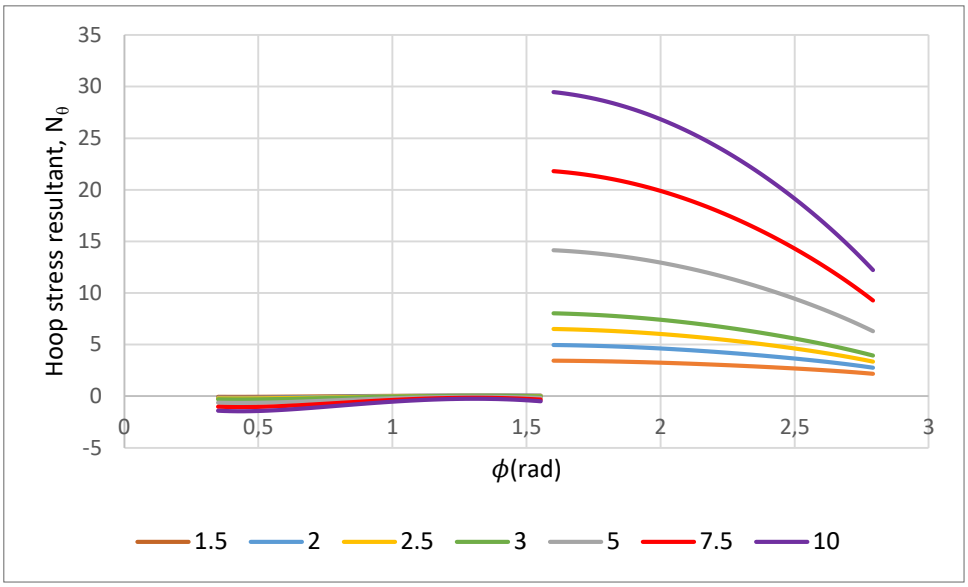

Figure 6-24: Hoop stress resultant, N_θ for a fixed aspect ratio of b/a=0.5 and varying opening ratios for the inner surface of an oblate elliptical torus

6.3.2.3. Variation of aspect ratio

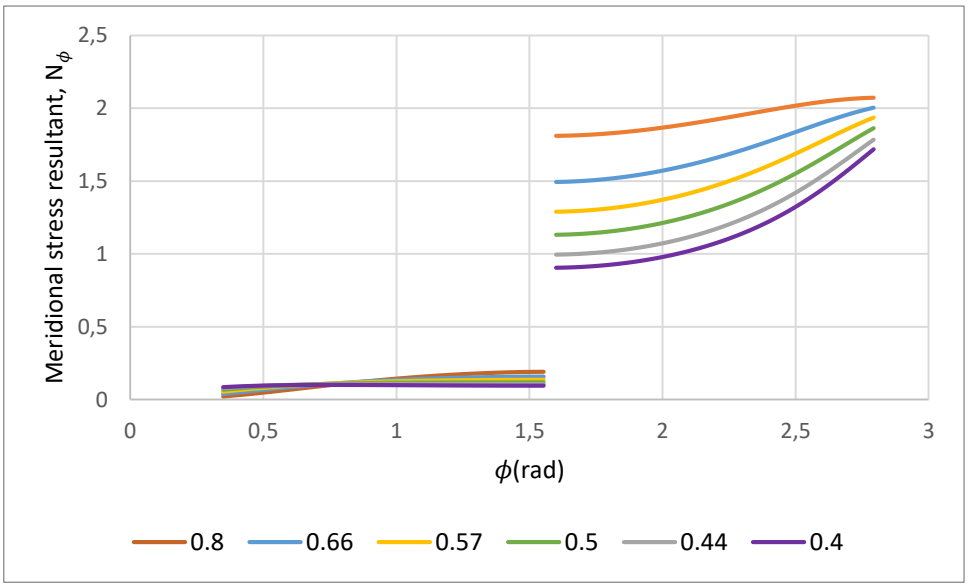

Figure 6-25: Meridional stress resultant, N_ϕ for a fixed opening ratio of A/a=3 and varying aspect ratios for the inner surface of an oblate elliptical torus

For a fixed opening ratio, a decrease in the aspect ratio for oblate toroidal shells decreases the meridional stress resultant slightly as ϕ increases for the inner-upper region of the tank. Examining the lower region shows that a decrease in the opening ratio corresponds to a decrease in the meridional stress of the shell. This is similar to the relationship between the decreasing opening ratio and values of N_ϕ found for the outer surface of the tank.

Throughout the inner surface of the tank, a decrease in the aspect ratio corresponds to a lower hoop stress resultant. As the aspect ratio is more circular in nature, the hoop stress for the upper-inner region of the tank is tensile, but as the cross-section of the oblate ellipse becomes more elongated, the hoop stress resultant decreases in magnitude.

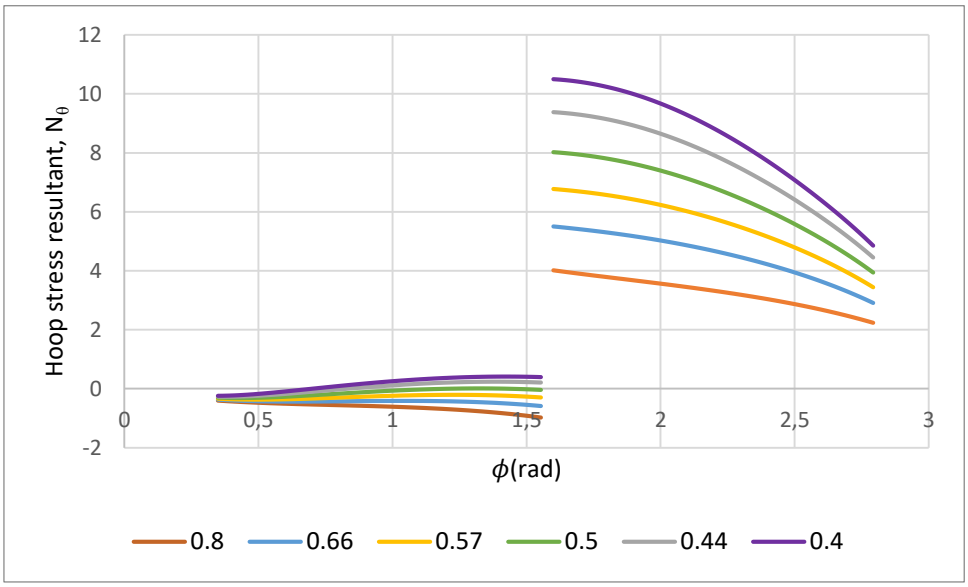

Figure 6-26: Hoop stress resultant, N_θ for a fixed opening ratio of A/a=3 and varying aspect ratios for the inner surface of an oblate elliptical torus

6.4 Circular toroidal shells

The derivation for the hydrostatically loaded circular torus has already been investigated by Enoma et al (2015). This section is used for comparison against prolate

and oblate elliptical toroidal shells. The geometry of the circular shell is vastly different to the elliptical, owing to the fact that a circular cross-section has an aspect ratio equal to 1. Consequently, only the effect of the opening ratio is examined for both the outer and inner surfaces of circular toroidal shells. Similarly, to the results presented for elliptical toroidal tanks, the value of a and γ are taken as unity.

6.4.1 Outer surface

As previously examined by Figure 6-5, Figure 6-27 shows the effect of increasing the aspect ratio has little effect on the meridional stress resultant of the outer-upper region of the tank. However, in the lower portion of the tank, an increase in the aspect ratio corresponds to an increase in the stress experienced, although it is noticed that an increase in the aspect ratio, does not correlate to a substantially large increase in the meridional stress, as there is little difference between peak values of $\frac{A}{a} = 1.5$ and $\frac{A}{a} = 10$, occurring towards the bottom of the vessel.

As seen from Figure 6-28, the opening ratio has a substantial effect on the value of N_θ, for both the upper and lower region of the outer surface of the tank. The effects appear to be proportional, as there are linear increases in the hoop stress resultant for a constant increase in the opening ratio. It is also interesting to observe for low opening ratios, the bottom of the tank is originally in compression after the support, but becomes more tensile in nature as ϕ tends to the bottom of the tank.

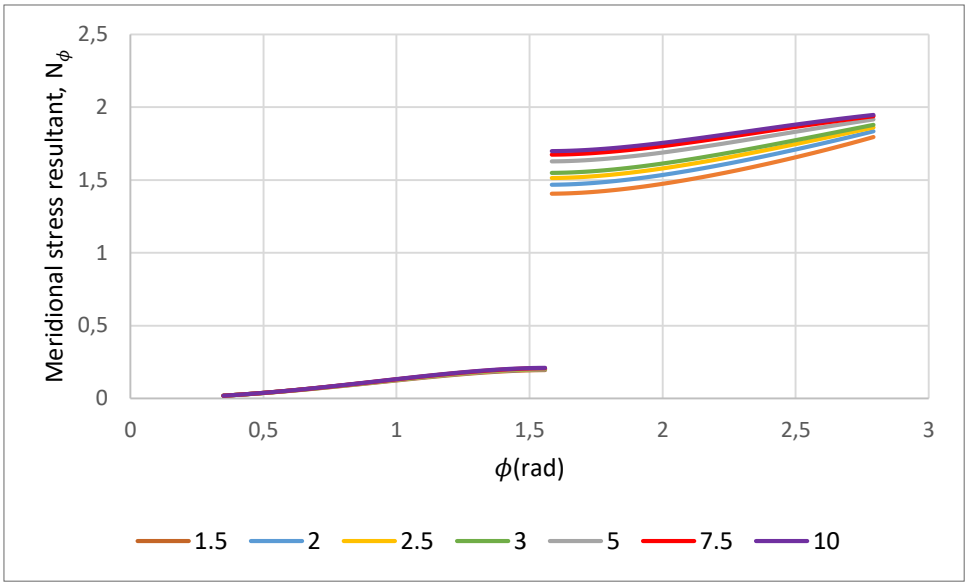

Figure 6-27: Meridional stress resultant for the outer surface of a circular torus, with varying aspect ratios

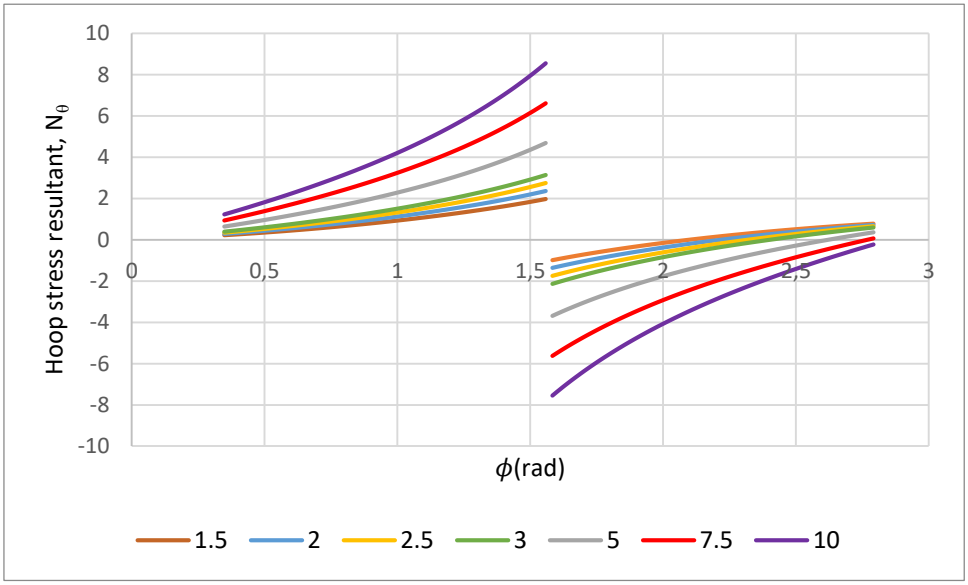

Figure 6-28: Hoop stress resultant for the outer surface of a circular torus, with varying aspect ratios

6.4.2 Inner surface

As was observed for both the prolate and oblate elliptical toroids, an increase in the opening ratio for the inner surface of circular toroidal shells corresponds to a lower meridional stress resultant experienced for the lower region of the tank. The values also converge as ϕ tends to the bottom of the vessel,

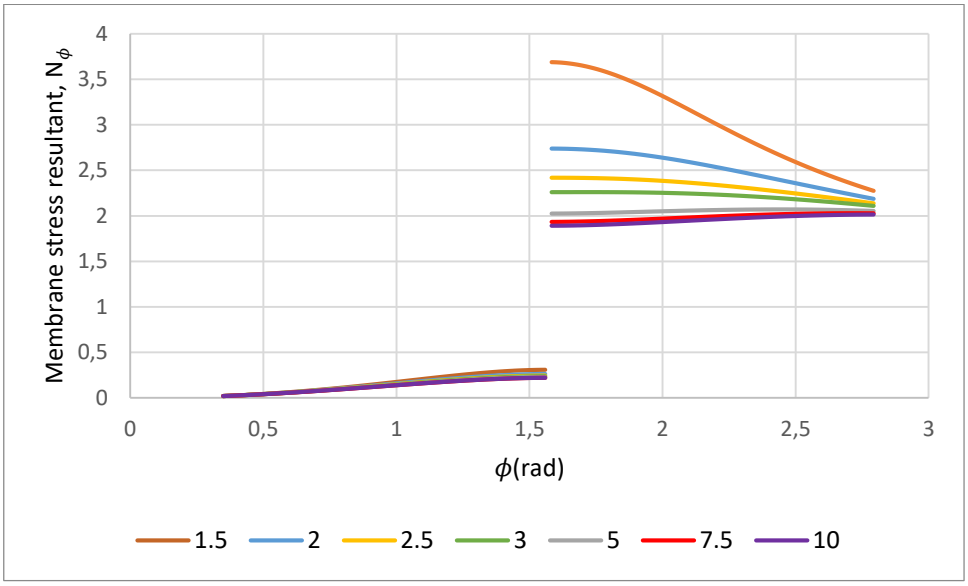

Figure 6-29: stress resultant for the inner surface of a circular torus, with varying aspect ratios

As similarly described for the outer surface, an increase in the opening ratio corresponds to higher magnitudes of hoop stress for both the upper and lower regions of the inner surface of the circular toroidal tank.

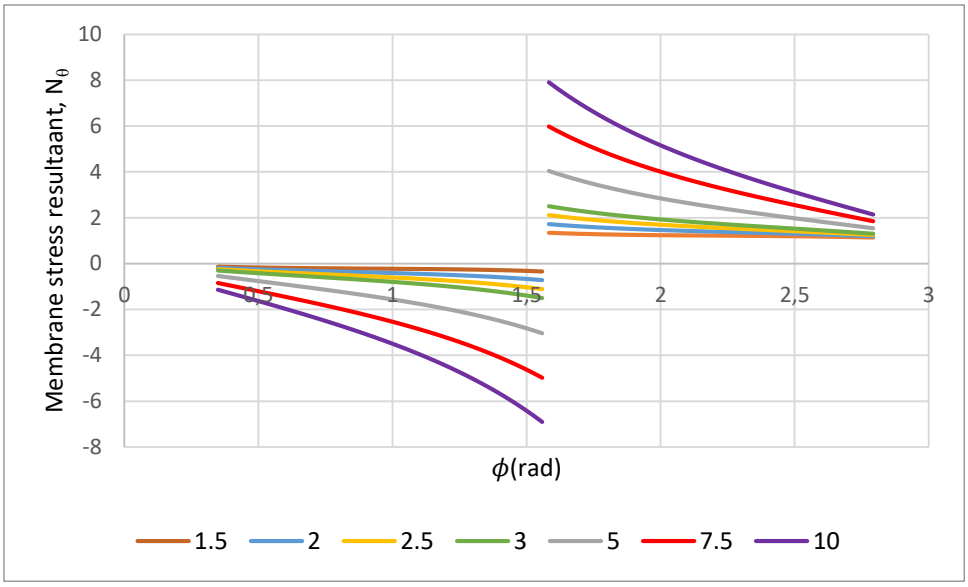

Figure 6-30: Hoop stress resultant for the inner surface of a circular torus, with varying aspect ratios

6.5 Conclusions

This chapter dealt with various cross-sectional profiles for prolate, circular and oblate toroidal tanks. Values, as far as possible, were taken at unity, to ensure that designers would have an idea of the sensitivity of stress distributions for various parameters of hydrostatically loaded toroidal tanks, relative to the parameters used. Membrane stress resultants were investigated, in both the meridional and hoop directions and it is recommended that designers investigate the stresses due to bending and edge effects when making final designs, as these effects are beyond the scope of this investigation.

Chapter 7

Numerical comparisons

In order to ensure that recommendations are made for designers, numerical examples are investigated for fixed volumes of toroidal tanks. Membrane stresses are examined comparing the various types of toroidal shells against each other. Two cases of toroidal tanks are investigated within this chapter, the first of which compares the aspect ratio for a fixed volume of elliptical and circular tanks, keeping the value of A constant throughout and examining the membrane stresses occurring throughout the tank, in addition to the surface area required for fabrication. Secondly, various prolate, oblate and circular shells, with constant aspect ratio but varying the opening ratio are compared in a similar manner. Thicknesses throughout this chapter are ignored as only the stress resultants are investigated.

7.1 Effect of aspect ratio

As similarly investigated in Chapter 6, the outer and inner surfaces are compared separately to each other. There are five different shells investigated, two prolate and oblate elliptical toroids and a circular. Their properties are as given below in m:

Table 7-1: Geometric properties of investigated shells for a fixed value of A

Type of shell	a(m)	b(m)	A(m)	Surface area(m^2)	Volume(m^3)
Prolate 1	10.6	21.21	30	19364	133239
Prolate 2	12.25	18.38	30	18320	133239
Circular	15	15	30	17765	133239

Oblate 1	18.38	12.25	30	18320	133239
Oblate 2	21.21	10.6	30	19364	133239

7.1.1 Outer surface

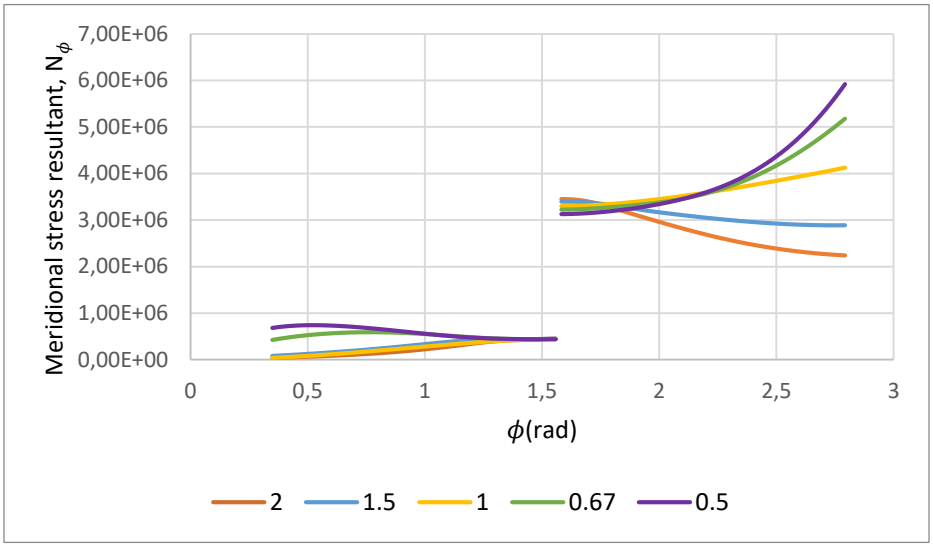

Figure 7-1: Meridional stress resultants for the outer surface of various toroidal tanks, defined by their aspect ratio for a fixed volume and opening

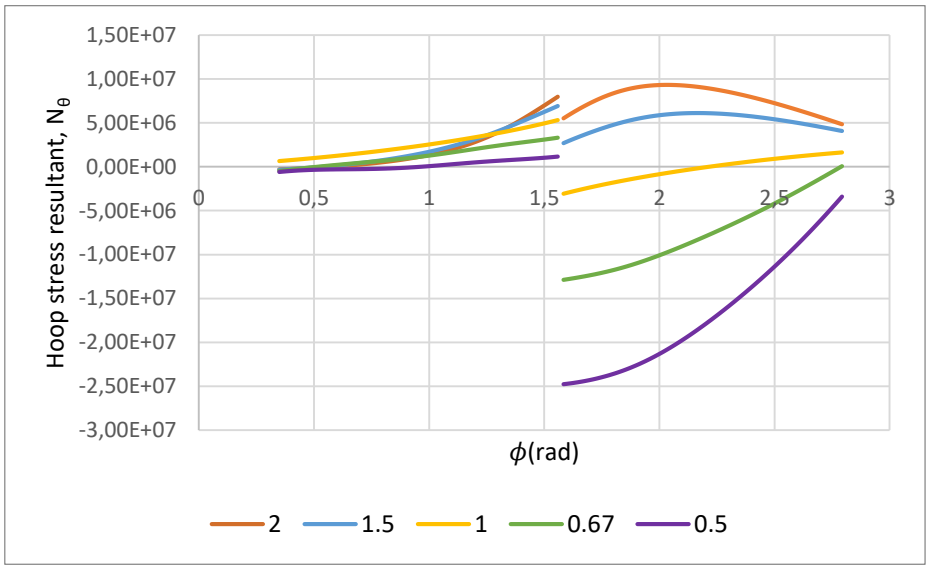

Figure 7-2: Hoop stress resultants for the outer surface of various toroidal tanks, defined by their aspect ratio for a fixed volume and opening

7.1.2 Inner surface

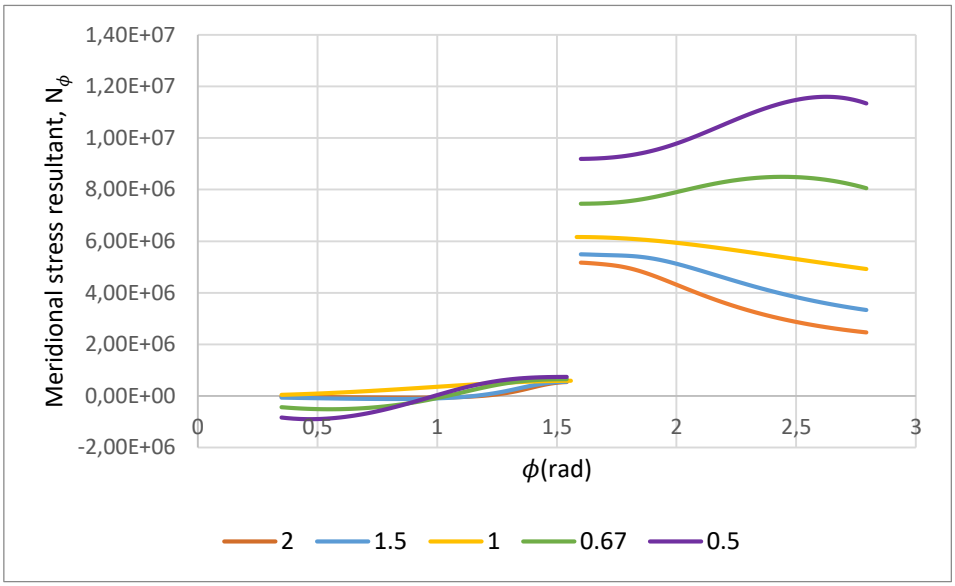

Figure 7-3: Meridional stress resultants for the inner surface of various toroidal tanks, defined by their aspect ratio for a fixed volume and opening

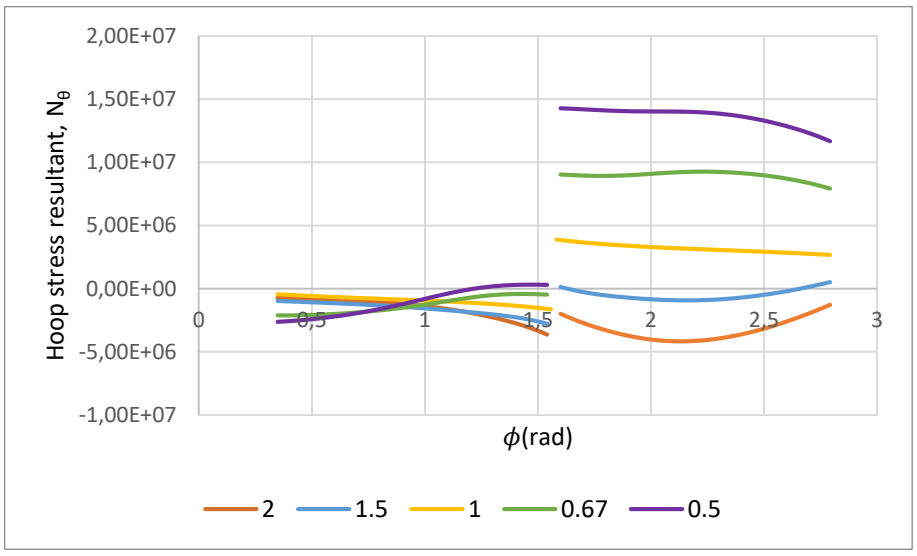

Figure 7-4: Hoop stress resultants for the inner surface of various toroidal tanks, defined by their aspect ratio for a fixed volume and opening

Examining Figure 7-1 and Figure 7-3, the oblate elliptical shell has the greatest magnitude for the meridional stress resultant, with peak stresses occurring towards the bottom of the tank for both prolate shells investigated. Circular toroidal shells, with an aspect ratio midway the prolate and oblate shells, have stresses occurring in between the prolate an oblate and are comparatively greater in magnitude than the prolate shells investigated. Prolate shells have comparatively the lowest meridional stress values, as an aspect ratio of $\frac{b}{a} = 2$ has stresses almost three times as less for the outer surface and almost six times as less for the inner surface when compared against the peak stresses of an oblate shell with an aspect ratio of $\frac{b}{a} = 0.5$. This indicates that when investigating the meridional stresses occurring sufficiently far away from the presence of edge effects a prolate shell, with increasing aspect ratio would be a favourable choice, for toroidal shells having a constant volume and constant opening.

Figure 7-2 and Figure 7-4 show the circumferential stresses for the same toroidal shells. Similar trends occur, with oblate elliptical shells having a greater magnitude for their stress resultants for both the inner and outer surfaces in comparison to circular and prolate cross-sections, with the peak value of N_θ being negative for the outer surface. Based on this, one would prefer to employ prolate shells, however, it is noted that as the aspect ratio is increased, compressive hoop stresses occur for the inner surface, which if increased sufficiently, may result in buckling occurring. However, the prolate shell with an aspect ratio of $\frac{b}{a} = 1.5$, has little compressive circumferential stresses occurring for both the inner surface, in addition to having lower peak values than the prolate cross section with an aspect ratio of $\frac{b}{a} = 2$.

Table 7-1 shows the surface area for each of the shells investigated and it can immediately be seen that circular cross-sections for a fixed volume and fixed value of A have the lowest surface area in comparison to its elliptical counterparts. Based on these factors, it is recommended that should designers are investigating the membrane stresses for a fixed volume and fixed opening, that a trade-off between prolate and circular cross-sections are made, in order to minimise the cost involved and ensure that structural integrity of the shell remains, similar to recommendations made by Vu et al (2010).

7.2 Effect of opening ratio

The effect of keeping the aspect ratio constant for prolate and circular toroidal shells for a fixed volume and varying the opening ratio is investigated in this section. Oblate shells are not investigated due to the better structural capabilities of prolate shells as established in 7.1. Aspect ratios are kept constant at $\frac{b}{a} = 2$. Prolate shells investigated have the following geometric properties:

Table 7-2: Geometric properties of investigated prolate shells for a fixed aspect ratio of 2

Opening ratio (A/a)	a(m)	b(m)	A(m)	Surface area(m^2)	Volume(m^3)
2	11.45	22.9	22.9	15962	118435
3	10	20	30	18262	118435
4	9.09	18.17	36.34	20100	118435

7.2.1 Prolate tanks

7.2.1.1. Outer surface

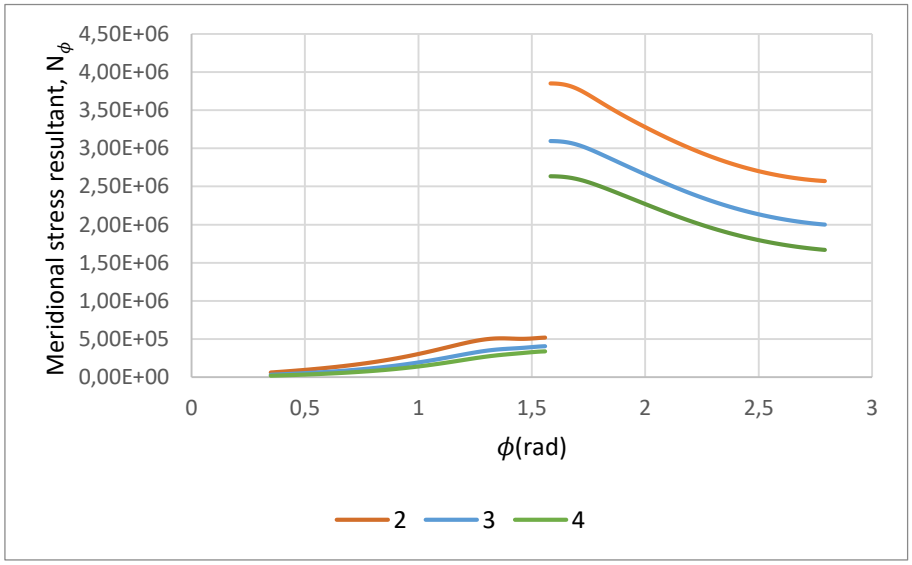

Figure 7-5: Meridional stress resultant profiles for the outer surface of prolate shells with a fixed aspect ratio of b/a = 2 and volume, with varying opening ratios

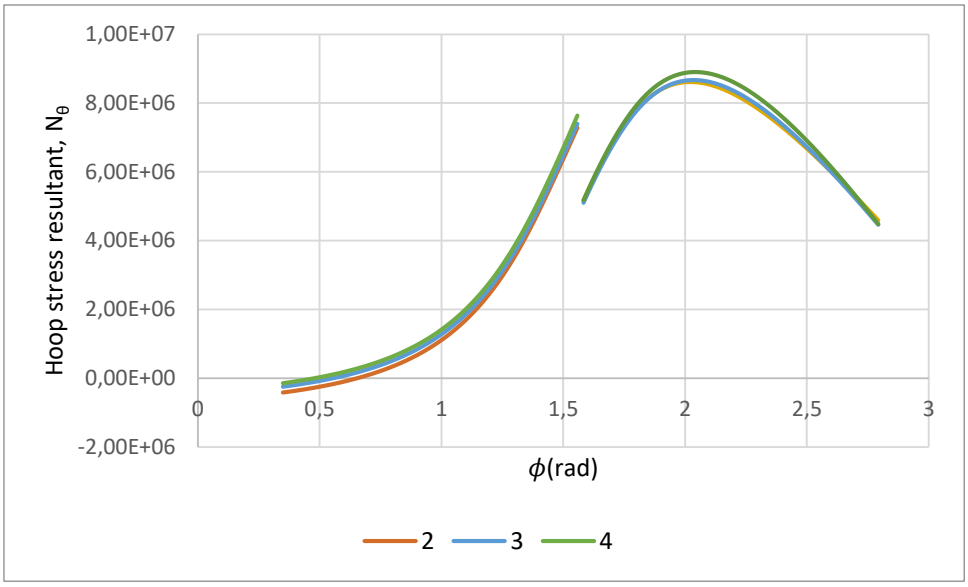

Figure 7-6: Hoop stress resultant profiles for the outer surface of prolate shells with a fixed aspect ratio of b/a = 2 and volume, with varying opening ratios

7.2.1.2. Inner surface

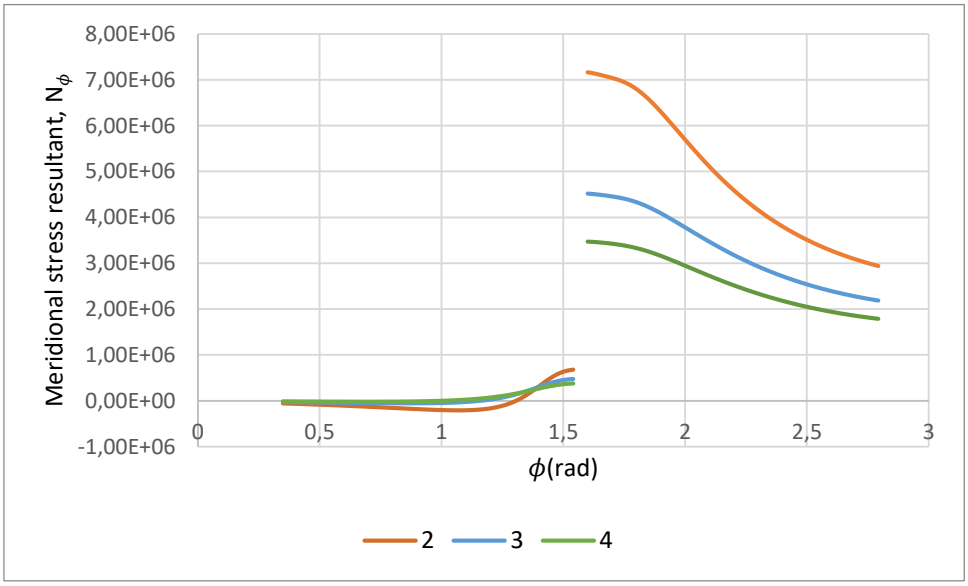

Figure 7-7: Meridional stress resultant profiles for the inner surface of prolate shells with a fixed aspect ratio of b/a = 2 and volume, with varying opening ratios

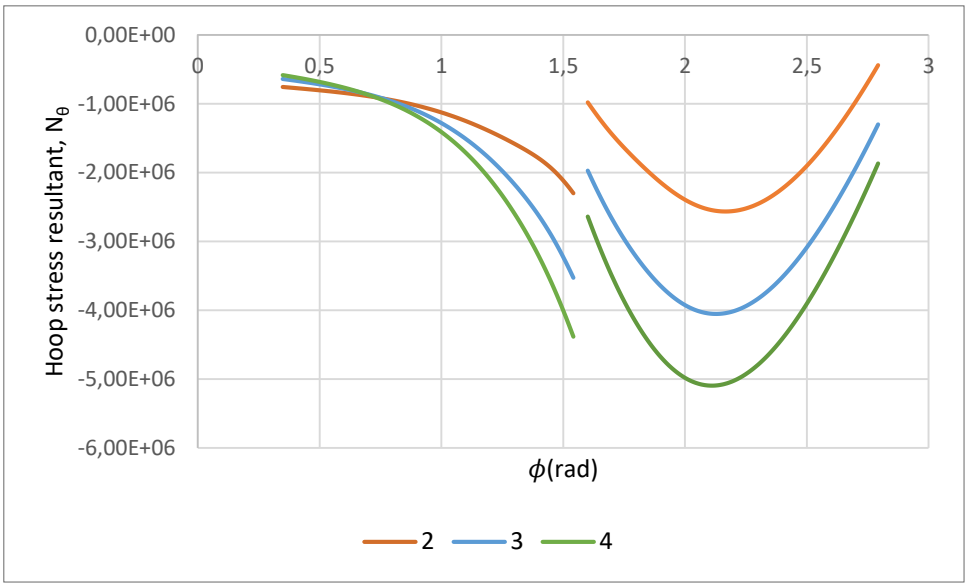

Figure 7-8: Hoop stress resultant for the inner surface of prolate shells with a fixed aspect ratio of b/a = 2 and volume, with varying opening ratios

Figure 7-5 and Figure 7-7 show the meridional profile for the outer and inner surface of the various prolate tanks respectively. For the fixed volume, opening ratios are varied, the charts indicate that mainly the lower region of the tank, for both the inner and outer surfaces are affected by the change in opening ratio. Peak membrane stresses occur just after the location of the support and a smaller opening ratio results higher stress resultants experienced by the shell. This reinforces the findings as established in Chapter 6.

Hoop stresses are however different in comparison. The outer surface sees no noticeable difference in the value of N_θ as the opening ratio is changed. The inner surface sees a far greater response to the opening ratio as an increase corresponds to greater compressive stresses experienced, which could possibly lead to the occurrence of buckling.

As expected, a smaller opening ratio corresponds to a smaller surface area obtained, but this also results in greater meridional stresses. Conversely, a larger opening ratio leads to larger compressive hoop stresses experienced, which may pose a greater problem, in

addition to a larger cost due to the increase in surface area. It is recommended that depending on the constraints the designer is facing, that a trade-off between keeping the opening ratio small, but not small enough to cause large meridional stresses is used when investigating the membrane stresses of prolate toroidal shells.

7.2.2 Circular tanks

For the same volume used for the prolate shells in 7.2.1, various aspect ratios of circular tanks are investigated in order to compare the surface area and structural integrity. Geometric aspects of these circular toroids are shown below.

Table 7-3: Geometric properties of investigated circular shells

Opening ratio (A/a)	a(m)	A(m)	Surface area(m^2)	Volume(m^3)
2	14.42	28.84	16418	118435
3	12.6	37.8	18802	118435
4	11.45	45.8	20702	118435

7.2.2.1. Outer surface

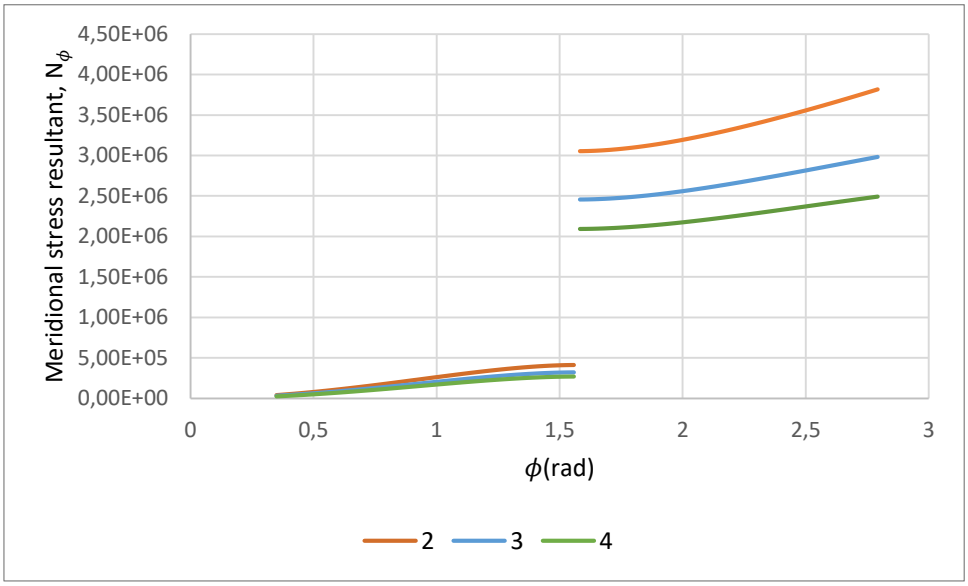

Figure 7-9: Meridional stress resultant for the outer surface of circular toroidal shells with a fixed volume, with varying opening ratios

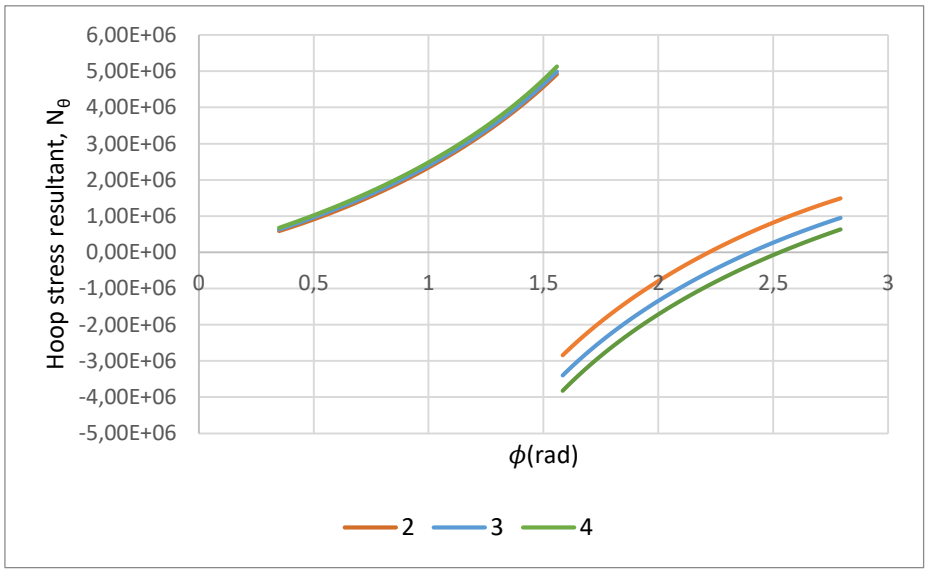

Figure 7-10: Hoop stress resultant for the outer surface of circular toroidal shells with a fixed volume, with varying opening ratios

7.2.2.2. Inner surface

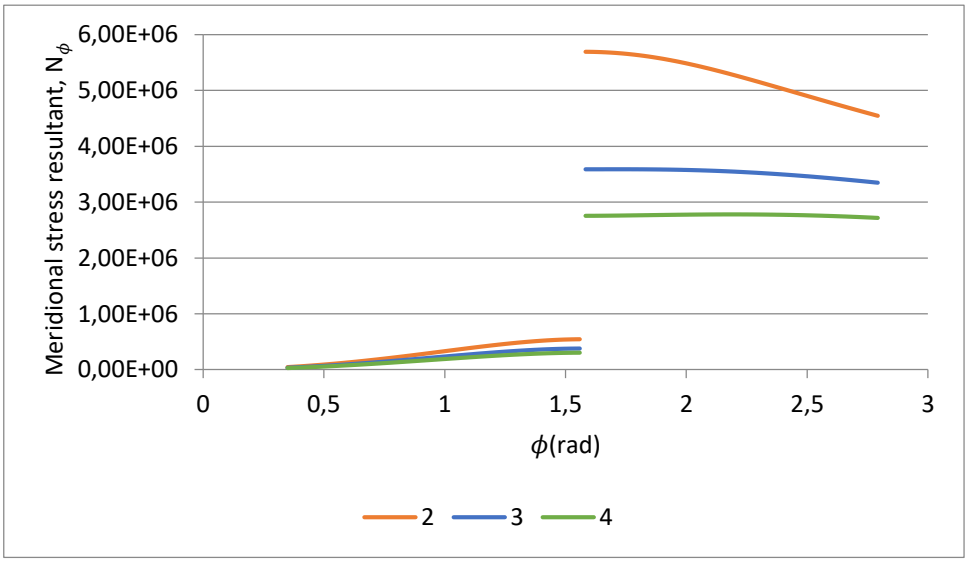

Figure 7-11: Meridional stress resultant for the inner surface of circular toroidal shells with a fixed volume, with varying opening ratios

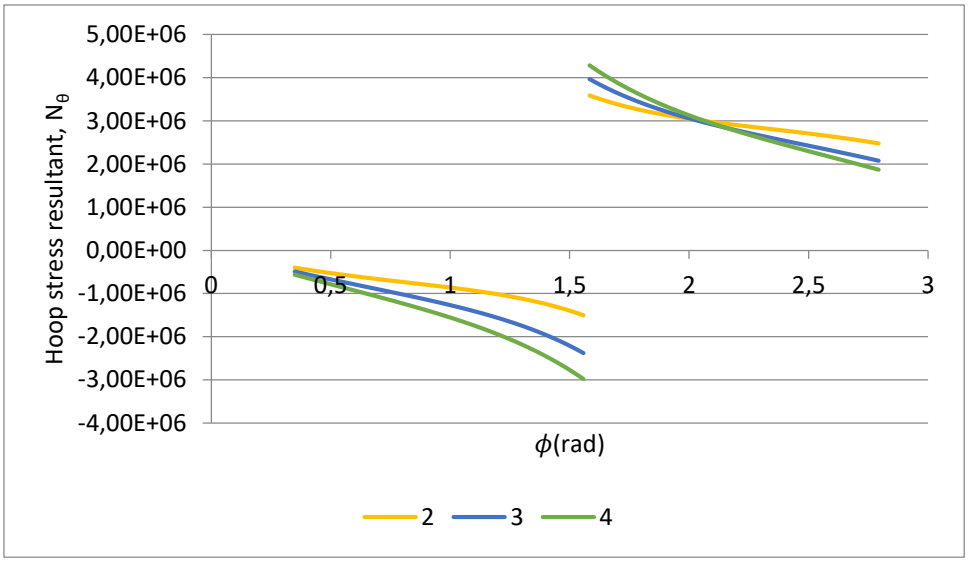

Figure 7-12: Hoop stress resultant for the inner surface of circular toroidal shells with a fixed volume, with varying opening ratios

The effect of the variation of the aspect ratio for circular tanks is similar to that experienced for the prolate tanks, as from Figure 7-9 and Figure 7-11, the smaller the opening ratio, the larger the peak meridional stress value will be, for the lower region for both the inner and outer surfaces of the circular toroidal tank. The upper regions of the tank are negligibly affected in comparison as only slight increases are noticed with a decrease in the opening ratio.

Hoop stresses have a different pattern, as the outer surface and inner surface of the tank react differently. Figure 7-10 and Figure 7-12 show the effects on the outer and inner surface respectively. It can immediately be seen that a larger opening ratio corresponds to higher magnitudes of peak hoop stresses in the lower region of the tank, as the hoop stress just sufficiently far away from the support is in compression, but becomes more tensile in nature as ϕ increases and the opening ratio increases. The inner surface behaves differently as higher peak stresses are experienced for a greater opening ratio.

Examining the surface area from Table 7-3, it is shown that for the same volume, circular toroidal shells with a larger cross-section and lower opening ratio yield the lower surface area, resulting in less sheet metal required to fabricate. As was discussed in examination of the prolate shell, a trade-off between keeping the opening ratio

sufficiently small, but not too small that large meridional stresses will be experienced is recommended, should designers only have a constraint of having a fixed volume, with no limitations on space required.

Chapter 8

Conclusions

8.1 Introduction

This study investigates the membrane stresses of elliptical and circular toroidal shells, subjected to complete hydrostatic pressure, supported on equatorial circles of latitude. Various parameters relating to toroidal shells such as the aspect and opening ratios are varied in order to obtain the membrane stress resultants in both the meridional and hoop directions. Using the membrane theory of shells, expressions were derived for elliptical toroidal shells whilst the corresponding expressions for circular shells were obtained from previous research undertaken by Enoma et al (2015).

The findings of this study lead to the development to further solutions for the bending solution of the elliptical toroidal shell subjected to hydrostatic loading and as well as recommendations to designers who are interested in the membrane stresses occurring at locations within toroidal shells sufficiently far away from bending disturbances.

8.2 Research objectives

The objectives of this study are as follows:

- To derive membrane expressions for elliptical toroidal shells and verify them using the finite element method
- To investigate the sensitivity of membrane stresses to a change in the aspect and opening ratio of circular and elliptical toroidal tanks

- To make economical recommendations to designers for practical values of toroidal tanks

8.3 Derivation and validation of the expression

Using the membrane theory of shells, membrane expressions for elliptical toroidal shells were derived. These expressions were validated against the finite element method software ADINA, for parameters of A, a, b, t and γ of 30m, 10m, 20m, 0.05m and 10kN/m^3 respectively. It was shown that excellent agreement occurred between the numerical and analytical results, with discrepancies occurring around locations of supports and the top and bottom of the tank, due to the presence of edge and bending effects occurring at these locations. It was therefore concluded that the derived expressions were suitable for examining the membrane stresses of elliptical toroidal tanks.

8.4 Membrane stress sensitivity

A parametric study into the membrane stress profiles of various prolate, oblate and circular toroidal shells was undertaken, with the assumption of dimensionless parameters and supports located at regions of $\phi = \frac{\pi}{2}$ and $\phi = \frac{3\pi}{2}$. Aspect and opening ratios were varied.

8.4.1 Aspect ratios

Aspect ratios were varied for elliptical toroidal shells, where it was found that whilst keeping all other parameters constant, the upper regions of meridional stress resultants of the inner and outer surface of both prolate and oblate elliptical toroidal tanks would have little effect. However, the inner and outer surface of the bottom half of the tank reacted differently, as both prolate and oblate cross-sections showed that an increase in the elongation of the cross-section corresponds to an increase meridional stress profiles for these regions. Oblate shells were also shown to have their peak stress occurring towards the bottom of the tank, contrasting prolate, where the peak meridional stress occurred just after the location of the support.

The circumferential stress profiles, were however different, as an increase in the aspect ratio for prolate shells corresponded to an increase hoop stress for both the inner and outer surface, but for oblate shells, an increase in the aspect ratio yielded a smaller hoop stress, due to the shell becoming more elongated.

8.4.2 Opening ratio

Similar trends were observed for prolate, oblate and circular toroidal tanks when investigating the opening ratio, keeping all else constant. The upper region of the tank, for both the inner and outer surfaces had very little change to its meridional stress resultant for an increase in the opening ratio, but lower region of the tank did not display the same trends. For the lower-outer region, an increase in the opening ratio corresponded to higher meridional stresses, although this was not proportionate to the increase. The lower-inner region experienced a different result, as a decrease in the opening ratio correlated with an increase in the meridional stress. This was found to be true for all types of toroidal shells investigated.

Circumferential stresses also seem to respond to their stress profiles irrespective of their cross-section as the hoop stresses for inner and outer surfaces of prolate, oblate and circular shells increase with an increase in the opening ratio.

8.5 Volumetric capability of toroidal shells

Numerical examples, using volume and surface area as constraints were used in order to make recommendations to designers on the type of toroidal shell to use. No optimisation function was created, due to the presence of elliptical integrals within the surface area of elliptical toroidal shells, from which the associated equations are complex.

8.5.1 Recommendations on cross-sectional profiles

For a shell with a fixed volume and fixed opening, it was determined that the optimal cross-sectional shape would be a trade-off between circular and prolate toroidal shells. This was established by comparing the area of metal required for fabrication and the maximum membrane stress experienced. It was found that comparing oblate shells to

prolate shells, for an inverse of the aspect ratio and same surface area and volume, the prolate shell would have better structural integrity for the same cost.

8.5.2 Recommendations on opening ratio

For the numerical examples investigated for prolate and circular toroidal tanks, for a fixed volume and fixed aspect ratio, it was shown that factoring cost and keeping volume constant, it is recommended that a sufficiently small opening ratio is used for design, however, this opening ratio should not be too small to induce large meridional stresses which may occur.

8.6 Recommendations for further research

- This study investigated the membrane stresses for elliptical and circular toroidal tanks. In reality, bending stresses will be present at the apex and bottom of the tank, in addition to the location of supports. It is recommended that bending solution is achieved for this. However, given the complexity of this, a finite element parametric study may be better suited for use.

- A large number of compressive stresses were seen throughout the various profiles in this study. It is therefore recommended that a buckling investigation is undertaken in order to obtain the critical pressures for elliptical and circular toroidal tanks. This may be done analytically or numerically.

References

Błachut, J. 2004. Buckling and first ply failure of composite toroidal pressure hull. Computers & Structures. 82(23):1981-1992.

Błachut, J. & Jaiswal, O. 2000. On buckling of toroidal shells under external pressure. Computers & Structures. 77(3):233-251.

Buchanan, G. & Liu, Y. 2005. An analysis of the free vibration of thick-walled isotropic toroidal shells. International Journal of Mechanical Sciences. 47(2):277-292.

Chandrupatla, T.R., Belegundu, A.D., Ramesh, T. & Ray, C. 2002. Introduction to finite elements in engineering. Prentice Hall Upper Saddle River, NJ.

Clark, R.A. 1950. On the theory of thin elastic toroidal shells. Journal of Mathematics and Physics. 29(1):146-178.

Combescure, A. & Galletly, G. 1999. Plastic buckling of complete toroidal shells of elliptical cross-section subjected to internal pressure. Thin-Walled Structures. 34(2):135-146.

Dahl, N. 1953. Toroidal-shell expansion joints. Journal of Applied Mechanics-Transactions of the Asme. 20(4):497-503.

Enoma, N., Egware, H.O., Itoje, H.J. & Unueroh, U.G. 2015. Membrane Solutions For Circular Toroidal Shells Under Internal Hydrostatic Pressure. 1(10).

Farshad, M. 2013. Design and analysis of shell structures. Springer Science & Business Media.

Fish, J. & Belytschko, T. 2007. A first course in finite elements. John Wiley & Sons.

Flugge, S. 1973. Stresses in shells. Berlin: Springer, 1973, 2nd Ed. 1.

Flugge, W. & Sobel, L. 1967. Stability of toroidal shells under uniform external pressure. AIAA Journal. 5(3):425-431.

Galletly, G. 1998. Elastic buckling of complete toroidal shells of elliptical cross-section subjected to uniform internal pressure. Thin-Walled Structures. 30(1):23-34.

Gavelya, S. & Kononenko, N. 1975. Characteristic oscillations and waves on a toroidal shell. International Applied Mechanics. 11(1):31-35.

Gol'denveizer, A. 1961. Theory of thin elastic shells. International Series of Monograph in Aeronautics and Astronautics.

Govender, N. 2013. A numerical investigation into the viscoelastic behaviour of round holes within pressurised HDPE pipes. Unpublished thesis.

Gradshteyn, I.S. & Ryzhik, I.M. 2014. Table of integrals, series, and products. Academic press.

Huang, D., Redekop, D. & Xu, B. 1997. Natural frequencies and mode shapes of curved pipes. Computers & Structures. 63(3):465-473.

Hung-bin, Z., Zhen-hui, W. & Zhu-pei, S. 1981. The Equations in Complex Variables under Axial Symmetric Loads and their Asymptotic Solutions. Journal of Tsinghua University (Science and Technology). 2:000.

Jiang, W. & Redekop, D. 2003. Static and vibration analysis of orthotropic toroidal shells of variable thickness by differential quadrature. Thin-Walled Structures. 41(5):461-478.

JORDAN, P.F. 1973. Buckling of toroidal shells under hydrostatic pressure. AIAA Journal. 11(10):1439-1441.

Kosawada, T., Suzuki, K. & Takahashi, S. 1986. Free vibrations of thick toroidal shells. Bulletin of JSME. 29(255):3036-3042.

Leung, A. & Kwok, N.T. 1994. Free vibration analysis of a toroidal shell. Thin-Walled Structures. 18(4):317-332.

Leung, A. & Kwok, N. 1995. Dynamic stiffness analysis of toroidal shells. Thin-Walled Structures. 21(1):43-64.

Liepins, A. & Sanders, J. 1963. Toroidal membrane under internal pressure. AIAA Journal. 1(9):2105-2110.

Manual, A.U. 2012. Version 6.12. Dassault Systémes Simulia Corp., Providence, RI.

Ming, R., Pan, J. & Norton, M. 2002. Free vibrations of elastic circular toroidal shells. Applied Acoustics. 63(5):513-528.

Novozhilov, V.V. 1959. The theory of thin shells. P. Noordhoff.

Novozhilov, V.V. 1951. On the Relation between Stresses and Strains in Nonlinearly Elastic Medium. Prikl.Mat.Mekh. 15(2):183-194.

Redekop, D. 1994. Dynamic response of a toroidal shell panel to blast loading. Computers & Structures. 51(3):235-239.

Redekop, D., Xu, B. & Zhang, Y. 1999. Stability of a toroidal fluid-containing shell. International Journal of Pressure Vessels and Piping. 76(9):575-581.

Reissner, E. 1946. Stresses and small displacements of shallow spherical shells. II. Journal of Mathematics and Physics. 25(1):279-300.

Ren, W. & Zhang, W. 1995. A survey of works on the theory of toroidal shells. Microstructures and Mechanical Properties of New Engineering Materials. :507-512.

Ruojing, Z. 1990. Thin Shell Vibrations in Low Frequency. Chinese Quarterly of Mechanics. 4:004.

Salley, L. & Pan, J. 2002. A study of the modal characteristics of curved pipes. Applied Acoustics. 63(2):189-202.

Sanders Jr, J.L. 1959. An improved first-approximation theory for thin shells.

Steele, C. 1965. Toroidal pressure vessels. Journal of Spacecraft and Rockets. 2(6):937-943.

Sun, B. 2010. Closed-form solution of axisymmetric slender elastic toroidal shells. Journal of Engineering Mechanics. 136(10):1281-1288.

Sutcliffe, W. 1971. Stress analysis of toroidal shells of elliptical cross-section. International Journal of Mechanical Sciences. 13(11):951-958.

Timoshenko, S.P. & Woinowsky-Krieger, S. 1959. Theory of plates and shells. McGraw-hill.

Tizzi, S. 2015. A free vibration analysis of toroidal composite shells in free space. Journal of Sound and Vibration. 337:116-134.

Tumarkin, S. 1959. Asymptotic solution of a linear nonhomogeneous second order differential equation with a transition point and its application to the computations of toroidal shells and propeller blades. Journal of Applied Mathematics and Mechanics. 23(6):1549-1565.

Veličković, V. 2007. Stress and Strain States in the Material of the Stressed Toroidal Container for Liquefied Petroleum Gas. Scientific Technical Review. 57(3-4):94-105.

Ventsel, E. & Krauthammer, T. 2001. Thin plates and shells: theory: analysis, and applications. CRC press.

Vu, V.T. 2010. Minimum weight design for toroidal pressure vessels using differential evolution and particle swarm optimization. Structural and Multidisciplinary Optimization. 42(3):351-369.

Vu, V.T. 2013. Optimum Shape of Constant Stress Toroidal Shells. Journal of Pressure Vessel Technology. 135(2):024501.

Vu, V.T. & Blachut, J. 2009. Plastic instability pressure of toroidal shells. Journal of Pressure Vessel Technology. 131(5):051203.

Wang, X. & Redekop, D. 2011. Natural frequencies analysis of moderately-thick and thick toroidal shells. Procedia Engineering. 14:636-640.

Wang, X., Xu, B. & Redekop, D. 2006. FEM free vibration and buckling analysis of stiffened toroidal shells. Thin-Walled Structures. 44(1):2-9.

Wang, X., Xu, B. & Redekop, D. 2006. Theoretical natural frequencies and mode shapes for thin and thick curved pipes and toroidal shells. Journal of Sound and Vibration. 292(1):424-434.

Wang, X.H. 2004. Free Vibration and Stability of Complete Orthotropic Circular Toroidal Shells.

Wissler, H. 1916. Festigkeitberechung von Ringsflachen. Promotionarbeit, Zurich.

Yamada, G., Kobayashi, Y., Ohta, Y. & Yokota, S. 1989. Free vibration of a toroidal shell with elliptical cross-section. Journal of Sound and Vibration. 135(3):411-425.

Zhan, H. 2008. Static and Dynamic Analysis of Toroidal LPG Tanks.

Zhan, H. & Redekop, D. 2008. Vibration, buckling and collapse of ovaloid toroidal tanks. Thin-Walled Structures. 46(4):380-389.

Zhan, H. & Redekop, D. 2009. Static and dynamic loading of an ovaloid toroidal tank. Thin-Walled Structures. 47(6):760-767.

Zhou, D., Cheung, Y. & Lo, S. 2010. Three-dimensional vibration analysis of toroidal sectors with solid circular cross-sections. Journal of Applied Mechanics. 77(4):041002.

Zingoni, A. 1997. Shell structures in civil and mechanical engineering. NY: Thomas Telford Publishing.

Zingoni, A. 2015. Liquid-containment shells of revolution: a review of recent studies on strength, stability and dynamics. Thin-Walled Structures. 87:102-114.

Zingoni, A., Enoma, N. & Govender, N. 2015. Equatorial bending of an elliptic toroidal shell. Thin-Walled Structures. 96:286-294.

Zwillinger, D. 2002. CRC standard mathematical tables and formulae. CRC press.

Appendix A

Sample ADINA File

.ADINA-AUI---

A. Model Building

Insert points corresponding to ellipse or circle in the +YZ Plane only

Point #	X2	X3
1	20	0
2	20.1	2.821347
3	20.2	3.97995
4	20.3	4.862098
5	20.4	5.6
6	20.5	6.244998
7	20.6	6.823489
8	20.7	7.35119
9	20.8	7.838367
10	20.9	8.292165
11	21	8.717798
12	21.1	9.11921
13	21.2	9.499474
14	21.3	9.861034

15	21.4	10.20588
16	21.5	10.53565
17	21.6	10.85173
18	21.7	11.15527
19	21.8	11.44727
20	21.9	11.7286
21	22	12
22	22.1	12.26214
23	22.2	12.51559
24	22.3	12.76088
25	22.4	12.99846
26	22.5	13.22876
27	22.6	13.45214
28	22.7	13.66894
29	22.8	13.87948
30	22.9	14.08403
31	23	14.28286
32	23.1	14.47619
33	23.2	14.66424
34	23.3	14.84722
35	23.4	15.02531
36	23.5	15.19868
37	23.6	15.3675
38	23.7	15.5319
39	23.8	15.69204
40	23.9	15.84803
41	24	16
42	24.1	16.14806
43	24.2	16.29233
44	24.3	16.43289
45	24.4	16.56985
46	24.5	16.70329
47	24.6	16.8333
48	24.7	16.95995
49	24.8	17.08333
50	24.9	17.20349
51	25	17.32051
52	25.1	17.43445
53	25.2	17.54537
54	25.3	17.65333

55	25.4	17.75838
56	25.5	17.86057
57	25.6	17.95996
58	25.7	18.05658
59	25.8	18.15048
60	25.9	18.24171
61	26	18.3303
62	26.1	18.4163
63	26.2	18.49973
64	26.3	18.58064
65	26.4	18.65905
66	26.5	18.73499
67	26.6	18.80851
68	26.7	18.87962
69	26.8	18.94835
70	26.9	19.01473
71	27	19.07878
72	27.1	19.14053
73	27.2	19.2
74	27.3	19.25721
75	27.4	19.31217
76	27.5	19.36492
77	27.6	19.41546
78	27.7	19.46381
79	27.8	19.51
80	27.9	19.55403
81	28	19.59592
82	28.1	19.63568
83	28.2	19.67333
84	28.3	19.70888
85	28.4	19.74234
86	28.5	19.77372
87	28.6	19.80303
88	28.7	19.83028
89	28.8	19.85548
90	28.9	19.87863
91	29	19.89975
92	29.1	19.91884
93	29.2	19.9359
94	29.3	19.95094

95	29.4	19.96397
96	29.5	19.97498
97	29.6	19.98399
98	29.7	19.991
99	29.8	19.996
100	29.9	19.999
101	30	20
102	30.1	19.999
103	30.2	19.996
104	30.3	19.991
105	30.4	19.98399
106	30.5	19.97498
107	30.6	19.96397
108	30.7	19.95094
109	30.8	19.9359
110	30.9	19.91884
111	31	19.89975
112	31.1	19.87863
113	31.2	19.85548
114	31.3	19.83028
115	31.4	19.80303
116	31.5	19.77372
117	31.6	19.74234
118	31.7	19.70888
119	31.8	19.67333
120	31.9	19.63568
121	32	19.59592
122	32.1	19.55403
123	32.2	19.51
124	32.3	19.46381
125	32.4	19.41546
126	32.5	19.36492
127	32.6	19.31217
128	32.7	19.25721
129	32.8	19.2
130	32.9	19.14053
131	33	19.07878
132	33.1	19.01473
133	33.2	18.94835
134	33.3	18.87962

135	33.4	18.80851
136	33.5	18.73499
137	33.6	18.65905
138	33.7	18.58064
139	33.8	18.49973
140	33.9	18.4163
141	34	18.3303
142	34.1	18.24171
143	34.2	18.15048
144	34.3	18.05658
145	34.4	17.95996
146	34.5	17.86057
147	34.6	17.75838
148	34.7	17.65333
149	34.8	17.54537
150	34.9	17.43445
151	35	17.32051
152	35.1	17.20349
153	35.2	17.08333
154	35.3	16.95995
155	35.4	16.8333
156	35.5	16.70329
157	35.6	16.56985
158	35.7	16.43289
159	35.8	16.29233
160	35.9	16.14806
161	36	16
162	36.1	15.84803
163	36.2	15.69204
164	36.3	15.5319
165	36.4	15.3675
166	36.5	15.19868
167	36.6	15.02531
168	36.7	14.84722
169	36.8	14.66424
170	36.9	14.47619
171	37	14.28286
172	37.1	14.08403
173	37.2	13.87948
174	37.3	13.66894

175	37.4	13.45214
176	37.5	13.22876
177	37.6	12.99846
178	37.7	12.76088
179	37.8	12.51559
180	37.9	12.26214
181	38	12
182	38.1	11.7286
183	38.2	11.44727
184	38.3	11.15527
185	38.4	10.85173
186	38.5	10.53565
187	38.6	10.20588
188	38.7	9.861034
189	38.8	9.499474
190	38.9	9.11921
191	39	8.717798
192	39.1	8.292165
193	39.2	7.838367
194	39.3	7.35119
195	39.4	6.823489
196	39.5	6.244998
197	39.6	5.6
198	39.7	4.862098
199	39.8	3.97995
200	39.9	2.821347
201	40	0
202	39.9	-2.82135
203	39.8	-3.97995
204	39.7	-4.8621
205	39.6	-5.6
206	39.5	-6.245
207	39.4	-6.82349
208	39.3	-7.35119
209	39.2	-7.83837
210	39.1	-8.29216
211	39	-8.7178
212	38.9	-9.11921
213	38.8	-9.49947
214	38.7	-9.86103

215	38.6	-10.2059
216	38.5	-10.5357
217	38.4	-10.8517
218	38.3	-11.1553
219	38.2	-11.4473
220	38.1	-11.7286
221	38	-12
222	37.9	-12.2621
223	37.8	-12.5156
224	37.7	-12.7609
225	37.6	-12.9985
226	37.5	-13.2288
227	37.4	-13.4521
228	37.3	-13.6689
229	37.2	-13.8795
230	37.1	-14.084
231	37	-14.2829
232	36.9	-14.4762
233	36.8	-14.6642
234	36.7	-14.8472
235	36.6	-15.0253
236	36.5	-15.1987
237	36.4	-15.3675
238	36.3	-15.5319
239	36.2	-15.692
240	36.1	-15.848
241	36	-16
242	35.9	-16.1481
243	35.8	-16.2923
244	35.7	-16.4329
245	35.6	-16.5699
246	35.5	-16.7033
247	35.4	-16.8333
248	35.3	-16.96
249	35.2	-17.0833
250	35.1	-17.2035
251	35	-17.3205
252	34.9	-17.4344
253	34.8	-17.5454
254	34.7	-17.6533

255	34.6	-17.7584
256	34.5	-17.8606
257	34.4	-17.96
258	34.3	-18.0566
259	34.2	-18.1505
260	34.1	-18.2417
261	34	-18.3303
262	33.9	-18.4163
263	33.8	-18.4997
264	33.7	-18.5806
265	33.6	-18.659
266	33.5	-18.735
267	33.4	-18.8085
268	33.3	-18.8796
269	33.2	-18.9484
270	33.1	-19.0147
271	33	-19.0788
272	32.9	-19.1405
273	32.8	-19.2
274	32.7	-19.2572
275	32.6	-19.3122
276	32.5	-19.3649
277	32.4	-19.4155
278	32.3	-19.4638
279	32.2	-19.51
280	32.1	-19.554
281	32	-19.5959
282	31.9	-19.6357
283	31.8	-19.6733
284	31.7	-19.7089
285	31.6	-19.7423
286	31.5	-19.7737
287	31.4	-19.803
288	31.3	-19.8303
289	31.2	-19.8555
290	31.1	-19.8786
291	31	-19.8997
292	30.9	-19.9188
293	30.8	-19.9359
294	30.7	-19.9509

295	30.6	-19.964
296	30.5	-19.975
297	30.4	-19.984
298	30.3	-19.991
299	30.2	-19.996
300	30.1	-19.999
301	30	-20
302	29.9	-19.999
303	29.8	-19.996
304	29.7	-19.991
305	29.6	-19.984
306	29.5	-19.975
307	29.4	-19.964
308	29.3	-19.9509
309	29.2	-19.9359
310	29.1	-19.9188
311	29	-19.8997
312	28.9	-19.8786
313	28.8	-19.8555
314	28.7	-19.8303
315	28.6	-19.803
316	28.5	-19.7737
317	28.4	-19.7423
318	28.3	-19.7089
319	28.2	-19.6733
320	28.1	-19.6357
321	28	-19.5959
322	27.9	-19.554
323	27.8	-19.51
324	27.7	-19.4638
325	27.6	-19.4155
326	27.5	-19.3649
327	27.4	-19.3122
328	27.3	-19.2572
329	27.2	-19.2
330	27.1	-19.1405
331	27	-19.0788
332	26.9	-19.0147
333	26.8	-18.9484
334	26.7	-18.8796

335	26.6	-18.8085
336	26.5	-18.735
337	26.4	-18.659
338	26.3	-18.5806
339	26.2	-18.4997
340	26.1	-18.4163
341	26	-18.3303
342	25.9	-18.2417
343	25.8	-18.1505
344	25.7	-18.0566
345	25.6	-17.96
346	25.5	-17.8606
347	25.4	-17.7584
348	25.3	-17.6533
349	25.2	-17.5454
350	25.1	-17.4344
351	25	-17.3205
352	24.9	-17.2035
353	24.8	-17.0833
354	24.7	-16.96
355	24.6	-16.8333
356	24.5	-16.7033
357	24.4	-16.5699
358	24.3	-16.4329
359	24.2	-16.2923
360	24.1	-16.1481
361	24	-16
362	23.9	-15.848
363	23.8	-15.692
364	23.7	-15.5319
365	23.6	-15.3675
366	23.5	-15.1987
367	23.4	-15.0253
368	23.3	-14.8472
369	23.2	-14.6642
370	23.1	-14.4762
371	23	-14.2829
372	22.9	-14.084
373	22.8	-13.8795
374	22.7	-13.6689

375	22.6	-13.4521
376	22.5	-13.2288
377	22.4	-12.9985
378	22.3	-12.7609
379	22.2	-12.5156
380	22.1	-12.2621
381	22	-12
382	21.9	-11.7286
383	21.8	-11.4473
384	21.7	-11.1553
385	21.6	-10.8517
386	21.5	-10.5357
387	21.4	-10.2059
388	21.3	-9.86103
389	21.2	-9.49947
390	21.1	-9.11921
391	21	-8.7178
392	20.9	-8.29216
393	20.8	-7.83837
394	20.7	-7.35119
395	20.6	-6.82349
396	20.5	-6.245
397	20.4	-5.6
398	20.3	-4.8621
399	20.2	-3.97995
400	20.1	-2.82135
401	20	0

-ok-

Geometry-Lines-Define-Add-Line Number 1-Type: Polyline-Curve Type: Spline:

	Point # [p]
1	1
2	2
3	3
4	4
5	5
6	6

7	7
8	8
9	9
10	10
11	11
12	12
13	13
14	14
15	15
16	16
17	17
18	18
19	19
20	20
21	21
22	22
23	23
24	24
25	25
26	26
27	27
28	28
29	29
30	30
31	31
32	32
33	33
34	34
35	35
36	36
37	37
38	38
39	39
40	40
41	41
42	42
43	43
44	44
45	45
46	46

47	47
48	48
49	49
50	50
51	51
52	52
53	53
54	54
55	55
56	56
57	57
58	58
59	59
60	60
61	61
62	62
63	63
64	64
65	65
66	66
67	67
68	68
69	69
70	70
71	71
72	72
73	73
74	74
75	75
76	76
77	77
78	78
79	79
80	80
81	81
82	82
83	83
84	84
85	85
86	86

87	87
88	88
89	89
90	90
91	91
92	92
93	93
94	94
95	95
96	96
97	97
98	98
99	99
100	100
101	101
102	102
103	103
104	104
105	105
106	106
107	107
108	108
109	109
110	110
111	111
112	112
113	113
114	114
115	115
116	116
117	117
118	118
119	119
120	120
121	121
122	122
123	123
124	124
125	125
126	126

127	127
128	128
129	129
130	130
131	131
132	132
133	133
134	134
135	135
136	136
137	137
138	138
139	139
140	140
141	141
142	142
143	143
144	144
145	145
146	146
147	147
148	148
149	149
150	150
151	151
152	152
153	153
154	154
155	155
156	156
157	157
158	158
159	159
160	160
161	161
162	162
163	163
164	164
165	165
166	166

167	167
168	168
169	169
170	170
171	171
172	172
173	173
174	174
175	175
176	176
177	177
178	178
179	179
180	180
181	181
182	182
183	183
184	184
185	185
186	186
187	187
188	188
189	189
190	190
191	191
192	192
193	193
194	194
195	195
196	196
197	197
198	198
199	199
200	200
201	201
202	202
203	203
204	204
205	205
206	206

207	207
208	208
209	209
210	210
211	211
212	212
213	213
214	214
215	215
216	216
217	217
218	218
219	219
220	220
221	221
222	222
223	223
224	224
225	225
226	226
227	227
228	228
229	229
230	230
231	231
232	232
233	233
234	234
235	235
236	236
237	237
238	238
239	239
240	240
241	241
242	242
243	243
244	244
245	245
246	246

247	247
248	248
249	249
250	250
251	251
252	252
253	253
254	254
255	255
256	256
257	257
258	258
259	259
260	260
261	261
262	262
263	263
264	264
265	265
266	266
267	267
268	268
269	269
270	270
271	271
272	272
273	273
274	274
275	275
276	276
277	277
278	278
279	279
280	280
281	281
282	282
283	283
284	284
285	285
286	286

287 287
288 288
289 289
290 290
291 291
292 292
293 293
294 294
295 295
296 296
297 297
298 298
299 299
300 300
301 301
302 302
303 303
304 304
305 305
306 306
307 307
308 308
309 309
310 310
311 311
312 312
313 313
314 314
315 315
316 316
317 317
318 318
319 319
320 320
321 321
322 322
323 323
324 324
325 325
326 326

327	327
328	328
329	329
330	330
331	331
332	332
333	333
334	334
335	335
336	336
337	337
338	338
339	339
340	340
341	341
342	342
343	343
344	344
345	345
346	346
347	347
348	348
349	349
350	350
351	351
352	352
353	353
354	354
355	355
356	356
357	357
358	358
359	359
360	360
361	361
362	362
363	363
364	364
365	365
366	366

367 367
368 368
369 369
370 370
371 371
372 372
373 373
374 374
375 375
376 376
377 377
378 378
379 379
380 380
381 381
382 382
383 383
384 384
385 385
386 386
387 387
388 388
389 389
390 390
391 391
392 392
393 393
394 394
395 395
396 396
397 397
398 398
399 399
400 400
401 401
402 1

-ok-

Geometry-Lines-Thickness-Define Line Thickness

	Line #	Thickness
1	1	0.5

-ok-

Model-Materials-Elastic-Isotropic-Add-Material Number:1 – Description-STEEL

Young's Modulus (>0): 205E9

Poisson's Ratio (-1.0<NU<0.5): 0.3

-ok-

Meshing – Element Groups – Add- Group Number: 1 – Type: Isobeam

Element Sub-Type: Axisymmetric Shell

-ok-

Meshing – Mesh Density – Define Line Mesh Density- Line Number: 1- Method: Use Number of Divisions – Number of Subdivisions: 1000

-ok-

Meshing-Create Mesh- Mesh Lines – Type: Isobeam

-ok-

B. Loading and BC's

Geometry-Spatial Function -Line-Define Line Function -Add-Function Number 1- Type: Linear- Values at Specific Points:

U=0: 0

U=1: 1

-ok-

Apply Load- Load Type: Pressure-Apply to: Line-Load Number -Define: Add-

Pressure Number: 1

Magnitude (Force/Area) 10E3

-ok-

Line	Deform. Dependent?	Load Direction	Time Function	Spatial Function
1	Default	Total (Normal)	1	1

-ok-

Model – Boundary Conditions – Apply Fixity- Apply to: Points:

	Point {p}	
1	201	ALL
2	1	ALL

-ok-

C. Analysis

Analysis Type: Static

D. Running the Program

Solution – Data File/Run

E. Post Processing

Create Model Line – Response Plot

View RR and TT Stress distributions

Export to Excel

Application for Approval of Ethics in Research (EiR) Projects
Faculty of Engineering and the Built Environment, University of Cape Town

APPLICATION FORM

Please Note:
Any person planning to undertake research in the Faculty of Engineering and the Built Environment (EBE) at the University of Cape Town is required to complete this form **before** collecting or analysing data. The objective of submitting this application prior to embarking on research is to ensure that the highest ethical standards in research, conducted under the auspices of the EBE Faculty, are met. Please ensure that you have read, and understood the **EBE Ethics in Research Handbook** (available from the UCT EBE, Research Ethics website) prior to completing this application form: http://www.ebe...ch/ethics/ethics.pdf

APPLICANT'S DETAILS		
Name of principal researcher, student or external applicant:		Nishalin Govender
Department		Civil Engineering
Preferred email address of applicant:		Nishalin.govender@hatch.com
If a Student	Your Degree: e.g., MSc, PhD, etc.,	MSc Eng
	Name of Supervisor (if supervised):	Prof Alphose Zingoni
If this is a research contract, indicate the source of funding/sponsorship		N/A
Project Title		A parametric investigation of the membrane stresses of hydrostatically loading toroidal tanks.

I hereby undertake to carry out my research in such a way that:

- there is no apparent legal objection to the nature or the method of research, and
- the research will not compromise staff or students or the other responsibilities of the University;
- the stated objectives will be achieved, and the findings will have a high degree of validity;
- limitations and alternative interpretations will be considered;
- the findings could be subject to peer review and publicly available; and
- I will comply with the conventions of copyright and avoid any practice that would constitute plagiarism.

SIGNED BY	Full name	Signature	Date
Principal Researcher/ Student/External applicant	Nishalin Govender	signature removed	07 Nov 2016

APPLICATION APPROVED BY	Full name	Signature	Date
Supervisor (where applicable)	Click here to enter text.	signature removed	Click here to enter a date.
HOD (or delegated nominee) Final authority for all applicants who have answered NO to all questions in Section1; and for all Undergraduate research (including Honours).	Click here to enter text.	signature removed	16/11/16 Click here to enter a date.
Chair : Faculty EiR Committee For applicants other than undergraduate students who have answered YES to any of the above questions.	Click here to enter text.		Click here to enter a date.

Page 1 of 1